

**INTEGRATION OF A COOLING SYSTEM WITH AN  
EXPERIMENTAL RIG FOR FILM EFFECTIVENESS  
MEASUREMENTS USING A FULL-STAGE HIGH-  
PRESSURE TURBINE**

A THESIS

Presented in Partial Fulfillment of the Requirements for the Degree Master of Science in  
the Graduate School of The Ohio State University

By

JACOB WARD HARRAL

\*\*\*\*\*

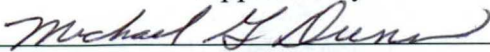
The Ohio State University  
2005

Thesis Committee:

Professor Michael G. Dunn, Advisor

Professor Tunc Aldemir

Approved by

  
\_\_\_\_\_  
Advisor

Graduate Program in Mechanical Engineering

## **ABSTRACT**

Increasing the efficiency in gas turbine engines requires constant improvement in the design tools currently available to the industry. One area for potential increases in efficiency deals with the film-cooling effectiveness in the high-pressure turbine section of the engine and the push to increase the temperature at the inlet of the turbine. Modeling of film-cooling effectiveness for incorporation into advanced CFD codes to be used for film effectiveness predictions and subsequent design of advanced engines is currently a major activity within the engine community. For the codes to be implemented as design tools one must gain confidence in their validity. One method that has been used for this purpose is to compare predictions obtained using these codes with experimental results obtained under as realistic conditions as is possible within the confines of controlled laboratory experiments. Under support of the NASA/DoD URETI, the OSU GTL has undertaken the task of performing detailed surface-pressure and surface heat-transfer measurements on the vane surfaces, on the blade surfaces, and on the stationary shroud of a fully cooled high-pressure turbine stage operating at design corrected conditions.

Several significant changes have been made to the OSU Gas Turbine Laboratory blowdown turbine facility and to the operating mode of that facility in order to make film effectiveness measurements. One of the major facility changes was the incorporation of a coolant gas supply system (LCF) into the facility. The major changes in operating mode involved operating in blowdown mode instead of shock tube mode. In order to achieve

this major change in operating procedure, it was necessary to incorporate a resistance heater into the rig just ahead of the high-pressure turbine vane inlet so that a resistance heater instead of the reflected shock could heat the test gas. The next major task was to sequence the main test gas flow with the coolant gas flow so that one could achieve the proper flow physics. This thesis will focus on the operation and integration of the LCF into the blowdown facility and on the experimental results acquired during the initial film-cooling experiment. Operation of the LCF is divided into three distinct areas: fast acting valve operation and sequencing with the main facility fast acting valve, cooling cycles, and facility controls. Successful integration of the LCF has been achieved and will be illustrated by the results of the initial film-cooling experiment. Through these experimental results and accompanying uncertainty analysis conducted as part of this thesis significant knowledge has been gained and will be applied to future film-cooling measurement programs.

With the demonstrated successful operation of the OSU turbine test facility in conjunction with the LCF, the OSU GTL is capable of conducting the critical experiments necessary to provide critical verification information for ongoing film effectiveness modeling and CFD code development.

## **ACKNOWLEDGMENTS**

I would like to start by thanking my advisor, Dr. Michael Dunn, for the opportunity to conduct my research at the OSU GTL and for his leadership, inspiration, and for the extra time spent on my thesis. I feel very privileged to have worked in a research facility that focuses on real world problems and works closely with industry following industry standards.

Also at the GTL, I would like to thank Dr. Charles Haldeman for teaching me to think from a scientific viewpoint and for the extra encouragement and guidance. Special thanks to the GTL staff and students: Jeff Barton, John Newkirk, Michael Jones, Ken Copley, Dr. Corso Padova, Randy Mathison, and Brian Cohen for ideas for solving problems and for the many trips to Roosters to keep our sanity. Working with these individuals has made my research career unforgettable and enjoyable, and I hope we stay in touch.

Finally, I would like to thank my family and friends for their support and encouragement throughout my collegiate career. Most of all I would like to thank my wife, Mary, who has given me endless love and support through the long nights of thesis writing and for her tolerance and patience as this chapter of my life comes to a close.

**VITA**

1980 .....Born - Chillicothe, Ohio

2003 .....B.S. Mechanical Engineering, University of  
Toledo, Toledo, OH

2003-Present .....Graduate Research Associate, The Ohio  
State University Gas Turbine Lab

**FIELDS OF STUDY**

Major Field: Mechanical Engineering

## TABLE OF CONTENTS

Abstract.....	ii
Acknowledgments.....	iv
Vita.....	v
List of Figures.....	ix
List of Tables.....	xiii
Nomenclature and Abbreviations.....	xiv
Chapter 1 Background Information and Direction of Research.....	1
1.1 Film Cooling Research.....	4
1.2 Film Cooling at The Ohio State University Gas Turbine Laboratory.....	5
1.3 Experimental Goals.....	6
1.4 Thesis Goals.....	7
Chapter 2 Description of Problem.....	8
2.1 Current Technology of Experimental Facilities.....	8
2.1.1 Facilities Designed for Flat Plate Measurements.....	9
2.1.2 Cascade Facilities.....	12
2.1.3 Rotating Facilities.....	26
2.2 Film Cooling at the OSU GTL.....	34
Chapter 3 Parameters Important for Film Cooling Experiments.....	37
3.1 Key Film Cooling Results.....	38

3.1.1 Blowing Ratio .....	38
3.1.2 Cooling Gas Mass Flow .....	40
Chapter 4 Operation and Integration of the LCF .....	42
4.1 Initial Design.....	43
4.2 Fast Acting Valve .....	44
4.3 Coolant System .....	56
4.4 LCF Controls .....	59
4.5 Integrating the LCF with the TTF.....	60
Chapter 5 Discussion of Calculations and Results .....	62
5.1 LCF Integration Results.....	62
5.2 Estimates of Blowing Ratio and Mass Flow.....	64
5.2.1 Blowing Ratio on the Blade.....	64
5.2.2 Coolant Gas Mass Flow Calculations .....	74
5.3 Uncertainty Analysis.....	78
5.3.1 Uncertainty in Blowing Ratio .....	78
5.3.2 Uncertainty in Mass Flow Supplied by LCF .....	81
5.3.3 Uncertainty in Mass Flow at Rotor Blade Cooling Holes .....	83
5.4 Future Experimentation .....	86
Chapter 6 Conclusions .....	89
Appendix A Experimental Results of FAV to Understand “Hic-cup” .....	92
Appendix B LCF Characterization Charts.....	95
Appendix C Coolant Gas Mass Flow Calculations.....	110

Appendix D Uncertainty Analysis Calculations .....	114
D.1 Blowing Ratio Influence Coefficients Characterization Plots .....	117
Bibliography .....	120



## LIST OF FIGURES

Figure 1. Two-shaft high bypass engine [1] .....	1
Figure 2. Typical cooled aircraft gas turbine blade [2].....	3
Figure 3. Two-dimensional coolant slot model with unsteady external pressure field [3] 4	
Figure 4. Film cooling test facility at University of Texas [12] .....	10
Figure 5. (a) Schematic of wind tunnel facility at University of Texas, (b) Side view of leading edge model [17].....	12
Figure 6. Schematic of blowdown facility at Texas A&M University [19] .....	13
Figure 7. The Stage-1 High-Pressure Turbine Blade for the GE CF6 [26] .....	14
Figure 8. Decay of maximum effectiveness (experiment by Dring <i>et al.</i> [4]).....	16
Figure 9. Film Cooling Effectiveness on Suction Surface Takeishi <i>et al.</i> [5] .....	17
Figure 10. Uncooled and Film Cooled Rotating Stage Measurements Compared with those from a Cooled Linear Cascade Abhari and Epstein [3].....	17
Figure 11. Rotating Bar Wake Generator [22].....	18
Figure 12. Conceptual view of unsteady wake effect on a model blade with film holes [24].....	19
Figure 13. Comparison at $x/s = 0.31$ on suction surface of MIT rotor and 2-D bar passing cascade test at 4% free-stream turbulence [27].....	19
Figure 14. Comparison on suction surface of MIT rotor ( $x/s = 0.08$ to $0.12$ ) with that from 2-D bar passing cascade test ( $x/s = 0.08$ ) at 4% free-stream turbulence [27]..	20

Figure 15. Different geometries of squealer tips [29].....	21
Figure 16. Geometry of film cooling holes [30].....	22
Figure 17. Conceptual view of flow in tip cavity [30].....	23
Figure 18. Uncooled rotating recess tip flow field [11].....	24
Figure 19. Cascade and shock apparatus at Virginia Tech [32] .....	25
Figure 20. Wind tunnel facility at Virginia Tech [32].....	26
Figure 21. MIT Time-resolved rotor heat transfer measurements [3] .....	29
Figure 22. Cross section of the rotating test equipment Takeishi <i>et al.</i> [5].....	30
Figure 23. Isentropic compression tube annular cascade facility at VKI .....	31
Figure 24. (a) Isentropic light piston facility at QinetiQ [35], (b) Current working section [36].....	32
Figure 25. Sketch of advanced turbine aerothermal research rig (TRF) configuration [37] .....	33
Figure 26. Shock tube facility (TTF) at the OSU GTL.....	34
Figure 27. Sketch of current OSU GTL Layout .....	35
Figure 28. Test rig mounted in dump tank.....	36
Figure 29. The effect of blowing ratio on single-row and double-row injection through different hole configurations [40] .....	39
Figure 30. LCF Connected to TTF for Film-Cooling Experiment .....	43
Figure 31. Breakdown of Internal LCF Construction.....	44
Figure 32. FAV in the open position (a) and the closed position (b).....	45
Figure 33. Cross-sectional view of FAV with sleeve in the open and closed position....	46

Figure 34. Timing sequence for FAV 3-way solenoid control valves .....	47
Figure 35. FAV internal chamber pressures and fiber optic sensors .....	48
Figure 36. FAV “hic-cup” while opening (a particularly severe case).....	50
Figure 37. Internal chamber pressure difference during “hic-cup” .....	51
Figure 38. Philtec sensor compared to current fiber optic pulse position sensor. ....	53
Figure 39. Effect of increasing the valve activation pressure .....	55
Figure 40. Difference in valve activation when extra ports at internal chambers are plugged.....	56
Figure 41. Time history of the FTS unit chilling the LCF coolant gas.....	58
Figure 42. Time history of the Julabo unit chilling the LCF coolant gas .....	58
Figure 43. Flow Path Temperature Rake Measurement .....	63
Figure 44. Stage Pressure Measurements .....	64
Figure 45. Normalized Static Pressure Distribution on Blade.....	65
Figure 46. Local Mach Number Distribution CFD Prediction (provided by Honeywell) .....	66
Figure 47. Estimated Blowing Ratio for Suction Surface Gill Holes.....	68
Figure 48. Estimated Blowing Ratio for Suction Surface Mid-Chord Holes .....	69
Figure 49. Estimated Blowing Ratio for Pressure Surface Holes near Mid-Chord.....	70
Figure 50. Internal Channel Pressure Measurements .....	71
Figure 51. FFT of Internal Pressure Measurements in Blade .....	72
Figure 52. Cooling Gas Internal Pressures .....	74

Figure 53. Influence Coefficient for the Static to Total Pressure Ratio in Blade Cooling Hole (x-axis: $\gamma_c$ , y-axis: Pr).....	80
Figure 54. Influence Coefficient for Static and Total Pressure Variables (Gamma=1.4) (x-axis: $P_s$ , y-axis: $P_{oc}$ ).....	81
Figure 55. Influence Coefficient for Gamma.....	82
Figure 56. Influence Coefficient for $M_p$ (x-axis: $\gamma$ , y-axis: $M_p$ ).....	84
Figure 57. Influence Coefficient for $M_t$ (x-axis: $\gamma$ , y-axis: $M_t$ ).....	85
Figure 58. Influence Coefficient for Gamma (x-axis: $M_t$ , y-axis: $M_p$ ).....	86

## LIST OF TABLES

Table 1. MIT blowdown experiment scaling parameters [3].....	28
Table 2. Mass flows at venturi chokes and at the vanes and blades .....	77
Table 3. Error Propagation Analysis for SS Gill Holes Blowing Ratio.....	79
Table 4. Error Propagation Analysis for Mass Flow Supplied by LCF .....	82
Table 5. Error Propagation Analysis for Mass Flow Calculated at Rotor Blade Cooling Holes .....	83

## NOMENCLATURE AND ABBREVIATIONS

GTL	Gas Turbine Lab		
TTF	Turbine Test Facility at The Ohio State University Gas Turbine Lab (OSU GTL)		
LCF	Large Calibration Facility at OSU GTL		
FAV	Fast Acting Valve – These are the valves that separate the driven tube and the LCF from the test section on the TTF		
T	Temperatures	PS	Pressure Surface
P, p	Pressure	SS	Suction Surface
$\rho$	Density	<b>Subscripts</b>	
$\gamma$	Specific Heat Ratio	o	Total property
$\nu$	Kinematic Viscosity	c	Coolant gas
V	Velocity	s	Static property
$\dot{m}$	Mass Flow	0	Without film-cooling
St	Stanton Number	F	Film-cooled
M	Mach Number	aw	Adiabatic wall
R	Gas Constant	$\infty, \alpha$	Freestream property
a	Speed of Sound	<b>Superscripts</b>	
$\tau$	Time Constant	*	Property at Mach 1
A	Area		
FO	Fiber Optic		

## CHAPTER 1

### BACKGROUND INFORMATION AND DIRECTION OF RESEARCH

Gas turbines are used in many applications ranging from aero and marine propulsion to power generation. Most gas turbine engines operate with the same basic underlying principles and physics, so they also tend to have similar limitations for performance. An exception to this might be a propulsion engine specifically designed for supersonic flight applications. One of the primary limitations in all gas turbines is the melting temperature of the hot section (combustor and high-pressure turbine) components, specifically the high-pressure turbine nozzle guide vanes and blades located directly behind the combustor as circled in red below in Figure 1.

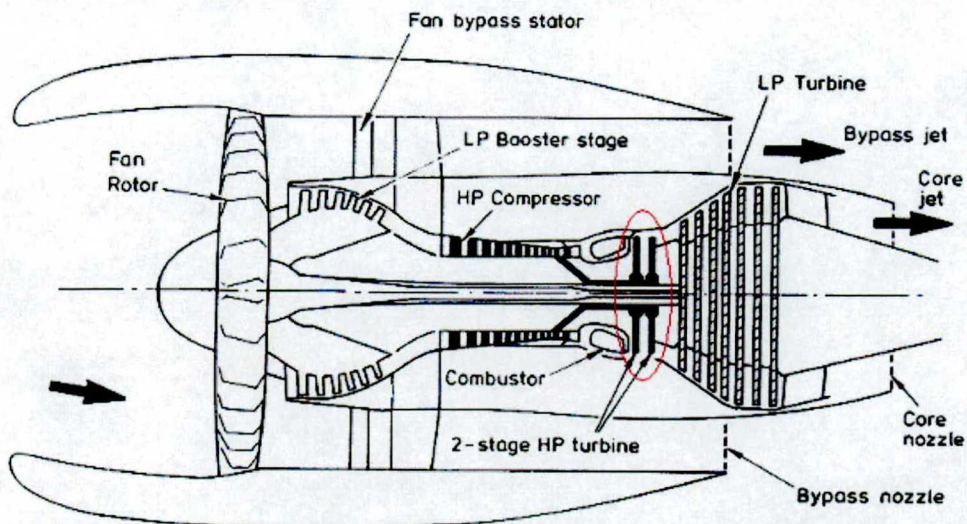


Figure 1. Two-shaft high bypass engine [1]

The turbine inlet temperature is continuously increasing with successive generations of engines because raising the turbine inlet temperature is one of the easier ways to achieve higher efficiency. For decades this temperature has been well above the melting temperature of the material used to construct the vanes and blades. It is possible to operate in this manner because cooling schemes like thermal boundary coatings (TBC), internal cooling, and external film cooling have been developed by the engine companies to protect the components. However, the technical problems associated with protecting these components are far from solved and there is significant research activity ongoing in the area.

An internal cooling scheme within airfoils directs the cooling gas through small channels prior to exiting the gas through external film cooling holes. Turbulators designed to trip the boundary layer are incorporated into these channels in order to increase the amount of heat that can be removed from the airfoil surface. The concept behind external film cooling is to bleed core flow air from the high-pressure compressor section of an engine and to direct that air through internal ducting to discrete holes in the surface of the blades, vanes, and shroud. The intent is to create a film of cool gas over the surface of the metal airfoil in order to reduce the local heat transfer coefficient. As long as the boundary layer is not blown off the surface by the introduction of this cold-gas film (a process which tends to entrain hot external gas), the metal will be offered some degree of protection from the higher temperatures of the main gas flow. Figure 2 is a sketch of a typical gas turbine blade with both internal cooling channels and external film cooling holes and slots. Figure 3 illustrates a conceptual two-dimensional model of



how the cooling gas exits through a discrete hole to form the protective film along the surface. In principle, this idea works since machines have been operating successfully for years with the turbine inlet temperature in excess of the material melting temperature. The primary intent of the ongoing research activity in this area is to significantly extend the useful operational life of current hot section components and to obtain more efficient cooling systems to allow for higher combustor exit temperatures. Focus of this thesis is placed on the experimentation related to the external film cooling so particulars of internal cooling schemes are not discussed.

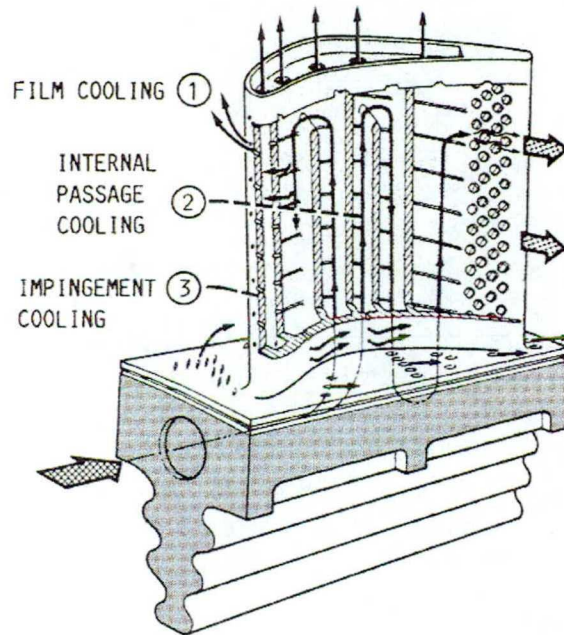


**Figure 2. Typical cooled aircraft gas turbine blade [2]**

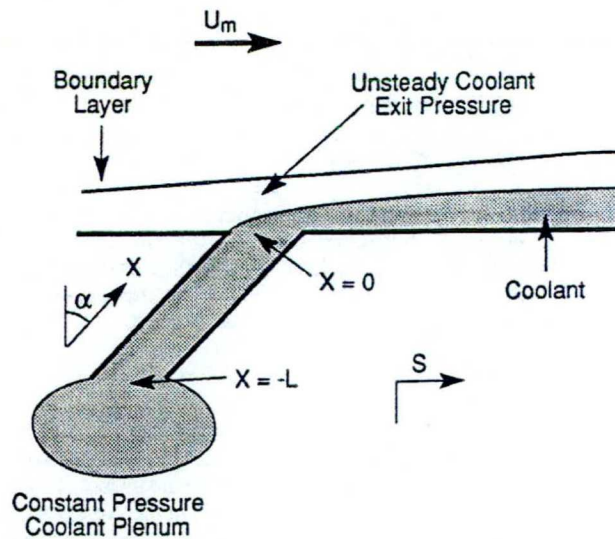


**Figure 3. Two-dimensional coolant slot model with unsteady external pressure field [3]**

### 1.1 Film Cooling Research

Film cooling research facilities can be broken down into three general categories, which reflect the complexities of the experimental apparatus: flat plates, cascades, and rotating rigs. Flat plate experiments are very useful for displaying the general physics and principles of film cooling along with making comparisons between configurations. Investigations of the effects of different cooling-hole geometries are often done in these types of facilities and the results used for various cooling models that are subsequently implemented into CFD codes. However, due to the simplicity of the flat plate it can be difficult to apply the results obtained in this manner directly to engine airfoils. This leads to much of the empiricism in this area of work, where results from flat-plate experiments are extrapolated based on engineering experience and implemented in airfoil designs without any further verification.

Cascade experiments are a step closer to the real world application than flat-plate experiments since these measurements capture the 3-D characteristics of the airfoil, specifically pressure gradient. These cascade experiments are very useful for film-effectiveness model development for the vane. However, several authors Dring *et al.* [4], Abhari and Epstein [3] and Takeshi *et al.* [5] have shown that cascade measurements for a rotating blade do not capture the importance of secondary flow on the pressure surface of the airfoil. To get as close to the real world environment as possible in the laboratory, the industry has an interest in fully-cooled high-pressure rotating turbine film cooling measurements in order to model film effectiveness and to develop the next generation of film cooling modeling for implementation into CFD predictive codes for design purposes. Because of the complexity of experimental rigs capable of performing these measurements and the cost of operation, only a few laboratories have invested in the infrastructure necessary to perform these experiments.

Short-duration facilities have been very successful in the past in obtaining full-stage rotating surface-pressure and heat-transfer measurements for uncooled high-pressure turbines. There have even been some measurements reported for limited cooling gas injection ([3], [4], [5], [6], [7], [8]), but none for a fully cooled stage. Both the experiment and the data interpretation and analysis of this type of an experiment are complex issues. A team of experimentalists and modelers/analysts working closely together will be required to achieve a successful outcome to this endeavor.

## **1.2 Film Cooling at The Ohio State University Gas Turbine Laboratory**

Under support of the NASA/DoD URETI, the OSU GTL has undertaken the task of performing surface-pressure and surface heat-transfer measurements on the vane

surfaces, on the blade surfaces, and on the stationary shroud of a fully cooled high-pressure turbine stage. In addition, the pressures and temperatures internal to the vane and blade coolant gas flows are measured since these parameters are important to the data analysis task. The OSU Turbine Test Facility (TTF) in which these measurements are performed, has been used by the researchers at the OSU GTL for the past twenty-one years, but significant modifications were necessary for this particular measurement program including obtaining a representative film cooled high-pressure turbine stage and designing, constructing, and putting into operation the supporting equipment. One of the necessary pieces of supporting equipment was a cooling gas (or cold gas) supply system. A facility of this type (known as the Large Calibration Facility [LCF]) was initially designed and constructed in 1997 [9] for use in film cooling experiments on the horizon, but it lay dormant until the first fully film cooled rig was operational at OSU in 2004. A significant portion of this thesis deals with the detailed integration of the cold-gas supply system into the film effectiveness measurement program.

### **1.3 Experimental Goals**

Film cooling experiments can be separated into two categories; optimization and code verification. Examples of optimization experiments include; comparing different geometries for the cooling hole, optimizing blowing ratios, and comparing new cooling schemes to existing cooling schemes. These involve changing one parameter of an experiment and are run in facilities capable of accommodating a flat plate configuration or in facilities capable of accommodating a cascade of airfoils due to the ease of making changes to the hardware. Code verification experiments may also be performed using a flat plate or a cascade configuration. One of the current efforts ongoing at the OSU GTL

is concerned with creating a valid data set for a fully cooled high-pressure turbine stage that will be used for CFD code verification. With the successful incorporation of the coolant gas supply, it is now possible to perform full stage rotating film cooling turbine experiments in the short duration TTF. Preliminary results will be presented in this thesis to demonstrate this capability along with some insight into the future of film cooling measurement programs. These data sets, along with others to follow, will be the primary data sets used by several of the engine companies for film cooling modeling and for film effectiveness predictions using selected CFD codes.

#### **1.4 Thesis Goals**

This thesis develops the physical parameters and experimental methods required to create and utilize short-duration fully-cooled rotating rig data. It also bridges the gap from the industry side which tends to focus on empirical design tools, towards the more academic aspects by discussing the key non-dimensional parameters that must be matched from a stage perspective in this environment. The information covered will include the current experimental technology, integration and operation of a coolant gas supply, particulars of conducting an experiment, and interpretation of the measurements. Current experiments are ongoing that will provide aerodynamic and heat transfer data results primarily on the first stage airfoil surfaces (vane and blade) and for the stationary shroud. Future experimental focus will expand to other portions of the stage to include the blade recessed tip and hub regions.

## **CHAPTER 2**

### **DESCRIPTION OF PROBLEM**

For gas turbine efficiencies to continue increasing, the engine designers need improved models and design tools capable of predicting the film effectiveness for the high-pressure stage. These new techniques are currently being created, but upon completion they must be verified by comparison with realistic experiments. The desire is to acquire these verification measurements within an environment for which the flow physics is as close to the engine environment as is possible for a controlled laboratory experiment. To this end, the facilities and the experience at the OSU GTL is a reasonable solution. There are a few other laboratories that could also perform comparable measurement programs as discussed in the following section, Section 2.1.

#### **2.1 Current Technology of Experimental Facilities**

Early turbine computer models were based on the underlying physics of simple experiments done in wind tunnels or blowdown facilities using flat plates or grouped airfoils (cascade) in the test section. Engine designers have used experimental results obtained using flat plates or cascades as the test vehicle to develop film-cooling models since film-cooling studies began in the mid 1940's. Increased computational power of modern computers has allowed incorporation of significantly more flow physics resulting in rather detailed CFD codes that have recently been shown to do a credible job of

predicting pressure and heat transfer distributions for portions of the blade not previously attacked [10], [11]. The current state of the art commercial codes, like Fluent and STAR-CD, use a full 3-D Navier-Stokes solver to predict pressure distributions and heat transfer. The expanded abilities of modern CFD codes have generated an increased need for more accurate and pragmatic experimental data sets that capture as much of the flow physics as is possible.

Historically there have been two separate methods for understanding gas turbine engines: analytical and empirical. Academia focuses on the analytical perspective of the physics in a gas turbine and their experiments tend to lean more toward the scientific side, and almost always involve a test article consisting of a flat plate or cascade. In some cases, the results of this effort are difficult to implement into real engines. The turbine industry follows a more empirical method that relies highly on past design experience with some support from their internal laboratories that may include a wide range of experimental facilities. Because the techniques developed by the engine companies for design purposes are highly proprietary, little data is published by industry in the open literature compared to the multitudes of publications by academia. The background information of this thesis will focus on the information available in the open literature.

### **2.1.1 Facilities Designed for Flat Plate Measurements**

Of the various types of experimental configurations to be discussed in Chapter 2, flat plate, cascade, and full-stage rotating, the facilities used to perform the flat plate measurements are by far the simplest and most economical. A typical flat plate facility for film cooling studies will consist of a wind tunnel or short duration blowdown tank,

flat plate with various cooling hole configuration(s), boundary layer bleed, and a cooling gas supply. Figure 4 is a sketch of the facility at the University of Texas [12].

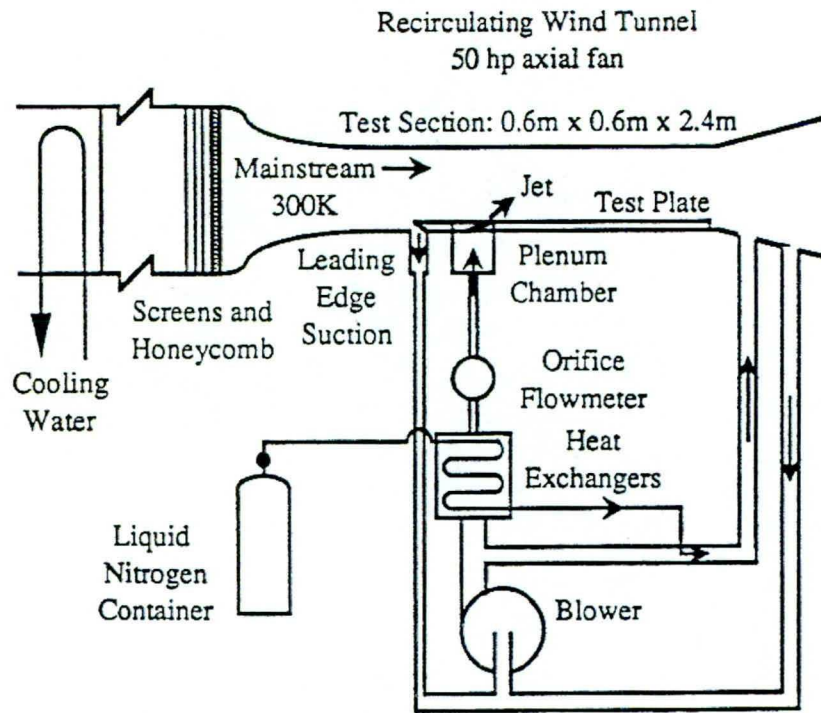


**Figure 4. Film cooling test facility at University of Texas [12]**

Flat plate facilities have some very economical advantages for film cooling experiments. The two biggest advantages are that only a small simple wind tunnel is required and the plate is simple, unlike airfoils with complex cooling hole configurations. Another advantage of the flat plate experiments is the simplicity of the instrumentation due to the quasi-steady flow characteristics. The instrumentation and data acquisition requirements are less stringent in flat plate experiments compared to the requirements of more sophisticated facilities. These facilities are commonly used for investigations dealing with hole geometry configurations as Sen *et al.* [12] has done. Results obtained using these flat plate experiments have proven to be instrumental in verifying very



detailed CFD models describing the flow physics of individual cooling holes in cross flow. Some of the researchers involved in this area and reference to their work are Leylek and Zerkle [13], Bernsdorf *et al.* [14], Burdet [15], and Montomoli *et al.* [16]

Along with the flat plate experiments are partial air foil curvatures configuration studies similar to Albert *et al.* [17] study of the leading edge model and Berhe and Patankar [18] with a curved-plate model. In Albert's *et al.* [17] experiment, instead of using traditional instrumentation like thermocouples and RTD's they used an IR camera to measure the surface temperature so that the film effectiveness on a leading edge model could be calculated. For this experiment the uncertainty in the temperature measurements were  $\pm 4.7^\circ\text{C}$ . This is typical of optical measurement techniques, which tend to show more quantitative results with contour plots but lack the accuracy of traditional measurement devices. The setup and model used in the experiment are shown below in Figure 5 (a) and (b).

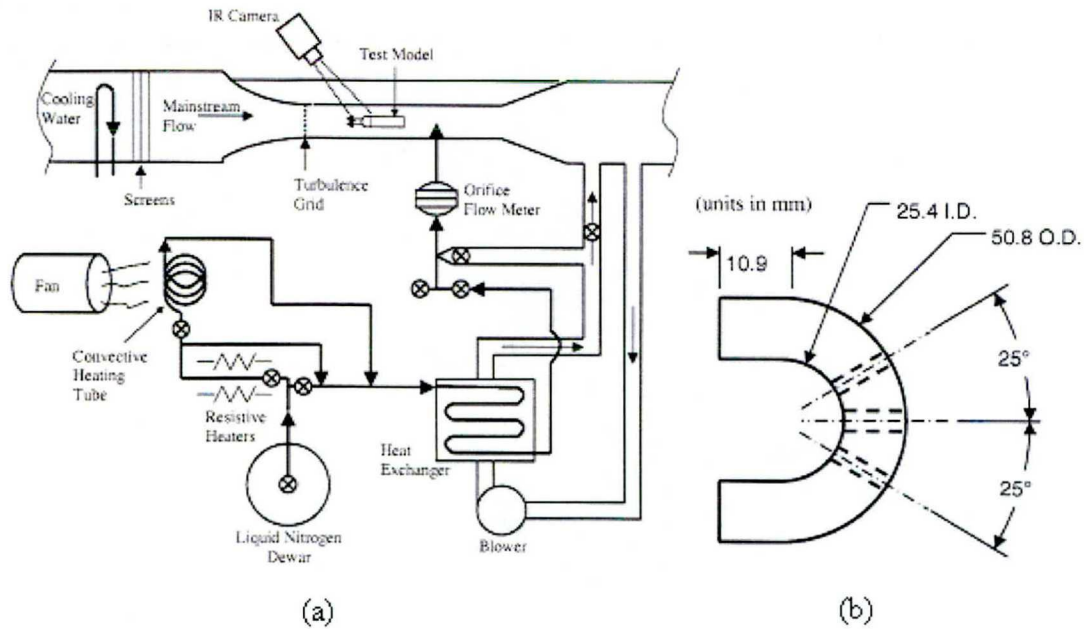


**Figure 5. (a) Schematic of wind tunnel facility at University of Texas, (b) Side view of leading edge model [17]**

### 2.1.2 Cascade Facilities

The facilities in which the flat plate experiments and the cascade experiments are performed are in many ways similar, but the geometry of the test article as it influences pressure gradient and the velocity vectors of the flow is significant. These variations can make a significant difference in the results depending upon the experimental goals.

Figure 6 shows a schematic of the test section and blowdown facility at Texas A&M.

Comparison of Figure 5 and Figure 6 suggests that an obvious difference between a flat plate facility and a cascade facility is the way in which the exit flow is turned. Cascade experiments are very popular because they are the closest representation to an engine configuration without introducing the complexity and expense of rotation.

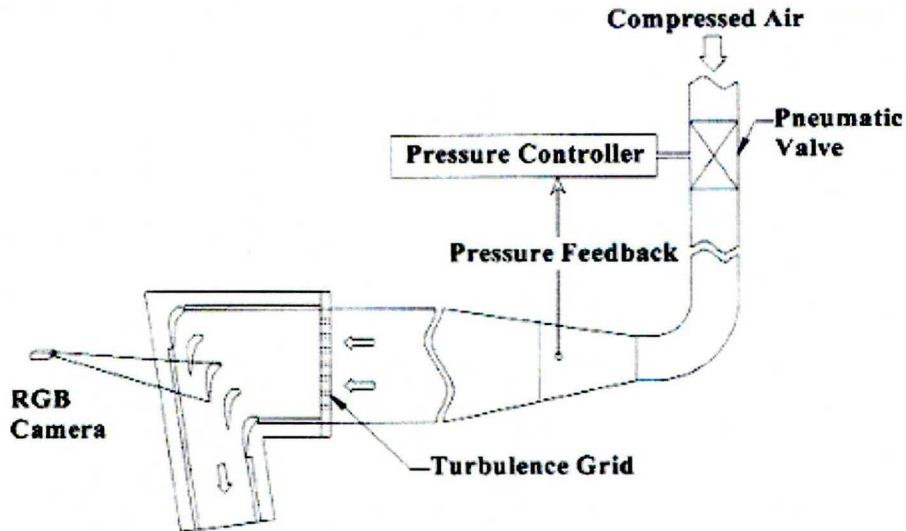


**Figure 6. Schematic of blowdown facility at Texas A&M University [19]**

A wide variety of experiments have been conducted using cascades and these measurements have proven to be very useful to engine designers. Over the past 60 years, literally thousands of different measurement programs have been performed for different vane and blade configurations using either uncooled or cooled geometries. The main parameters set by the investigator are the inlet Reynolds number and temperature ratios between the main flow and the coolant flow (in the case of cooled experiments) and/or the wall. When using a blade as the test article, the blade is fixed with a rotated orientation in order to obtain the proper incidence angle. When investigating problems related to blades, some researchers have used an upstream row of rotating bars to simulate vane wakes and shocks [20], [21], [22], [23], [24]. It is much more difficult to simulate the relative motion at the blade/outer air seal interface, but some authors have used a moving wall [25]. When using a vane as the test article, the missing piece of the flow physics is the multiple reflection of the wave system (which will be shock and

expansion waves in the case of a transonic turbine) from the downstream blades, but this effect is most important on the suction side of the vane and can sometimes be rather significant.

From this point on, the discussion will be confined to airfoils with film cooling and the immediate discussion will deal with the blade of the high-pressure turbine. For discussion purposes the airfoil will be divided into five separate parts: pressure surface, suction surface (not seen in figure), tip, leading edge, and platform (hub) as labeled in Figure 7 on a sketch of a GE CF6 high-pressure turbine blade.

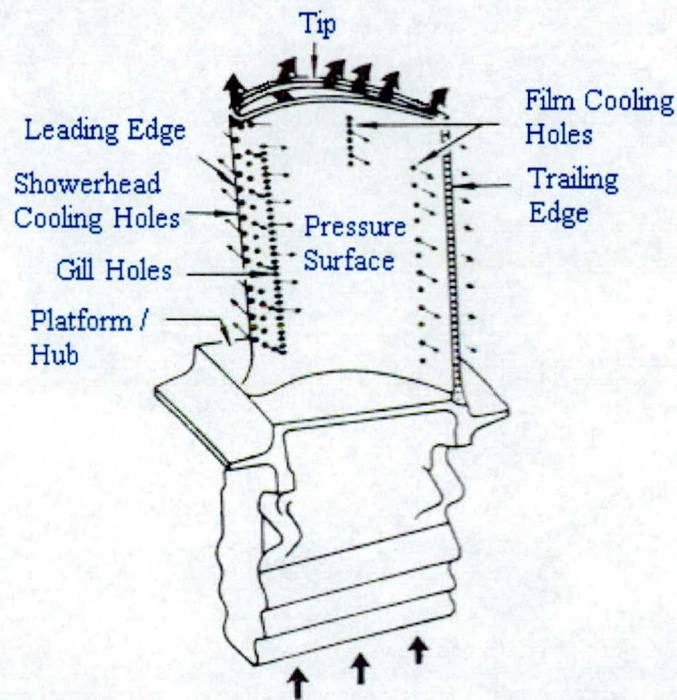


**Figure 7. The Stage-1 High-Pressure Turbine Blade for the GE CF6 [26]**

### ***2.1.2.1 Pressure and Suction Surfaces***

Limited data exists on the pressure and suction surfaces for rotating blades that have the same geometry as cascade data. Dring *et al.* [4], Takeishi *et al.* [5], and Abhari and Epstein [3] were the first to compare film cooled blade data taken in a rotating environment to film cooled blade data taken in a cascade facility. It is important to make note that the rigs operated by Dring and by Takeishi were not run at design corrected conditions corresponding to a high-pressure turbine, but that the facility operated by Abhari and Epstein was operated at the proper design corrected conditions. All three of the comparisons show little difference between the rotating and cascade data for the suction surface as demonstrated by results from the three measurement programs, which are shown in Figure 8, Figure 9, and Figure 10. Figure 8 illustrates that on the pressure surface of the blade, the film effectiveness is dramatically less than that of the cascade data. This decrease in effectiveness is felt to be a direct result of the influence of the blade secondary flow on the coolant flow. Takeishi *et al.* [5] also mentions this phenomenon in his discussion, but due to difficulties with the experiment he had insufficient data to publish a conclusive result. For the results presented in Figure 9, the gauge locations on the rotating blade were at constant span between cooling holes so the red rotating data should be compared to the blue cascade data. Takeishi *et al.* [5] noted the clear 30% drop in effectiveness at a non-dimensional distance of  $x/d=60$  near the trailing edge on the suction surface in Figure 9. Conclusions drawn from the Abhari and Epstein experiment included reduced heat transfer on the suction surface of the rotor compared to the cascade and the time-resolved data revealed that the cooling both reduced the time-averaged level of heat transfer and changed the shape of the unsteady

wave form. The unsteady driver for film cooling on the pressure surface has been shown to be caused by the vane/blade interactions [3].

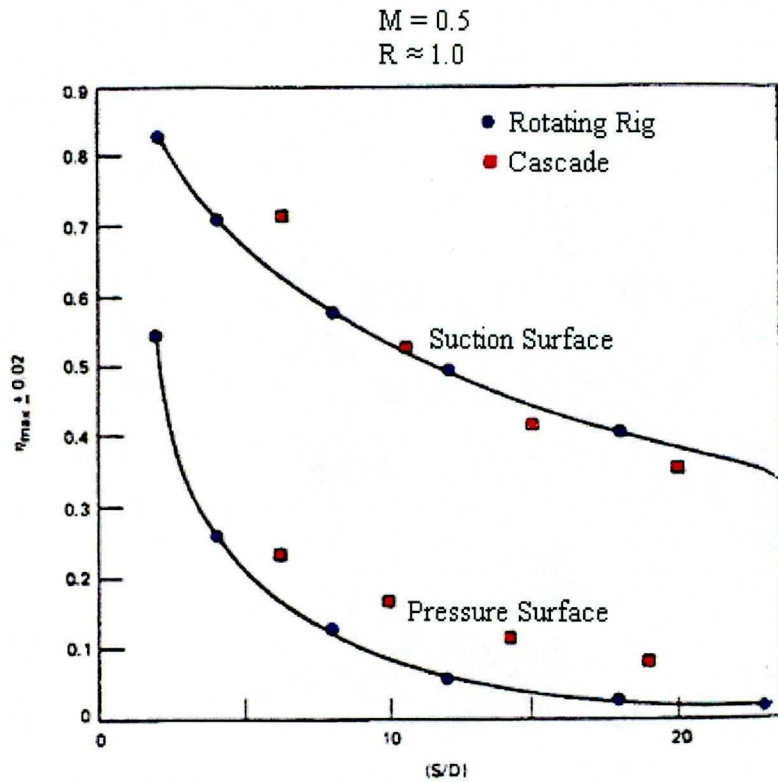


Figure 8. Decay of maximum effectiveness (experiment by Dring *et al.* [4])

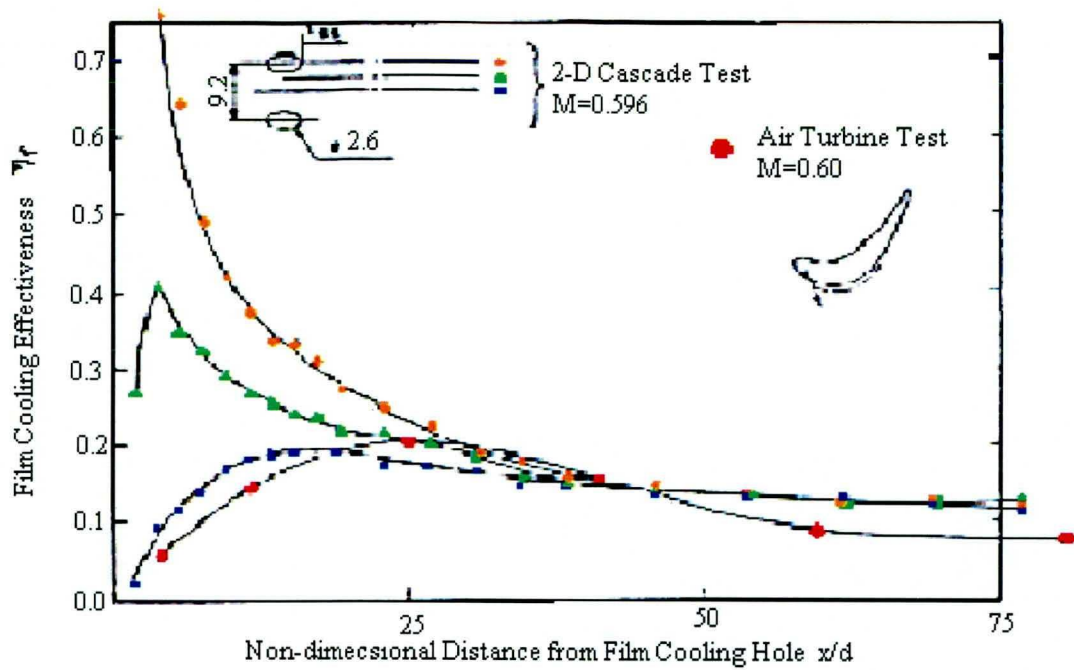


Figure 9. Film Cooling Effectiveness on Suction Surface Takeishi *et al.* [5]

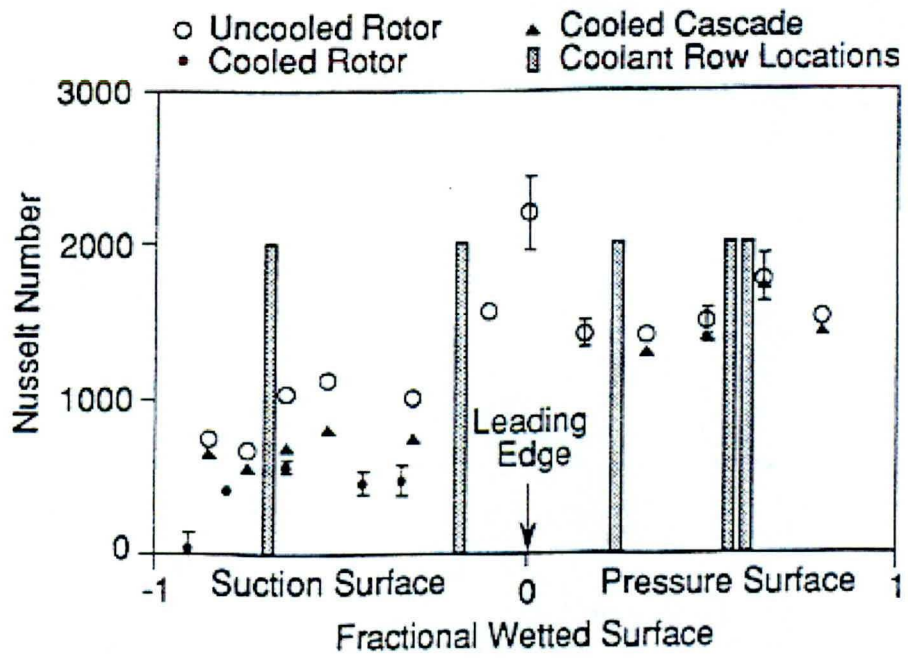
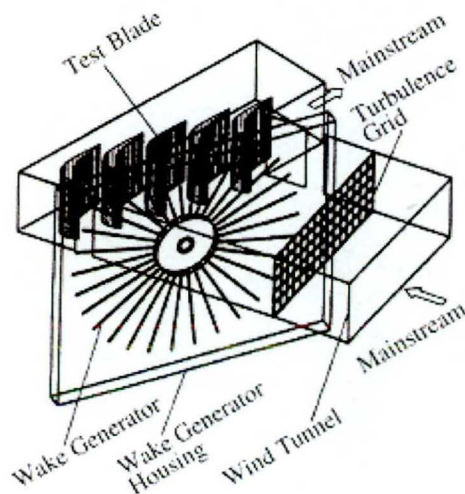


Figure 10. Uncooled and Film Cooled Rotating Stage Measurements Compared with those from a Cooled Linear Cascade Abhari and Epstein [3]

One method attempted by cascade experimentalists to create the vane/blade shock interaction is with the use of rotating bars. By rotating a wheel with multiple rods, (approximately 0.125-in diameter) pressure wakes generated by the rods can be seen on the blade. The concept is shown in Figure 11 and Figure 12 with results of an Oxford cascade experiment with rotating bars compared to an MIT rotor in Figure 13 and Figure 14. From the results, the phase and magnitude of the pressure disturbance produced by the rotating bars is inconsistent with that produced from the vane/blade interaction in the rotating experiment.



**Figure 11. Rotating Bar Wake Generator [22]**



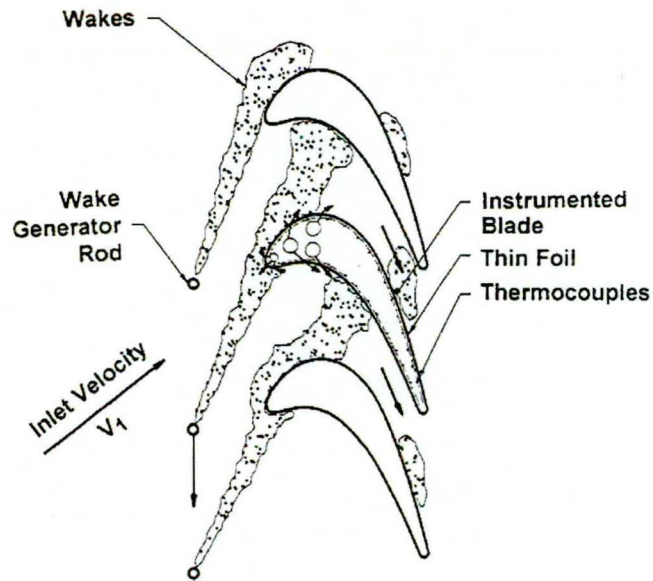


Figure 12. Conceptual view of unsteady wake effect on a model blade with film holes [24]

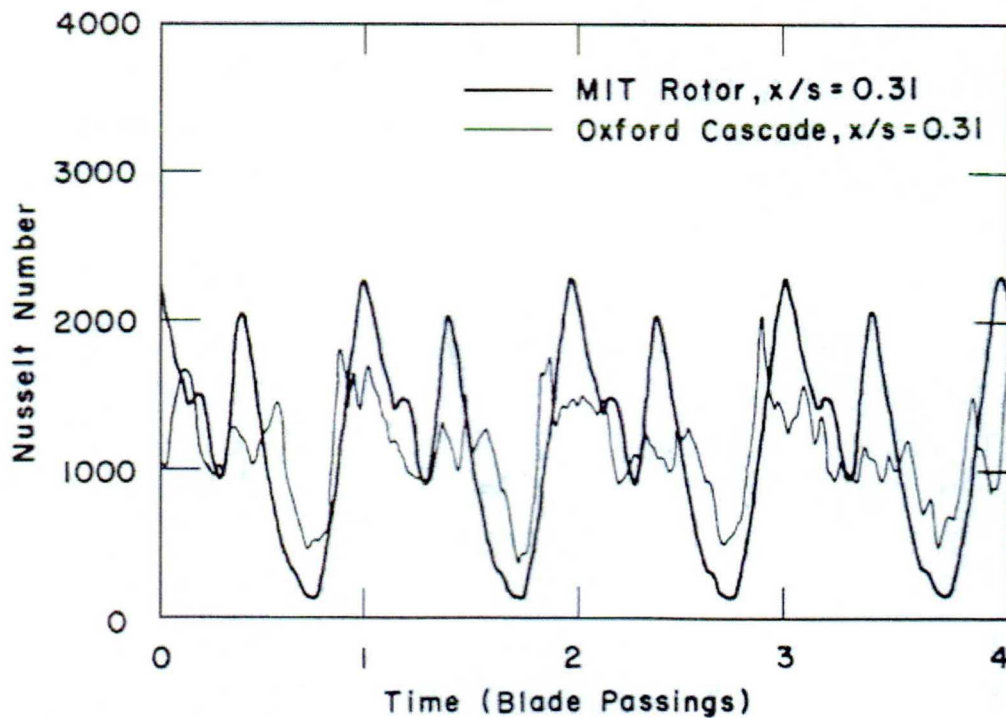
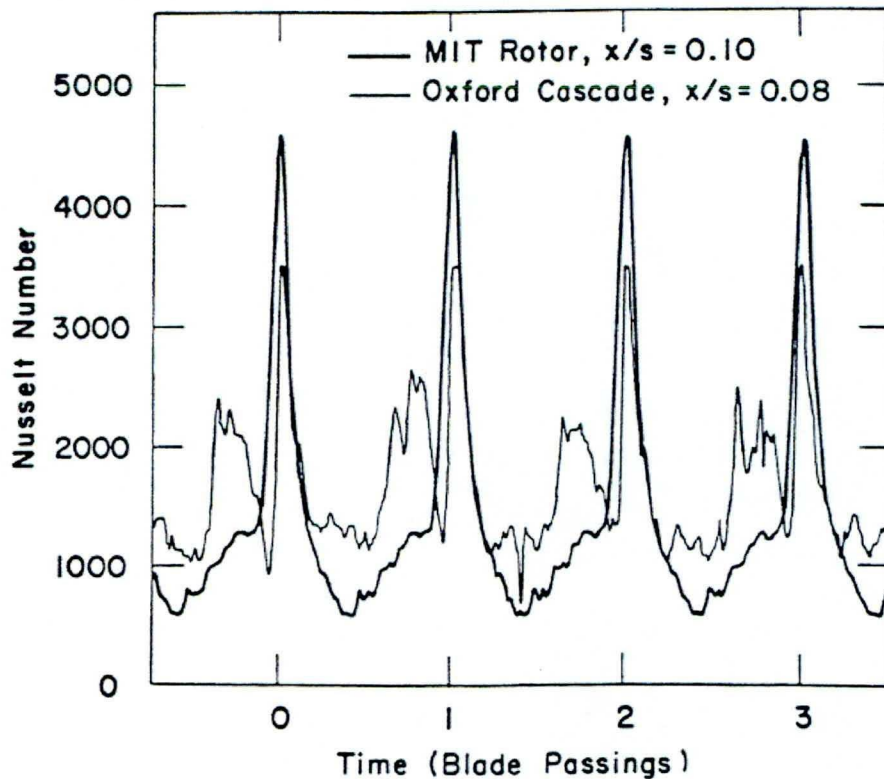


Figure 13. Comparison at  $x/s = 0.31$  on suction surface of MIT rotor and 2-D bar passing cascade test at 4% free-stream turbulence [27]



**Figure 14. Comparison on suction surface of MIT rotor ( $x/s = 0.08$  to  $0.12$ ) with that from 2-D bar passing cascade test ( $x/s = 0.08$ ) at 4% free-stream turbulence [27]**

### ***2.1.2.2 Tip Region***

Blade tip cooling receives a significant amount of attention within the gas turbine community because of the high heat transfer levels in this location and because of the desire to continually reduce the tip/shroud clearance in order to improve aero performance, which merely aggravates the heat transfer situation. The flow environment in the tip region is responsible for a significant percentage of blade failures. Insufficient cooling at the tip leads to increased thermal stresses and when combined with the potential for an occasional tip/shroud rub sequence, causes a portion of the blade to

eventually liberate. Blade tip loss increases the gap between the tip and the stationary shroud, resulting in a direct loss of power and efficiency of the turbine [28].

Many different experimental configurations and facilities have been and are being used for tip region investigations. These studies frequently involve varying the blowing ratios, the tip gap, the tip geometries (as shown in Figure 15), and different film cooling schemes like cooling the tip with injection of the film coolant from the pressure surface as investigated by Kwak *et al.* [29] in Figure 16. While many of the tips will be compared to a plane tip geometry the global goal is to adequately cool the squealer tip geometry. The squealer tip is greatly preferred because in the case of an unfortunate tip rub significantly less damage is done to the blade if the tip is recessed as opposed to being flat. However, in the process of selecting the proper recessed tip configuration, it is important to understand the accompanying flow physics. Figure 17 contains a schematic of potential air patterns in the recessed (squealer) tip cavity predicted by Kwak and Han [30] based upon their experimental results.

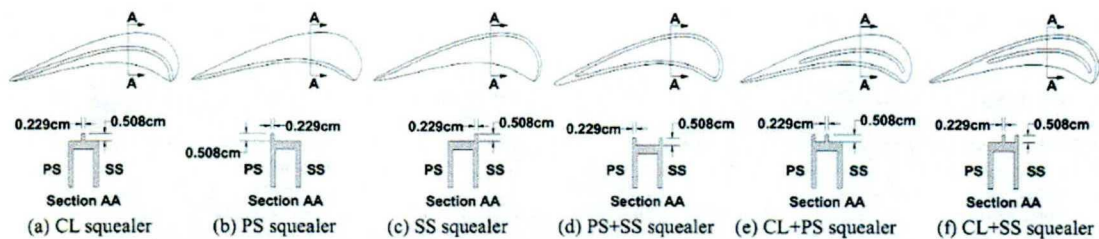
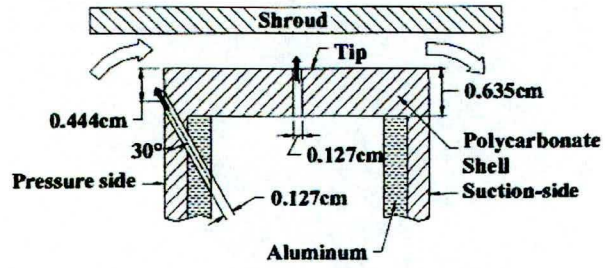
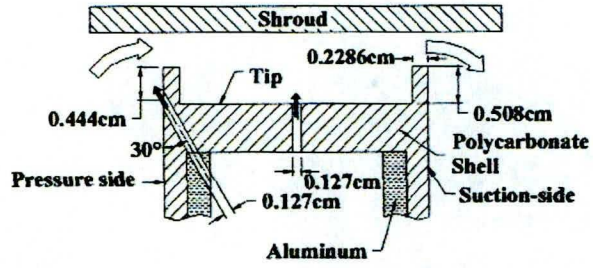


**Figure 15. Different geometries of squealer tips [29]**



(a) Plane Tip



(b) Squealer Tip

Figure 16. Geometry of film cooling holes [30]

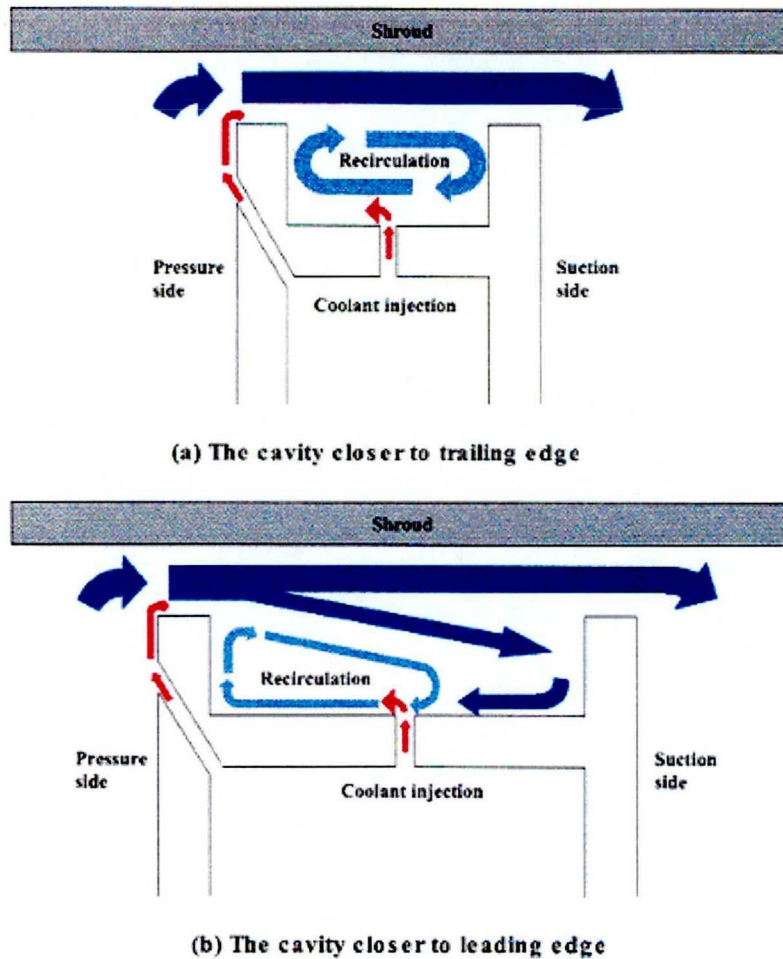


**Figure 17. Conceptual view of flow in tip cavity [30]**

Researchers using cascade facilities to perform blade tip investigations, whether cooled or uncooled, emphasize that the pressure difference from the pressure to the suction surface drives the physics of the tip flow. Yaras and Sjolander [25] used a cascade setup and added a moving outer belt to simulate the influence of rotation on the tip gap. The results of this study indicated that relative motion has a significant effect on the tip leakage vortex and passage vortex structures [31]. Molter *et al.* [11] modeled the tip region for an uncooled rotating blade which demonstrates the complexities involved in

the flow field that affect heat transfer. The flow field predicted by Molter over a recessed tip is shown in Figure 18.

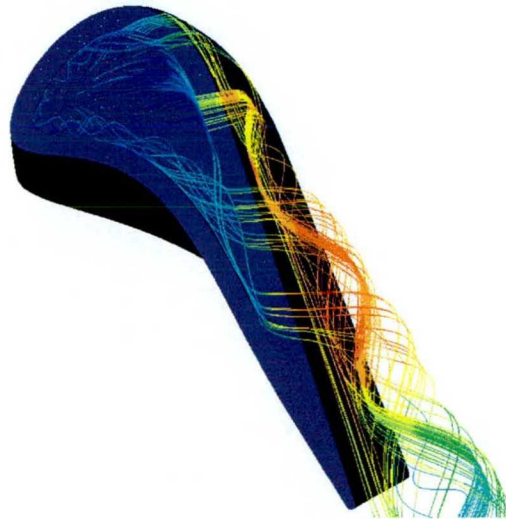


**Figure 18. Uncooled rotating recess tip flow field [11]**

### ***2.1.2.3 Leading Edge Region***

The leading edge of the vane is subjected to the relatively high turbulence generated by the combustor and the leading edge of the blade is subjected to what is left of this combustor turbulence, to the injected cooling gas (especially from the vane trailing edge slots), and to the wakes and shock wave reflections from the trailing edge of the vane which presents a very unsteady flow field environment to the blade. Since the turbulence at the leading edge of the vane is very difficult to measure in an operating gas turbine, experimentalists have run multiple experiments varying the turbulence levels to measure the effect of turbulence on film cooling. To simulate the unsteadiness at the leading edge of the blade cascade experimentalists have come up with a couple of creative solutions. Either using rotating bars as discussed in Section 2.1.2.1 or with a separate shock generator to simulate the pressure wakes and shocks associated with the

upstream vane and blade rows impinging on the leading edge of a downstream airfoil [32]. The experimental setup for using a shock generator is shown in Figure 19 along with the cascade facility at Virginia Polytechnic Institute and State University in Figure 20.

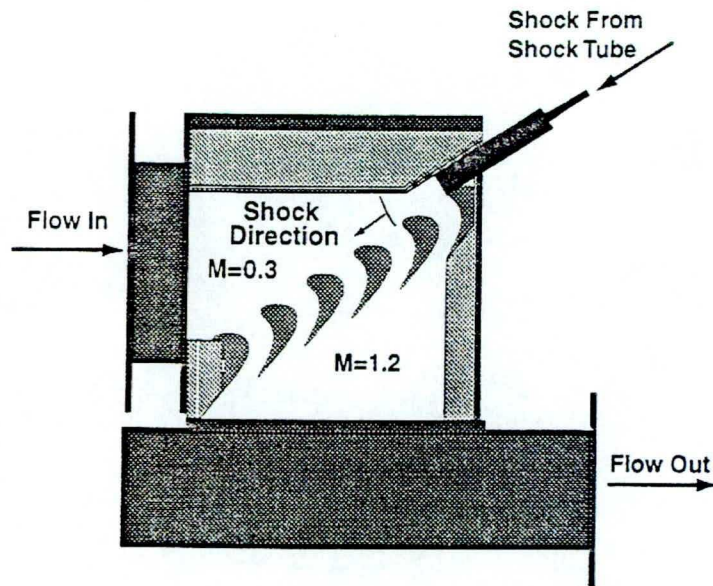


**Figure 19. Cascade and shock apparatus at Virginia Tech [32]**

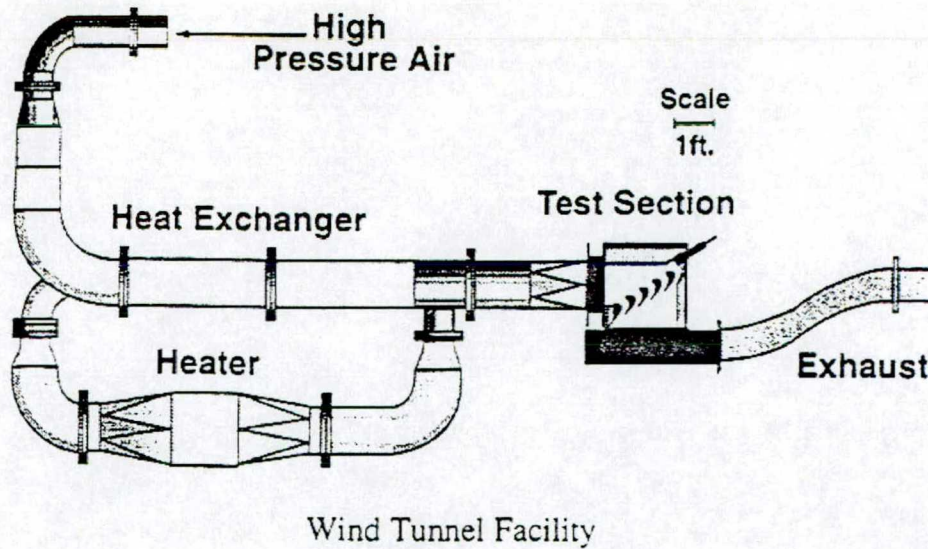


**Figure 20. Wind tunnel facility at Virginia Tech [32]**

Both the spinning rod method and the shock generation technique have produced unsteadiness in the air flow to the leading edge of the airfoil. But it has yet to be demonstrated that either method can produce an unsteady effect consistent with that experienced in an engine.

### **2.1.3 Rotating Facilities**

As compared to the multitude of cascade facilities in operation, only a few rotating facilities exist. This is primarily due to the complexity of the rigs, cost to build and operate each rig, and the amount of time involved from initial design to completion of the experiment. However, these facilities are capable of producing results for an environment representative of the flow physics associated with an engine including the vane blade interaction, tip and shroud interaction, and the centrifugal and Coriolis effects on the secondary (coolant) flow.



In 1980, Dring *et al.* [4] conducted the first set of film cooled turbine experiments at the United Technologies Research Center (UTRC). Some of the key features of the setup were that the airfoils were approximately five times engine size, the speed was 405 RPM, and the study focused on the cooling flow from a single hole. As mentioned in 2.1.2.1, the results were compared to cascade data and are presented in Figure 8. The findings proved to be very valuable for understanding the centrifugal and Coriolis effects on the secondary flow.

Until now, the most comprehensive film cooling experiment and analysis conducted at engine corrected conditions was completed by Abhari and Epstein [3] at the Massachusetts Institute of Technology (MIT). The parameters of the experiment are compared to a full-scale turbine in Table 1. Some of the key features of this facility and experiment are that it included cooling gas from the trailing edge of the vane, but not from individual holes on the vane; utilized new double sided heat flux gauges as developed by Epstein *et al.* [33], and generated high frequency response heat transfer data, shown in Figure 21. The geometry of the blades is the same as the cascade experiment conducted by Rigby *et al.* [34] at Oxford University which allowed for the comparison to the rotating bars in a cascade facility in Figure 13 and Figure 14.

<b>MIT BLOWDOWN TURBINE SCALING</b>		
	<b>Full Scale</b>	<b>MIT Blowdown</b>
Fluid	Air	Ar-Fr 12
Ratio specific heats	1.28	1.28
Mean metal temperature	1118°K (1550°F)	295°K (72°F)
Metal/gas temp. ratio	0.63	0.63
Inlet total temperature	1780°K (2750°F)	478° (400°F)
True NGV chord	8.0 cm	5.9 cm
Reynolds number*	$2.7 \times 10^6$	$2.7 \times 10^6$
Inlet pressure, atm	19.6	4.3
Outlet pressure, atm	4.5	1.0
Outlet total temperature	1280°K (1844°F)	343°K (160°F)
Prandtl number	0.752	0.755
Eckert number**	1.0	1.0
Rotor speed, rpm	12,734	6,190
Mass flow, kg/sec	49.0	16.6
Power, watts	24,880,000	1,078,000
Test time	Continuous	0.3 sec

\* Based on NGV chord and isentropic exit conditions

\*\*  $(\gamma-1)M^2T/\Delta T$

**Table 1. MIT blowdown experiment scaling parameters [3]**

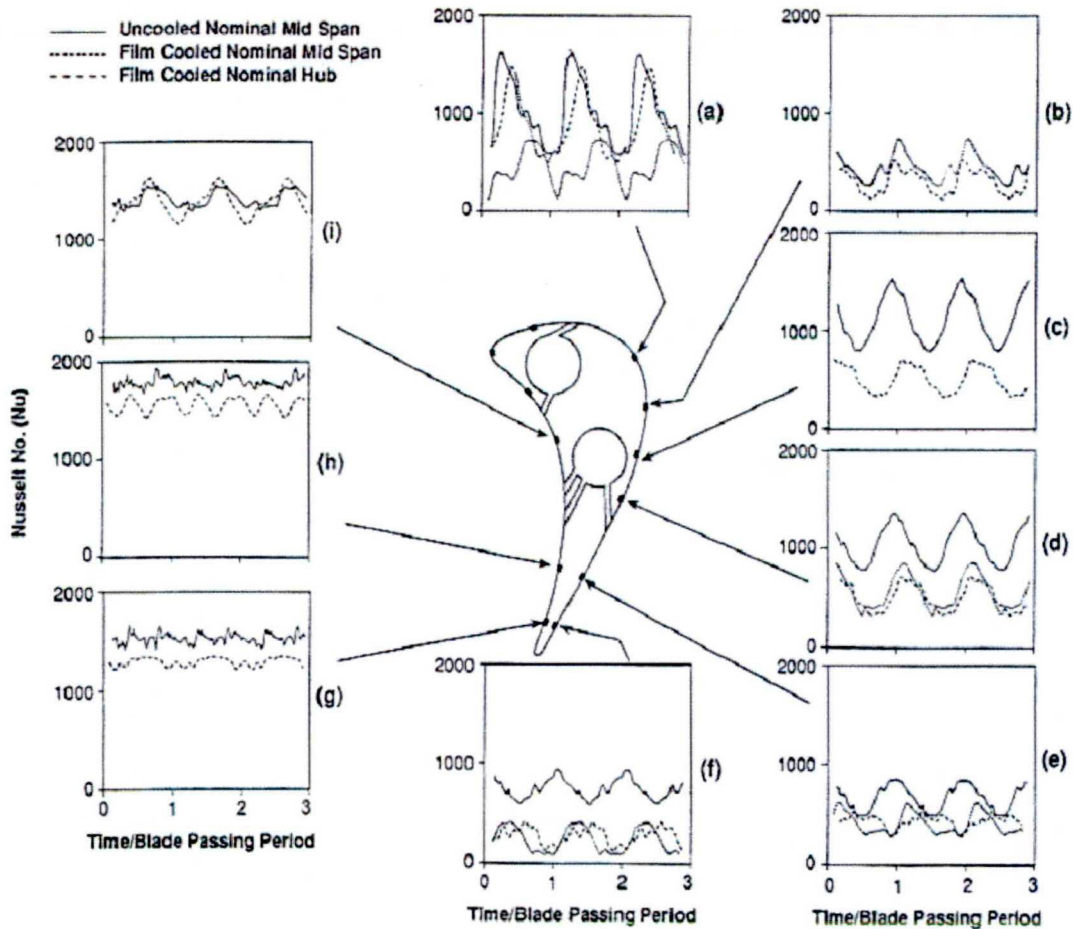


**Figure 21. MIT Time-resolved rotor heat transfer measurements [3]**

Takeishi *et al.* [5] at the Takasago Research & Development Center were the next to conduct a film cooled rotating experiment. Similar to Dring, this experiment was done in conjunction with a 2-D cascade experiment for comparison as mentioned in 2.1.2.1. The facility is a wind tunnel with a water brake attached to the rotor for setting the proper speed (up to 6260 rpm) and pressure ratio across the stage. The cross section of the test rig in Figure 22 shows the complexity involved with rotating experiments. As opposed to the traditional measurement techniques, Takeishi used suction taps to pull a small amount of gas from the boundary layer and analyzed the concentration for the CO<sub>2</sub> gas that was

used as a tracer. From the measurement technique used the experiment was limited to time-averaged data and could not attain the time-resolved data as did Abhari and Epstein. The Scanivalve used to collect the gas from the rotor is limited by channel count as well as to the fact that it can only take one sample for each suction tap, resulting in the inability to measure the unsteadiness of the core flow.

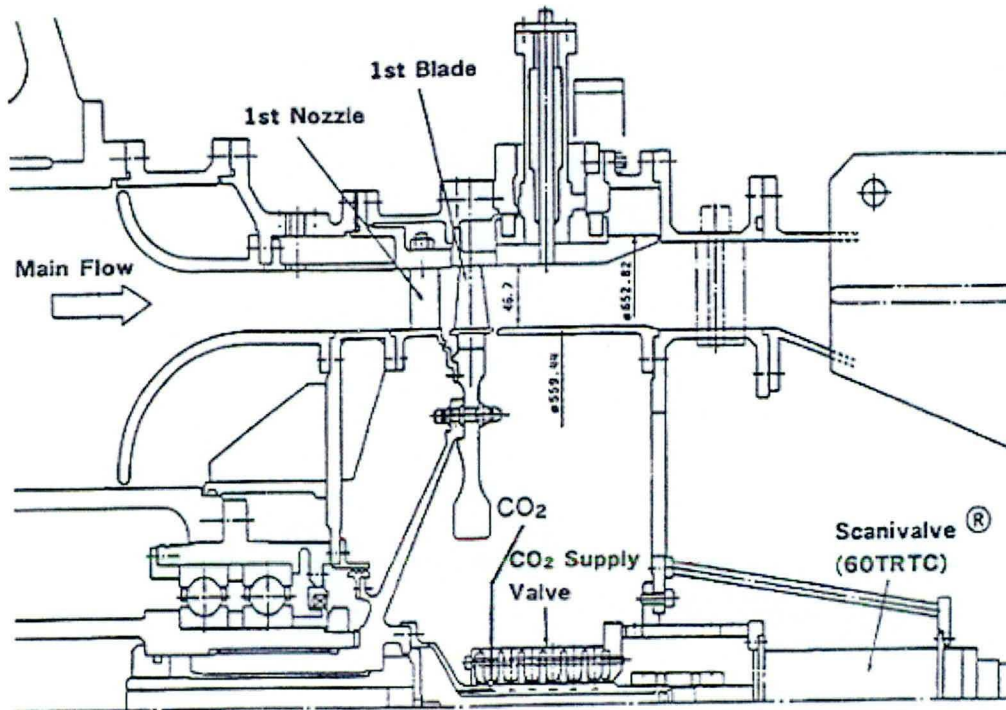


**Figure 22. Cross section of the rotating test equipment Takeishi *et al.* [5]**

Von Karman Institute (VKI) has multiple facilities for cascade and rotating turbine research, but only the isentropic compression tube annular cascade facility (CT-3) has the capability of accommodating film cooling experiments. A diagram of this facility can be seen in Figure 23. To date the only cooling experiments performed using this facility were partially cooled and have included a vane trailing edge discharge with hub

cavity flow, [7], [8]. The facility currently has two key limitations with a top rotor speed of 6500 rpm and only 16 rotating channels of data acquisition from the rotor that are limited in frequency response to 78 kHz.

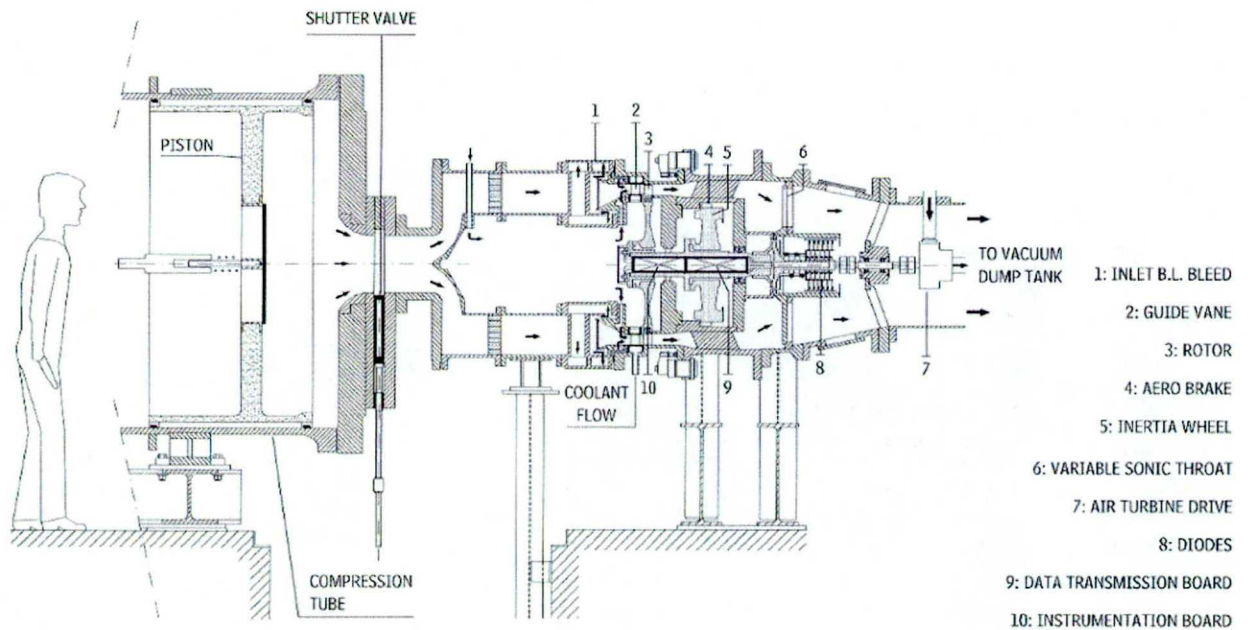
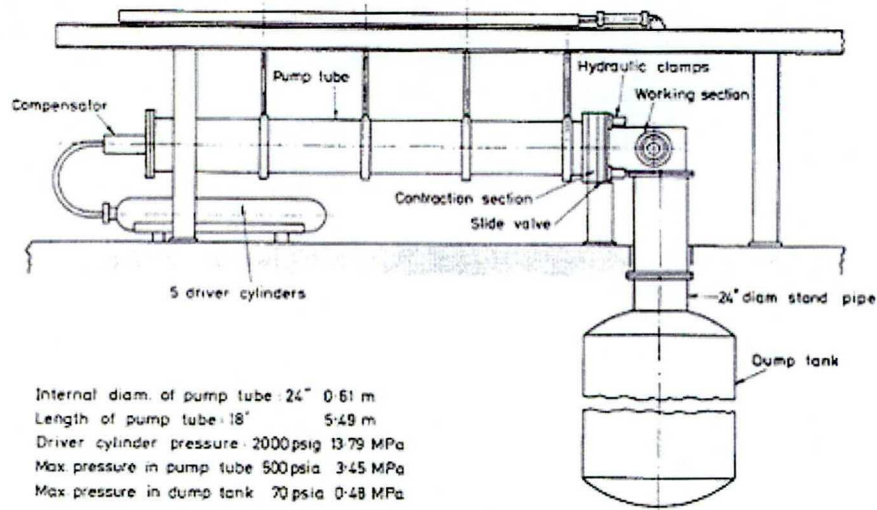
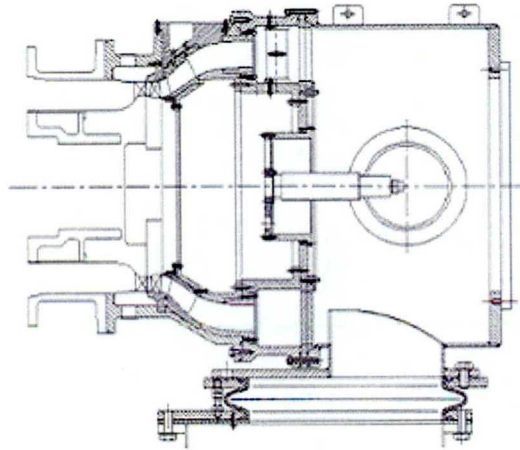


**Figure 23. Isentropic compression tube annular cascade facility at VKI**

Another Isentropic Light Piston Facility (ILPF Figure 24) is in operation at QinetiQ with the University of Oxford. This facility can easily reach speeds of 9500 rpm and has 150 total data channels. Currently, incorporation of film cooling into the experiments has not been published for this facility.



(a)



(b)

**Figure 24. (a) Isentropic light piston facility at QinetiQ [35], (b) Current working section [36]**

The most newly operational rotating facility is located at the Wright Patterson Air Force Base in Dayton Ohio. The TRF (Turbine Research Facility shown in Figure 25) was designed and built to be the all-encompassing facility for film cooling high-pressure gas turbine experiments and features high-speed capabilities with an eddy brake and boundary layer bleeds. The researchers at Wright Patterson have recently (2004)

conducted their first experiment which involved studying details of the unsteadiness caused from the vane blade interactions.

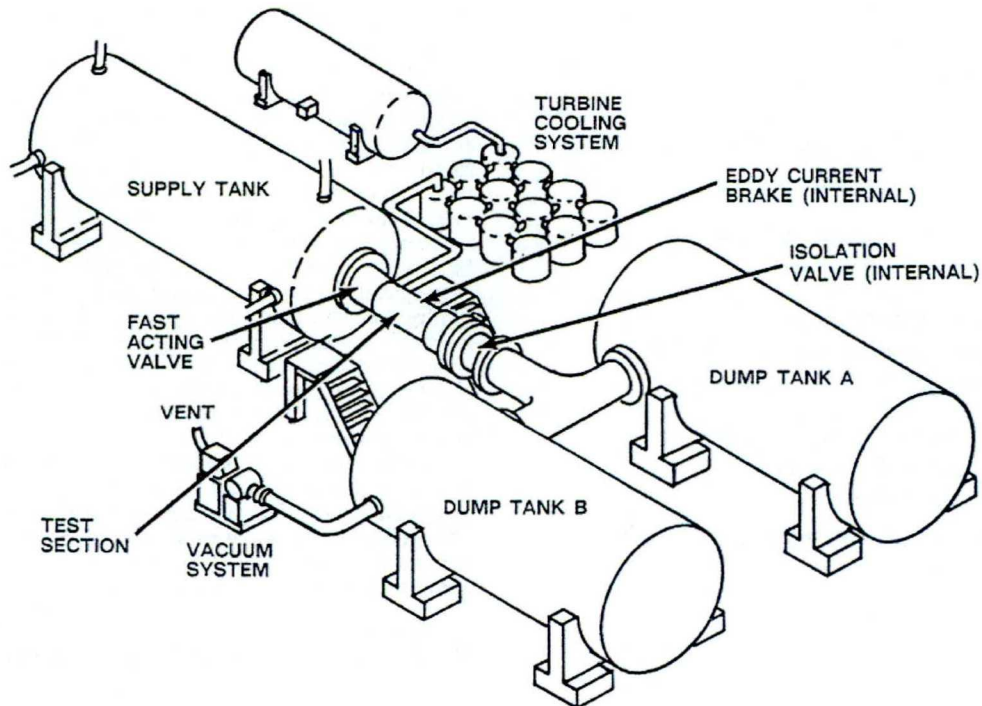


**Figure 25. Sketch of advanced turbine aerothermal research rig (TRF) configuration [37]**

The shock tube facility (TTF for turbine test facility) at The Ohio State University is extremely unique compared to the other rotating facilities because the design was derived from other shock tunnels used for hypersonic research. The TTF was design and built at the Calspan Corporation (Buffalo, NY) in 1983 then moved to OSU with the creation of the OSU GTL in 1995. The facility consists of a shock tube that is 18.5-in diameter and 100' long with a FAV connecting to a Mach 6 nozzle and a 33' long by 9-ft. diameter dump tank, which contains the test rig. Dunn *et al.* [38] provides a detailed description of the facility which is shown in Figure 26. When the shock tube was used to heat the gas that would eventually pass through the turbine stage, researchers would send

a shock wave down the tube to heat the supply gas in reflected-shock mode, and then open a FAV to allow the shock processed gas to pass into the dump tank, and subsequently close the FAV approximately 100 milliseconds later. Operation in this mode allowed approximately 36 milliseconds of time over which data could be acquired. The key features of the TTF are the high speed capabilities, large number of high frequency data acquisition channels with a total of 640 channels with up to 300 rotating channels (assuming two slip rings per channel), and the ability to adapt each set of experimental goals with a new rig for each rotor.



**Figure 26. Shock tube facility (TTF) at the OSU GTL**

## **2.2 Film Cooling at the OSU GTL**

Conducting film cooling experiments at the OSU GTL requires three major changes in facility operation: use of the TTF in blowdown mode rather than in shock



mode, construction of an electrical convective heater, and incorporation of the LCF to supply the film cooling gas. Operation of the TTF in blowdown mode allows for potentially longer test times compared to the 36 milliseconds supplied by operating in shock mode. However, it should be noted that the flow establishment process is a bit slower when operating in blowdown mode compared to shock mode. Also, by eliminating the uncertainty associated with rupture of the two diaphragms used when operating in shock mode, the initiation of the core flow gas is controlled with precise timing by the FAV. The use of the convection heater has added the option of introducing hot streaks to more accurately simulate real combustors. Details of the design, construction, and controls of the convective heater can be found in [39]. The heater can be seen in a sketch of the current facility layout shown in Figure 27 and a cross-section of the experimental rig in Figure 28. The process involved in incorporating the LCF with the TTF is described in detail in Chapter 4.

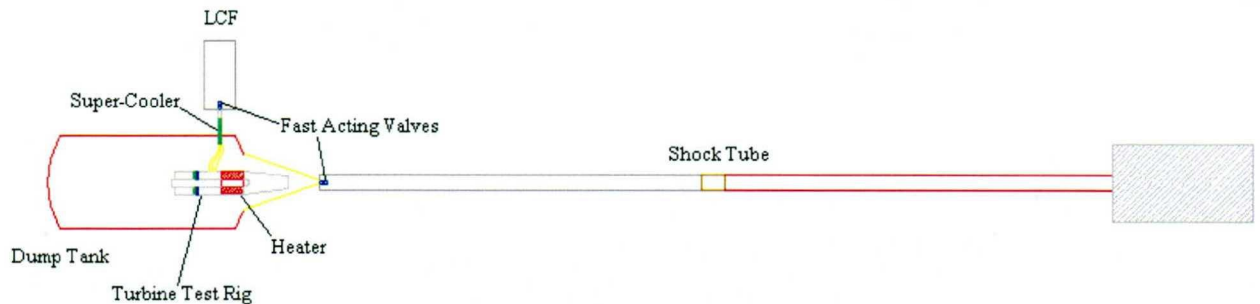


**Figure 27. Sketch of current OSU GTL Layout**

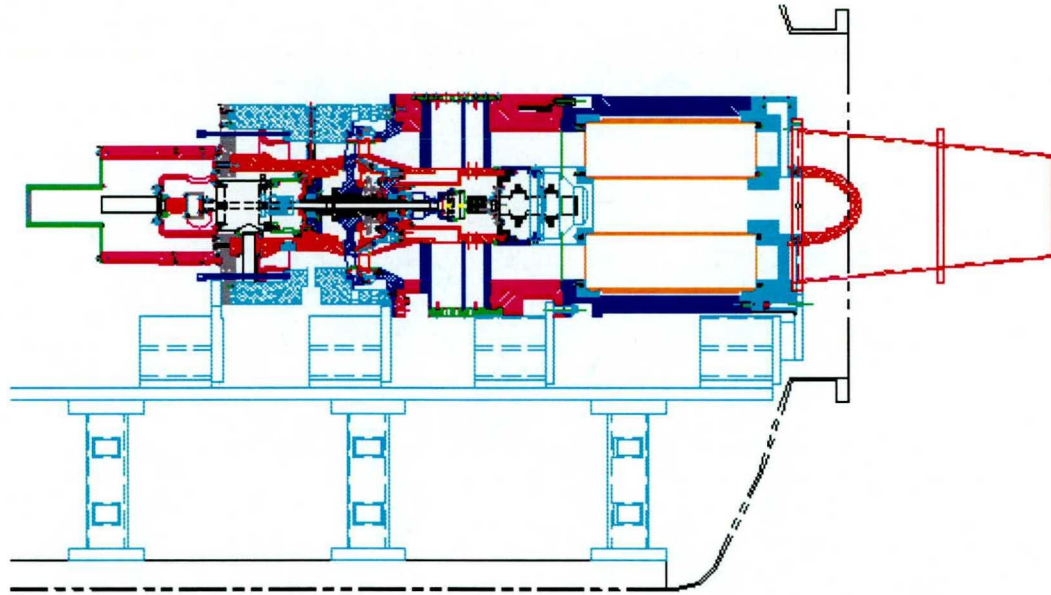


**Figure 28. Test rig mounted in dump tank**

## CHAPTER 3

### PARAMETERS IMPORTANT FOR FILM COOLING EXPERIMENTS

One of the primary reasons for performing the measurement program described herein is to assist in the development of CFD codes that will be used to provide advanced thermal protection designs for machines of the future. For the industry to have confidence in the capability of these CFD codes, reasonable comparisons between prediction and measurement must be demonstrated for cases that closely represent the flow physics associated with a gas turbine engine. To this end, properly run experiments can produce non-dimensional results that can be incorporated into the CFD codes in order to explain the flow physics representative of an engine by operating at design corrected conditions with as many other relevant parameters as possible duplicated. In order for this comparison to be meaningful to the turbine designer, the measurement program must duplicate several of the key non-dimensional parameters noted below. The primary

parameters typically matched are flow function ( $\frac{\dot{m} \sqrt{T_o/T_{ref}}}{P_o/P_{ref}}$ ), pressure ratio across the

turbine stage, important temperature ratios, Reynolds number ( $\frac{VL}{\nu}$ ), blowing ratio

( $\frac{\rho_c V_c}{\rho_\infty V_\infty}$ ) in the case of film cooled measurements, and corrected speed ( $\frac{N_{phy}}{\sqrt{T_o/T_{ref}}}$ ).

Other parameters that may be duplicated include Prandtl numbers, specific heat ratio ( $\gamma$ ),

Mach number, and density ratio of coolant gas to the main flow ( $\frac{\rho_c}{\rho_\infty}$ ). The parameters duplicated will depend upon the experimental goals and the facility's capabilities.

### 3.1 Key Film Cooling Results

Cooled high-pressure turbine experimental goals focus primarily upon the film effectiveness results along with the heat-transfer and surface pressure measurements.

Whether film effectiveness is presented in terms of NHFR (Net Heat Flux

Reduction,  $1 - \frac{q''_F}{q''_0}$ ), SNR (Stanton Number Reduction,  $1 - \frac{St_F}{St_0}$ ), or adiabatic

effectiveness ( $\eta_{aw} = \frac{T_{aw} - T_\infty}{T_c - T_\infty}$ ) the two key parameters from the cooling perspective are

the coolant temperature and the blowing ratio. Both of these parameters are controlled by the coolant gas supply which makes the functionality of the LCF critical for conducting film cooling experiments.

#### 3.1.1 Blowing Ratio

The blowing ratio parameter is a non-dimensional parameter designed to characterize the coolant flow, which also serves as an indicator of the likelihood of the coolant flow penetrating the boundary layer and entraining hot freestream gas that could potentially result in a significant increase in the local heat transferred to the airfoil surface. Film cooling effectiveness is therefore closely linked to the blowing ratio, which leads to the importance of the parameter. Film cooling effectiveness results are often presented as a function of the blowing ratio as can be seen from Figure 29. Note Figure

29 presents the results as  $\frac{St_F}{St_0}$  instead of  $1 - \frac{St_F}{St_0}$  but the blowing ratio clearly affects the film effectiveness.

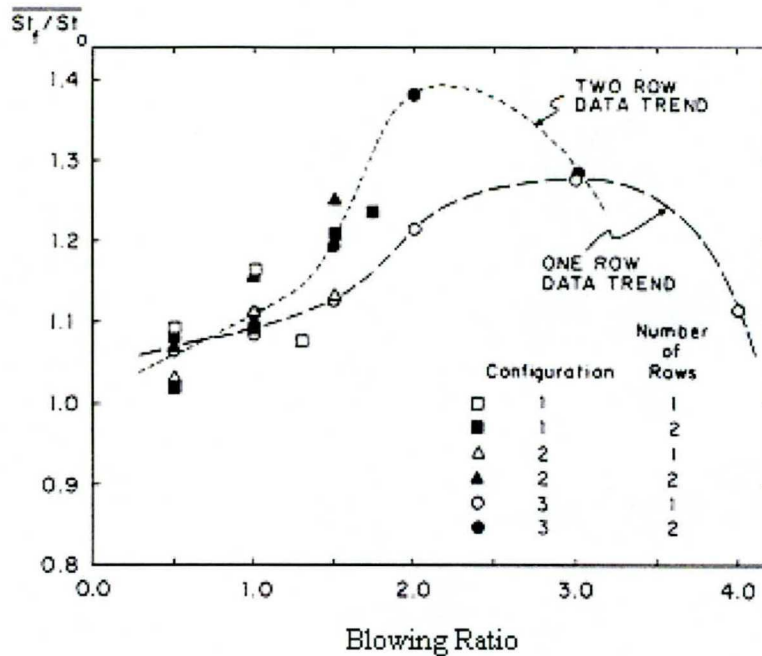


**Figure 29. The effect of blowing ratio on single-row and double-row injection through different hole configurations [40]**

In the case of the full stage fully cooled experiments described in this thesis, the value of the blowing ratio parameter is a function of specific location on the airfoil, and thus it is not reasonable to present the resulting film effectiveness as a function of a single global blowing ratio, but rather the results are presented as a function of local blowing ratios for each row of cooling holes at a given span. Global blowing ratios are much simpler to calculate since the mass flow and total area of cooling holes are measured. However, rotating rigs will have the same pressure ratios across the stage and pressure gradients along the surfaces of an airfoil as an engine and the supply coolant flow to all

parts of the blades come from a single supply, leaving blowing ratios ranging from 1.4 to 6.4. Due to the large fluctuation in the local blowing ratio the global blowing ratio is of little use for comparing to other experiments like flat plate experiments and cascade experiments where the local blowing ratio is easily calculated. Measuring the local blowing ratio in a rotating experiment leads to the uncertainty of measuring the velocity of the cooling gas in the holes along with measuring inherent mass flow leaks caused by rotation. Two assumptions are made to calculate the velocity of the coolant gas in the holes, first is to assume the static pressure on the exterior surface of the airfoil is equivalent to the static pressure in the cooling holes. The second assumption made is to estimate the total coolant gas pressure in the airfoil. The total pressure can either be set as a constant which indicates the internal chamber is acting as a plenum to the cooling holes (Method A) or in the case of the blade the total pressure can be set equal to the internal channel pressure which varies with vane passing (although slightly) and would imply the flow is slow but cannot be treated as a plenum (Method B). The calculation details and results are presented in Chapter 5 for both assumptions. Ideally the blowing ratio should always be presented on the local level but the important information resulting from the blowing ratio is how much it changes between experiments. For this purpose either the global blowing ratio or the normalized coolant mass flow (with core mass flow) is sufficient for adjusting the blowing ratio between experiments in rotating rigs.

### **3.1.2 Cooling Gas Mass Flow**

The coolant gas mass flow to the rig is set by the temperature and pressure of the LCF and with six venturi chokes which divide the flow into the three sections: inner

vane, outer vane, and rotor. The mass flow is also calculated at the airfoil exit holes for each section using the data from each experiment prior to the start of the core flow. Prior to introducing the core flow, the cooling gas flow through the holes is choked due to the vacuum in the dump tank setting the Mach number equal to 1. Comparing the mass flow at the venturi chokes with the mass flow at the airfoils allows the experimentalists to conduct a useful check on the system to find any possible leaks along with verifying a proper cooling supply setup. Mass flow calculations are carried out in detail in Chapter 5.

## **CHAPTER 4**

### **OPERATION AND INTEGRATION OF THE LCF**

The LCF was designed and built at the OSU GTL in 1997 with the primary purpose of running in conjunction with the TTF for film cooled turbine experiments. In order to properly link the LCF to the main facility and to the turbine rig inside (Figure 30), there were three major areas that had to be addressed: (1) coordination of a fast acting valve (FAV) with the primary flow coming from the TTF, (2) definition of the proper cooling cycles to provide the desired temperature and pressure of the cooling gas at the vane and blade, and (3) establishment of controls for interfacing the LCF with the TTF facility. The FAV was built and in reasonably good working order prior to initiation of the 2004 measurement program, but there was no information for timing and operation.



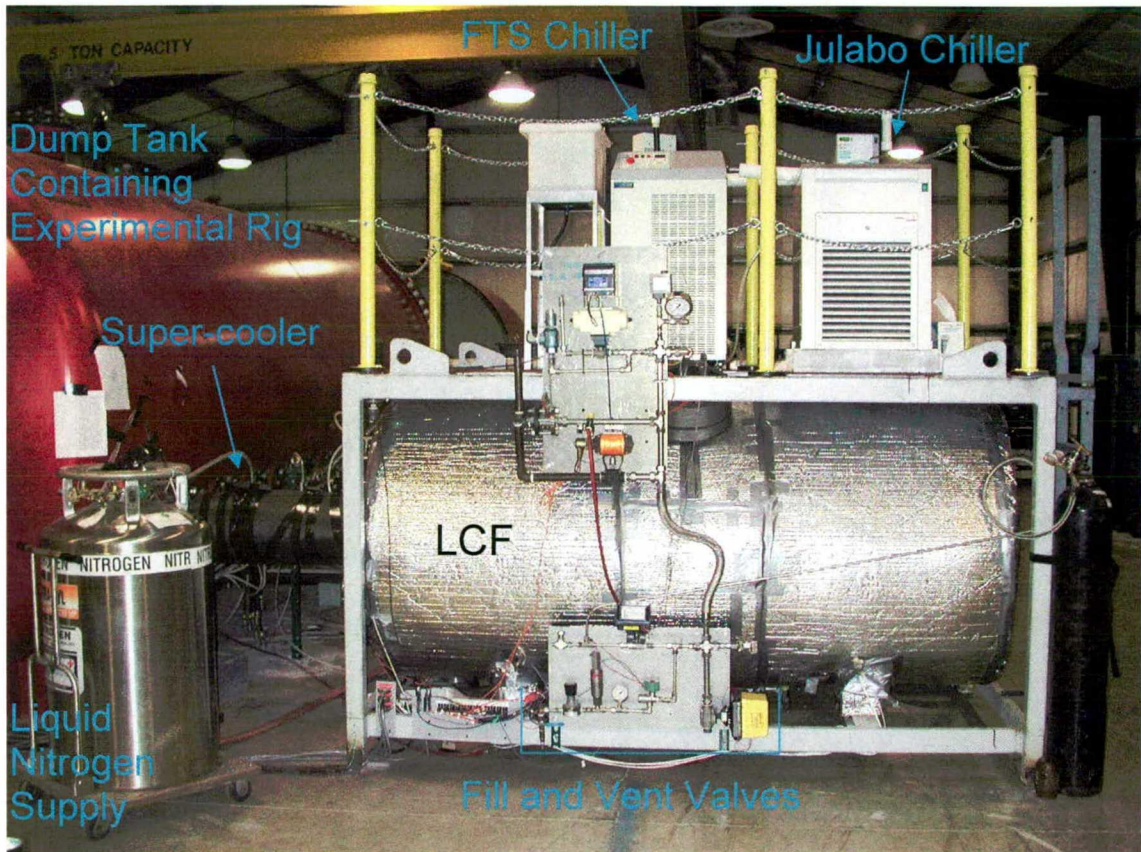


**Figure 30. LCF Connected to TTF for Film-Cooling Experiment**

#### **4.1 Initial Design**

The cooling gas supply tank used for the film cooling experiments was initially designed for a dual purpose. First purpose is to be used in conjunction with the TTF for supplying cooling gas for film cooling gas turbine experiments. Second purpose is for the unit to be used as a large calibration facility with different test sections similar to the Small Calibration blowdown Facility (SCF) still in use at the OSU Gas Turbine Laboratory.

Ideally the LCF tank would be sized accordingly for each experiment in the TTF so the time constant of the shock tube and the LCF would be approximately the same. This would result in constant blowing ratios from the film cooling to the freestream flow

as the total pressures decrease during longer experiments. However, since the LCF will be used in many future experiments it was sized as large as feasible at the time of construction resulting with an internal volume of 45 ft<sup>3</sup>. The core design of the LCF calls for a triple jacketed tank with the inner tank as the main pressure vessel, the second to circulate fluid, and the third to contain the insulation as shown in Figure 31. All three jackets of the tank came from the same batch of stainless steel so the thermal expansion coefficient of each jacket is the same. The rest of the LCF can be broken up into three distinct areas: Fast Acting Valve (FAV), Coolant System, and Controls.

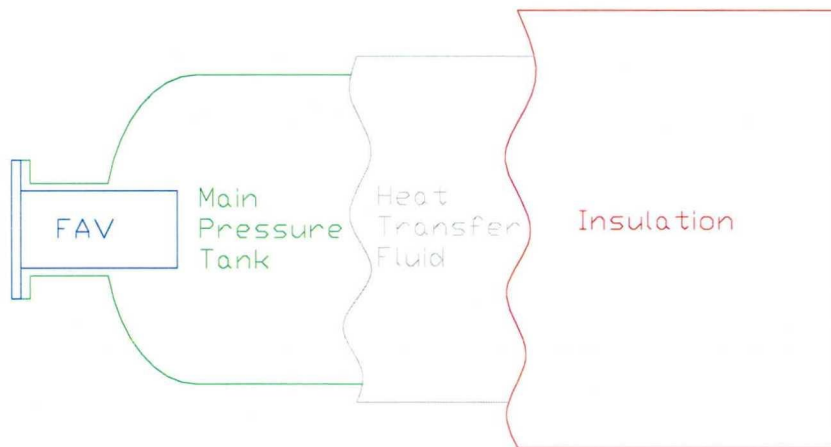


**Figure 31. Breakdown of Internal LCF Construction**

#### **4.2 Fast Acting Valve**

The two primary design parameters of the FAV are fast actuation for operating in conjunction with the TTF and for smooth clean air flow for calibration purposes.

The valve is a fast acting sleeve valve that was designed for pneumatic actuation and opens in about 10 ms with clean air flow at the exit of the valve. To get clean air flow at the exit of the valve the flow path was designed with an elliptical shape and modeled in

Star-CD [9]. The contour of the flow path can be seen in both Figure 32 (a) and Figure 33.

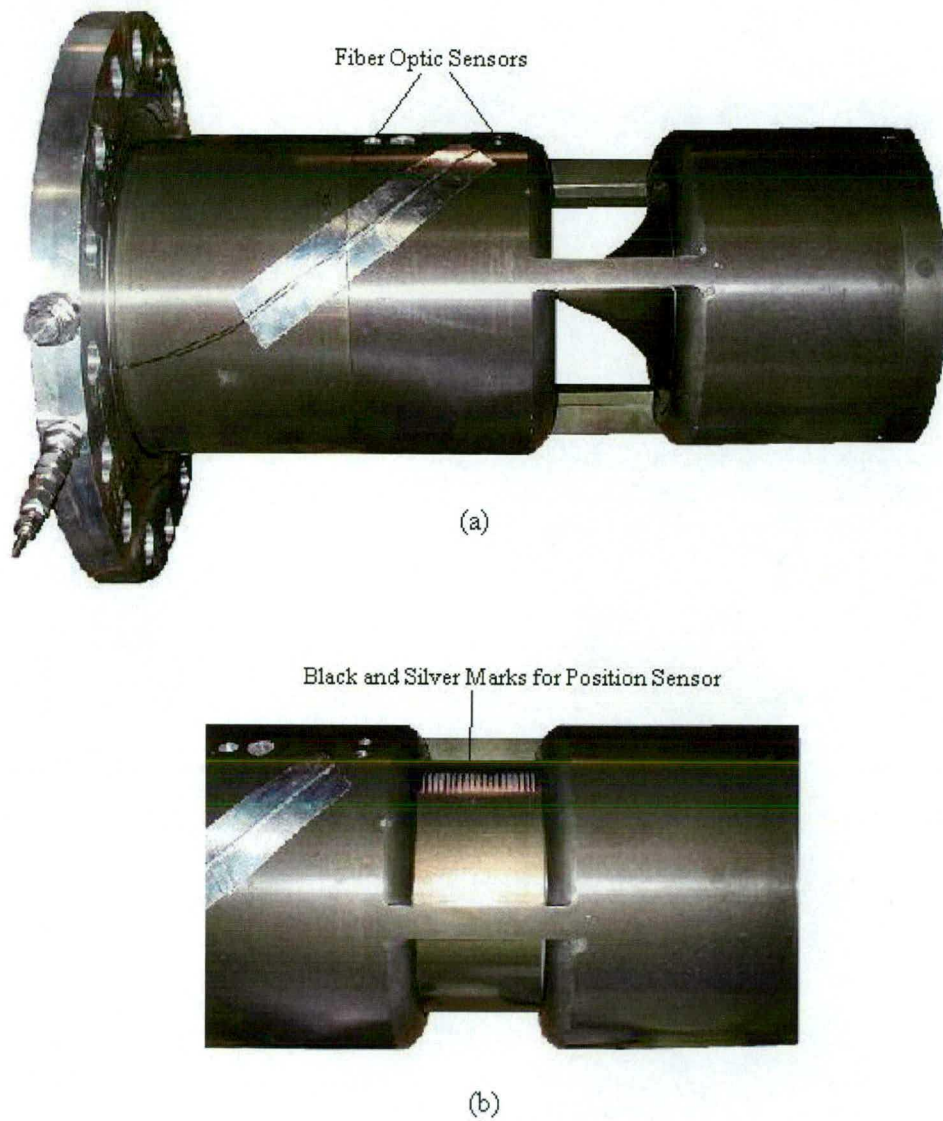


**Figure 32. FAV in the open position (a) and the closed position (b)**

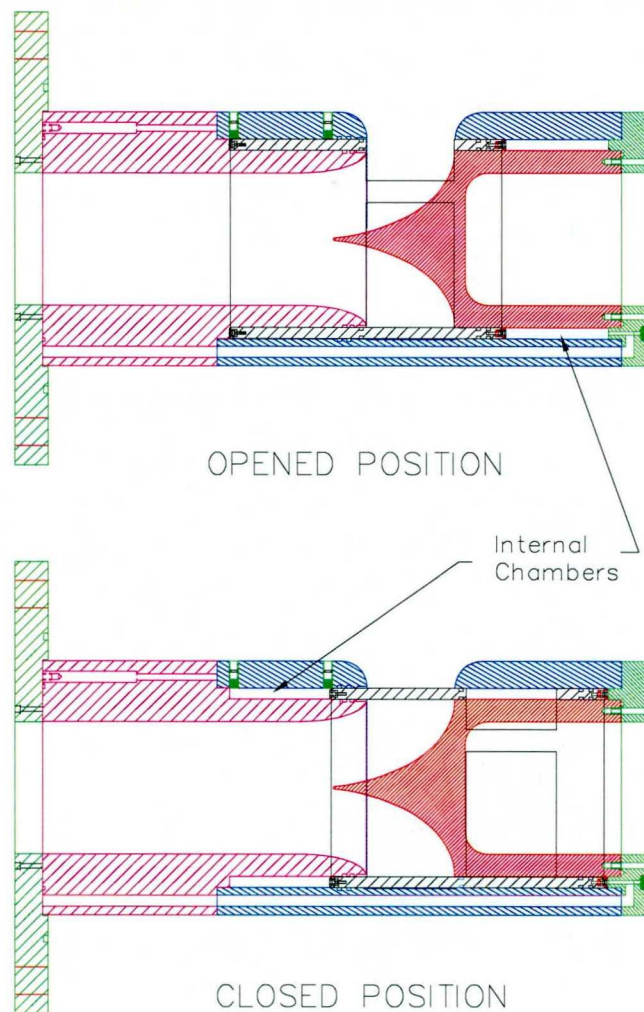


**Figure 33. Cross-sectional view of FAV with sleeve in the open and closed position**

The motion of the valve is controlled with timers that actuate two 3-way solenoid valves which fill and vent the internal chambers to move the sleeve. Movement of the sleeve uses air pressure in the chambers to push and catch the sleeve. To open the FAV, the first 3-way control valve is activated which fills the aft chamber and pushes the sleeve to the open position. Then activating the second 3-way valve for 0.1 s puts a small burst of air into the fore chamber and catches the sleeve before it can slam into the endplate.

For closing the sleeve the process is reversed using the second 3-way valve to move the sleeve and the first 3-way valve to catch the sleeve. A schematic of the timing sequence for the 3-way solenoid valves is shown in Figure 34. The chamber pressures are recorded along with the fiber optic sensors (explained on page 51) and are displayed in Figure 35 for the FAV when operated at room temperature. The internal chambers that move the sleeve can be seen in the cross-section view of the valve in Figure 33. To operate the LCF with the TTF, the timers are triggered with a constant 5 volt signal that allows the LCF FAV to open and fill all internal cooling cavities in the rig and establish cooling flow before the FAV for the TTF opens and releases the core flow.

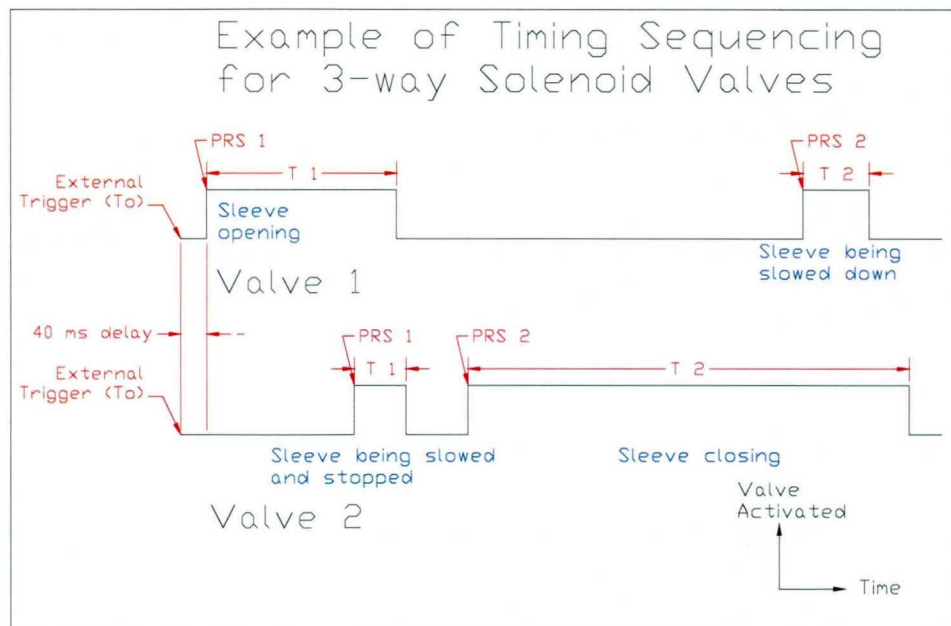


**Figure 34. Timing sequence for FAV 3-way solenoid control valves**

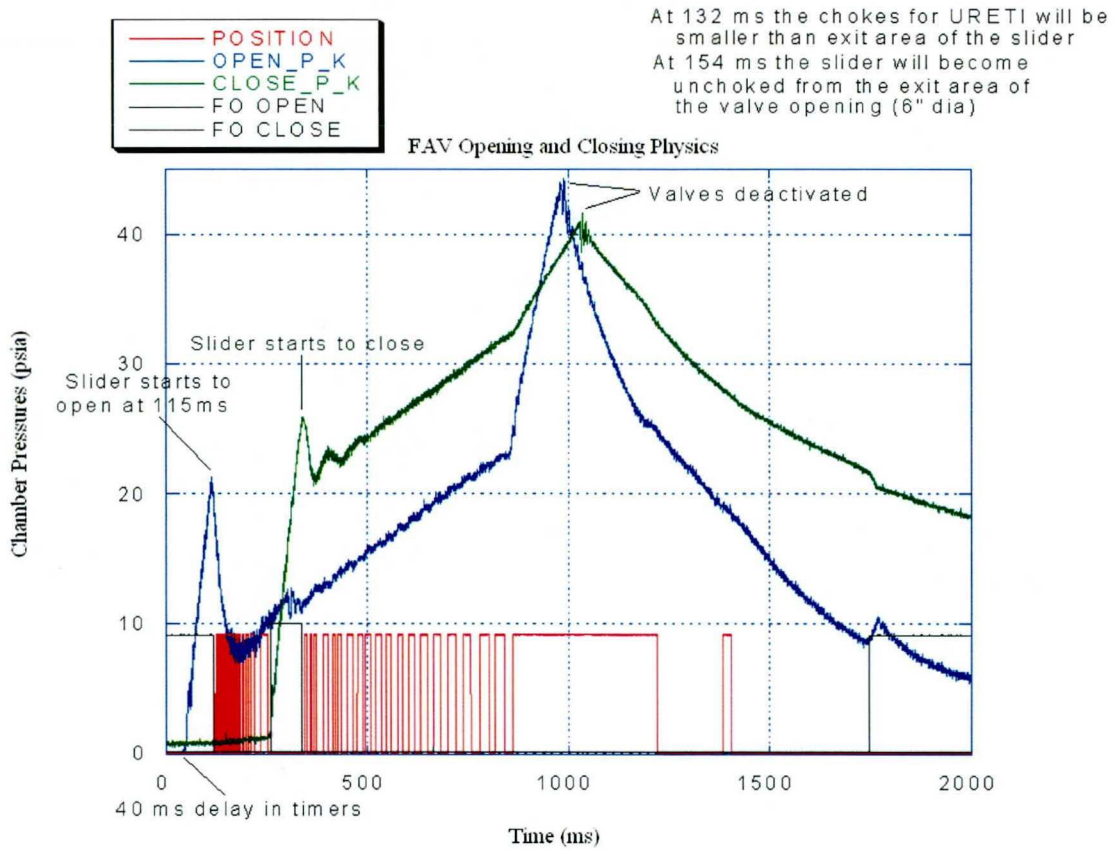


**Figure 35. FAV internal chamber pressures and fiber optic sensors**

In order for the LCF to operate in conjunction with the TTF the FAV must be very reliable and consist of very repeatable opening times. With proper operation and the proper timing of the 3-way control valves the FAV has had successful activation in excess of 300 runs which has included experiments to determine proper timing scenarios with different operation cycles and preliminary experiments measuring mass flow and understanding the flow characteristics from the LCF into the rig. Throughout the experiments the opening sequence of the FAV has proven to open repeatable to within 6 milliseconds when operated at consistent conditions (primarily tank temperature and

valve activation pressures). This degree of repeatability is sufficient for the purposes of these experiments.

A new phenomena, referred to as a “hic-cup”, begun appearing after about 100 activations where the sleeve either slows down or pauses moments after motion begins as in Figure 36. The sleeve motion is governed by the pressure difference between the internal chambers and friction acting on the internal seals. Figure 37 suggests that the pressure difference in the internal chambers is not the cause as there is no jump in the close chamber pressure which places focus on the friction. In an effort to characterize the “hic-cup” an extensive test matrix (included in Appendix A with results) was conducted that varied LCF pressure, LCF temperature, valve activation pressure, test section pressure, and a test section bleed. The experiments produced inconclusive results as to which variable may be the driving factor. The internal seals in the valve are the only variables unaccounted for in the test matrix and with the “hic-cup” slowly fading over time it is believed this change in friction may have been caused from the seals becoming broken in. Even with the slowly changing friction the valve has proven to be very repeatable run to run and is reliable for the turbine film cooling experiments.

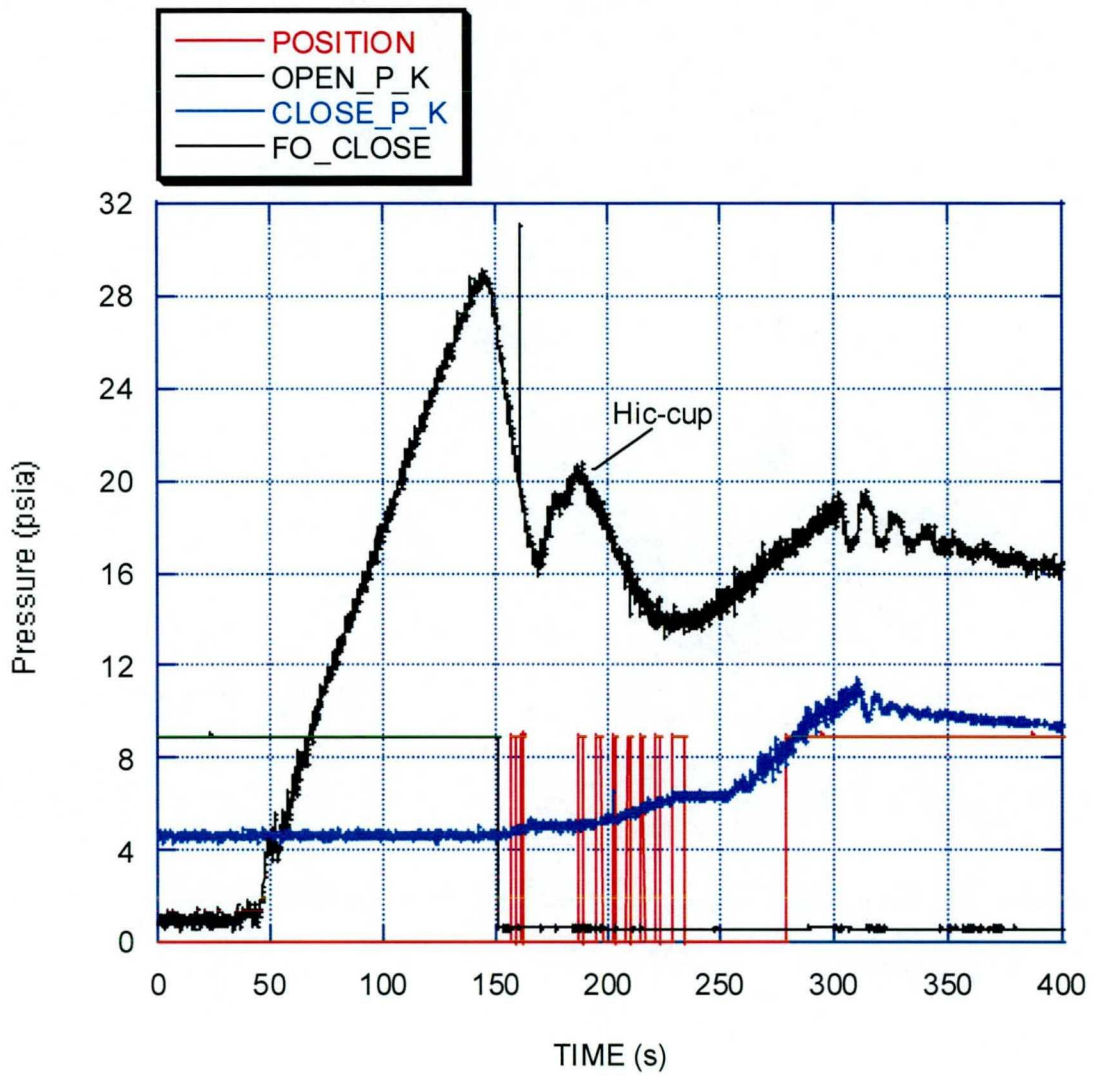
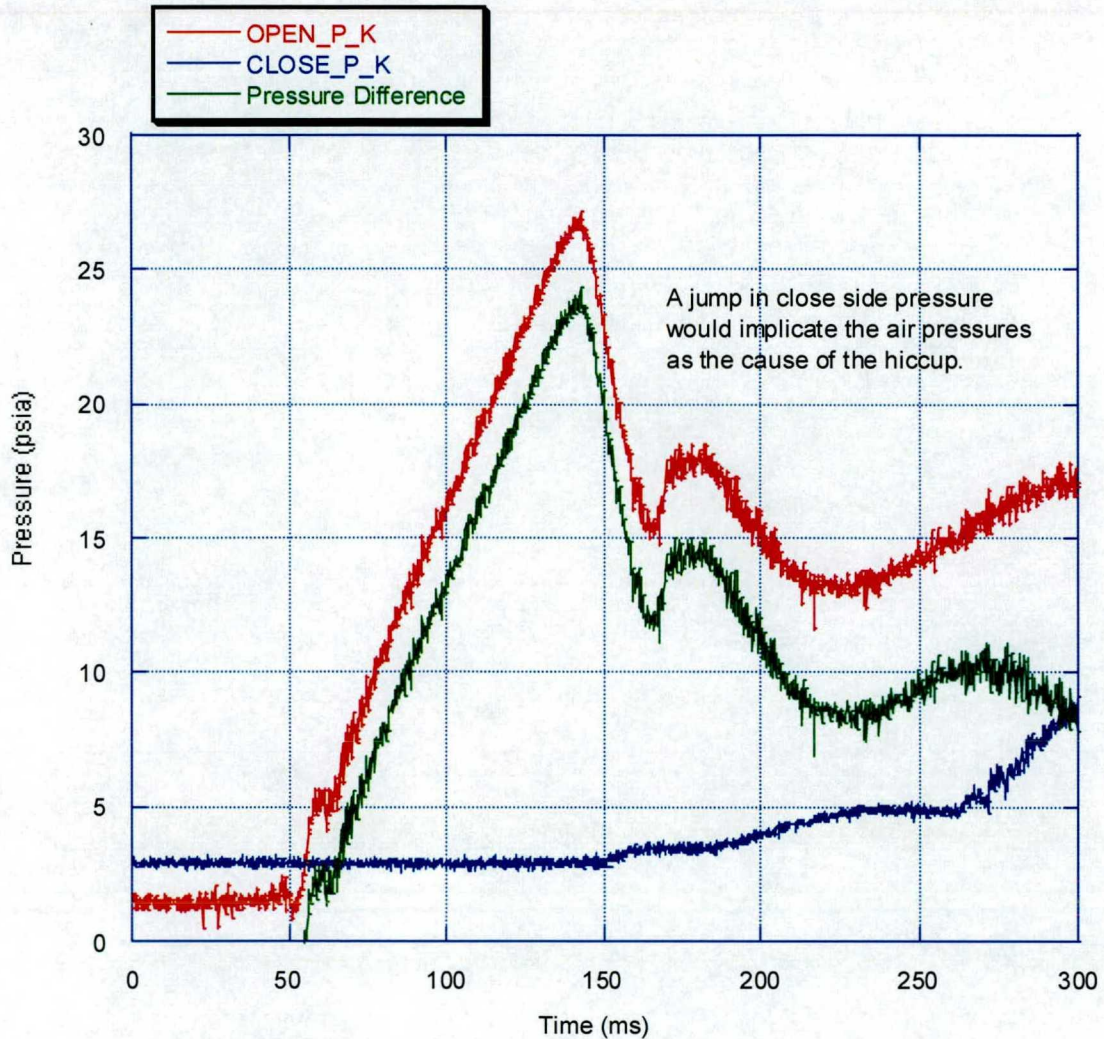


Figure 36. FAV “hic-cup” while opening (a particularly severe case)





**Figure 37. Internal chamber pressure difference during “hic-cup”**

Other key features of the valve include the coating and fiber optic sensors. Valve parts were coated to decrease both friction and wear acting upon the seals and sleeve of the valve. The coating consisted of Teflon impregnated into an anodized aluminum oxide formed on the surface by the electrochemical reaction of aluminum with oxygen [9]. Position of the valve is tracked with three fiber optic sensors. Two of these sensors are

used as “clear indicators” to tell the operator that the sleeve is either in the fully open or fully closed position. The third sensor reads the silver and black lines that are 0.1 inches wide on top of the sleeve as seen in Figure 32b. Output of this sensor can be tracked on a computer to measure how far the sleeve has moved (within 0.1 inches) as shown in red in Figure 35. The disadvantage of this sensor is the silver and black marks will wear off on the seals with time. For this reason a Philtec D-170 position sensor was investigated as a possible replacement. The comparison of the output of the Philtec D-170 sensor with the fiber optic sensor is shown in Figure 38 where the position pulses were converted to distance. Based upon these results, a Philtec D-171 (better model for intended use but unavailable as demo) will be installed into the valve when time allows.

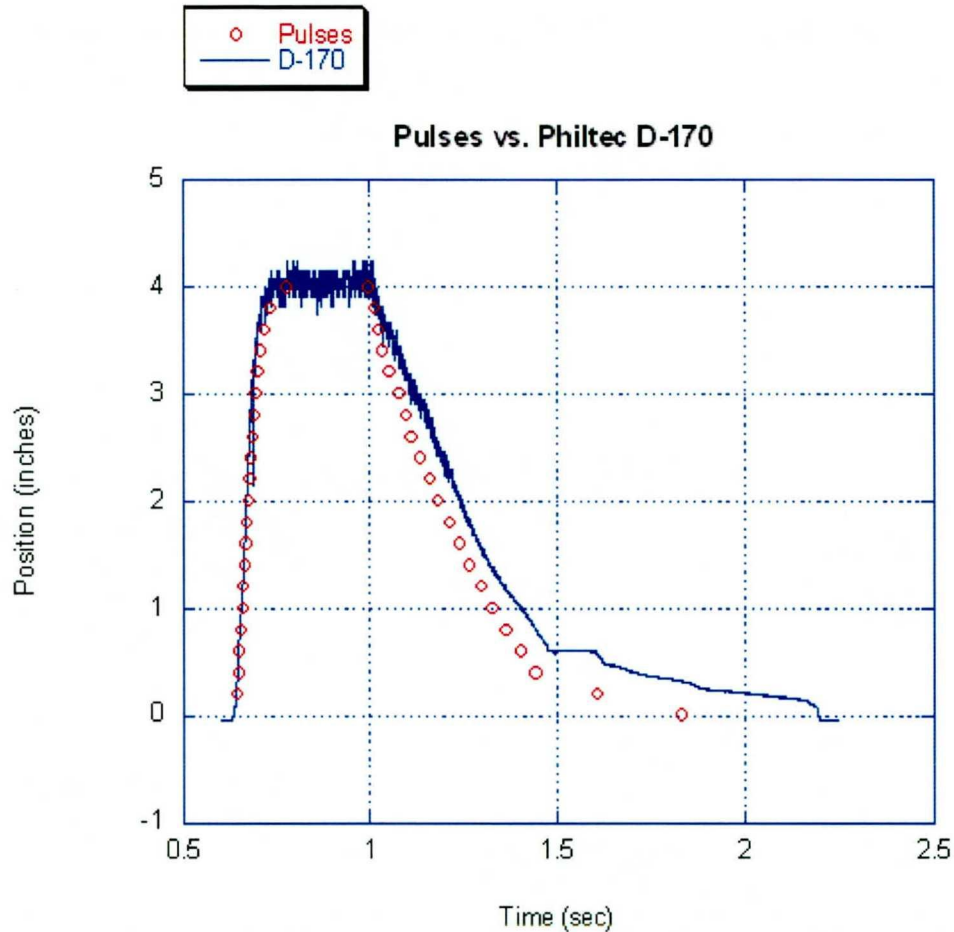


**Figure 38. Philtec sensor compared to current fiber optic pulse position sensor.**

Valve operation for the URETI experiment uses an activation of 40 ms as opposed to the 10 ms that is theoretically possible by design. Three options exist to allow for more rapid operation of the valve. The first is to replace the two 3-way solenoid valves with valves that have larger openings; the control valves presently being used have open areas of  $0.1 \text{ in}^2$  and cause a choke point from the internal chambers to the external pressure supply and vacuum tank. The second option is to increase the activation pressure; for example from the normal 75 psia to 122 psia will open the valve 35 ms faster as seen in Figure 39. The third option is to utilize the two extra ports (already

existing in the valve) to the opening chamber and a single unused port to the closing chamber to accommodate extra control valves allowing more mass flow of the activation gas into the internal chambers which will speed up the sleeve motion. A fourth option to increase the activation speed was implemented prior to conducting the experiments determining the proper activation timing. This option added plugs to block off the unused ports near the internal chambers effectively reducing the chamber volume for the activation gas to fill. This successfully reduced the time for initiation of sleeve motion by 30 milliseconds as seen in Figure 40. For the URETI film cooling experiments, a delay of the TTF is needed to allow coolant passages in the rig to fill and flow to establish. Due to this delay the slower activation of the valve is sufficient and preferred for the life of the valve.

### Effect of Increasing Valve Activation Pressure

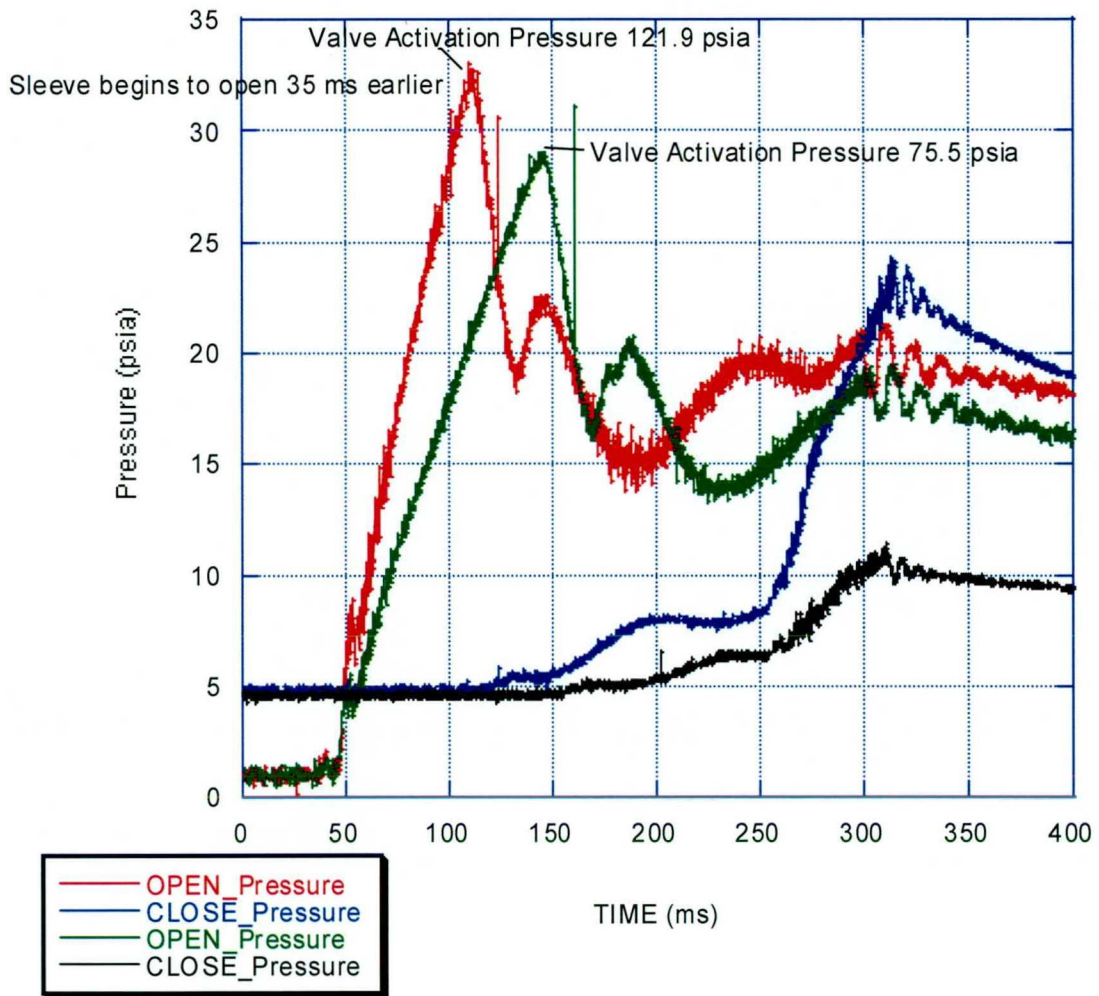
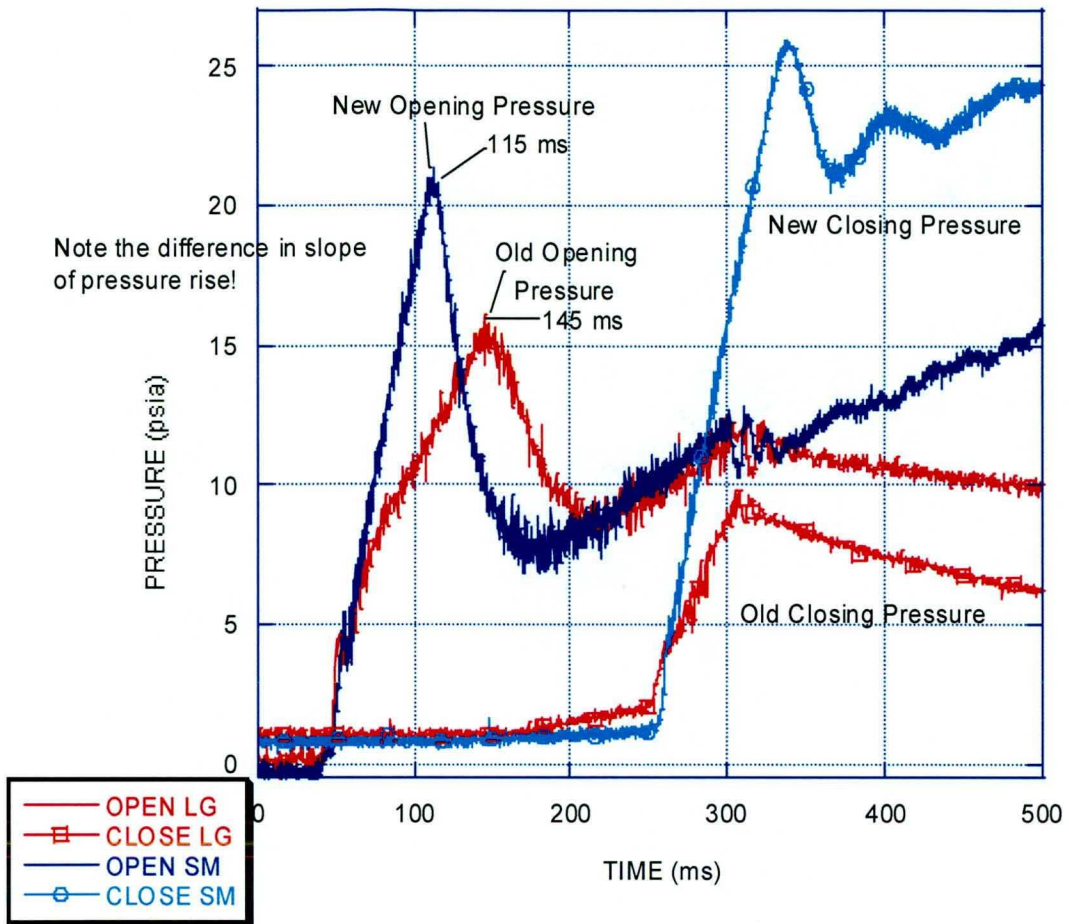


Figure 39. Effect of increasing the valve activation pressure

Difference in Valve Activation from Plugging  
Extra Ports at Internal Chambers



**Figure 40. Difference in valve activation when extra ports at internal chambers are plugged**

### 4.3 Coolant System

Cooling the gas contained within the LCF for film cooling experiments was intended to serve two purposes; (1) to obtain the necessary cold temperatures for film cooling gas and (2) to provide sufficient mass flow for large rigs. Cooling the LCF to cryogenic temperatures can be done with either of two recirculating chillers on top of the LCF. The FTS unit has proved to reach lower temperatures but allows water into the

Syltherm XLT (heat transfer fluid) which collects on the heat transfer plates. This water accumulation causes a steady decay of the heat extraction capability of the unit and does not allow the LCF to remain at low temperatures as shown in Figure 41 (the temperature begins to increase at the right side of the figure). To fix the water issue a molecular sieve was added to the side of the LCF to remove the water from the heat transfer fluid when the facility is at room temperature. The Julabo unit is rated for higher heat reduction capabilities and prevents water from getting into the system but the price one pays is that it is not possible to reach the desired lower temperatures due to the slow pumping of the unit. The cooling curve for the Julabo unit is in Figure 42, which covers a 50-hour time span but the unit has proven to only increase 3-4 degrees from a maximum low when operated continuously for 2 weeks. A booster pump may be added to the Julabo chiller to increase the cooling capabilities of the LCF but for the current set of experiments the Julabo chiller is used alone to cool the facility and assist in attaining the necessary mass flows required. In the case of the URETI experiments, reduction of the cooling gas temperature was assisted by installation of a liquid nitrogen cooled heat exchanger downstream of the LCF as is described below.

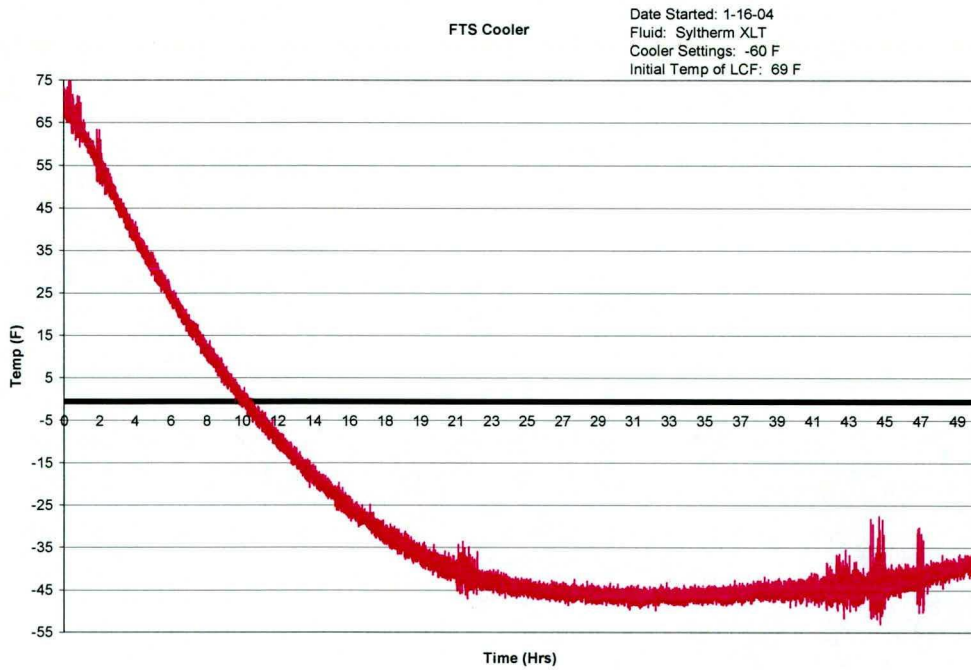


**Figure 41. Time history of the FTS unit chilling the LCF coolant gas**

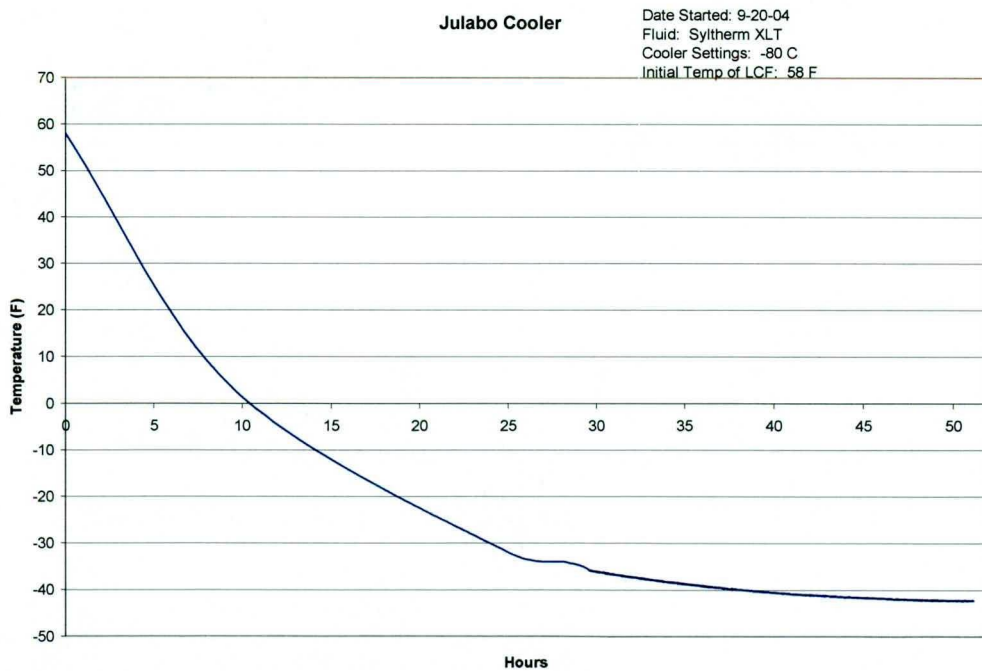


**Figure 42. Time history of the Julabo unit chilling the LCF coolant gas**



A minimum coolant gas temperature was obtained by using the Julabo chiller to cool the gas to  $-43^{\circ}\text{F}$  and then turning on the FTS chiller to reduce the temperature further to  $-56^{\circ}\text{F}$ . However, this minimum temperature was obtained with the LCF isolated such that the FAV connection was well insulated. Since the chillers are operating at maximum capacity, connecting anything to the LCF will potentially result in a heat source and thus increase the minimum temperature that can be attained. As an example, plumbing the LCF to the TTF and then to the rig containing the turbine stage for the URETI experiments has resulted in minimum coolant gas temperatures of  $-30^{\circ}\text{F}$  from the Julabo chiller alone and  $-45^{\circ}\text{F}$  when using the FTS unit along with the Julabo.

From preliminary experiments the long multiple tubes required to get the coolant gas from the LCF into each turbine section (inner vane, outer vane, and rotor) proved to be a very good heat exchanger that resulted in room temperature gas at the exit of the film cooling holes on the vanes and blades, which was clearly an unacceptable situation. To fix this problem a liquid nitrogen heat exchanger (super-cooler) was designed to lower the temperature of the gas leaving the LCF, shortened the tubes carrying the gas from the LCF to the turbine, and heat was extracted from the tubes extending to the turbine via conduction. Using the super-cooler in conjunction with the LCF lowered the cooling gas to  $17.3^{\circ}\text{F}$  at the exit of the vane and blade cooling holes. Operation of the LCF with the super-cooler still requires using the Julabo chiller to cool the LCF coolant gas in order to obtain the proper mass flow into the turbine stage.

#### **4.4 LCF Controls**

Controls for the LCF were designed and built for total control of the facility from either within the control room or next to the facility. This is important for the different

operating modes of calibration or film cooling experiments. Total control includes the ability to fill the tank with different gases, vent the tank fast or slow, and operate the FAV. Filling the LCF is controlled with three valves, one for dry shop air, one for compressed gas from a bottle (size K), and the third for evacuating the tank. Using relays the control panel has built in delays and safeties to assure only one valve can open at a time and the vacuum valve cannot open if the tank pressure is above 16 psia which protects the vacuum pump from positive pressure. Venting the LCF can be done in a fast action by opening a 1" diameter pneumatic valve or in a slow controlled manner using a finely adjustable valve which can be used for pressure calibrations. Activation of the FAV can be conducted by using the timer controls for fast activation and an external trigger source or using a manual toggle switch to slowly open and close the valve. The facility is protected against over-pressurization (tank rating 464 psia) with three devices, a rupture disc (486 psia, above tank rating but acceptable due to factor of safety in tank design), a blow-off valve (454 psia), and an adjustable pressure switch currently set to open the fast vent valve at 434 psia. The control panel has digital meters to visually inspect the tank temperature and the valve activation pressures for the FAV. Using a PC the internal temperature, pressure, and FAV chamber pressures can be monitored or recorded at high sampling frequency during an experiment.

#### **4.5 Integrating the LCF with the TTF**

In conducting a film cooling experiment, many operating parameters must be matched in preparation for an experiment. These parameters include tunnel pressure, LCF pressure, LCF temperature, super-cooler temperature, and heater temperature. Operating the LCF in conjunction with the TTF requires intricate timing and the

activation of both facilities and multiple data acquisition systems. Once the rotor is rotating at the proper speed the LCF FAV is activated first to allow coolant passages to fill and for the cooling film to be established. With the use of three adjustable timers the TTF FAV is activated 1.5 seconds after the LCF. Data acquisition is divided into three sets; monitor, coolant flow, and main flow. The monitor data is recorded at low sampling frequency throughout the experiment to measure initial conditions of the system. Coolant flow path and LCF sensors are recorded at high sampling frequency and are initiated with the triggering of the LCF FAV. With the activation of the TTF FAV the main flow high sampling frequency data acquisition system is triggered. To conclude an experiment, both FAVs close and the remaining gas in the TTF and LCF are vented.

Future film cooling experiments are expected to be conducted similar to the one described above. So as a design aid to future experiments the mass flow capabilities of the LCF was characterized using a series of charts located in Appendix B. The charts plot the mass flow as a function of time for a given choke area, initial pressure, and initial temperature. Initial temperature values were determined from the current experimental setup by using the low temperature attainable from only using the Julabo chiller (-30°F) and using both the Julabo and the FTS chillers (-45°F).

## **CHAPTER 5**

### **DISCUSSION OF CALCULATIONS AND RESULTS**

The two key calculations related to the film cooling gas are the blowing ratio and the mass flow calculations as discussed in Chapter 3. This chapter will show the successful integration of the LCF with the TTF and discuss the calculation details of the blowing ratio and the mass flow calculations along with the uncertainties associated with these values. All calculations and results presented in this chapter are from the initial fully cooled single stage high-pressure turbine experiment conducted using the newly integrated TTF/LCF system.

#### **5.1 LCF Integration Results**

Successful integration of the LCF with the TTF is best described from the data results presented in Figure 43 and Figure 44. Figure 43 displays the upstream and downstream total temperature measurements starting when the trigger signal was given to the LCF. This data also clearly shows the 1500 ms delay between the TTF and the LCF trigger signals. The pressure measurements in Figure 44 start at 1500 ms on Figure 43 and display some of the pressure measurements obtained during the activation of the core flow. From these two graphs it can be concluded that the timing and activation of the FAV on the LCF was successful.

### Normalized Rake Temperatures During Experiment

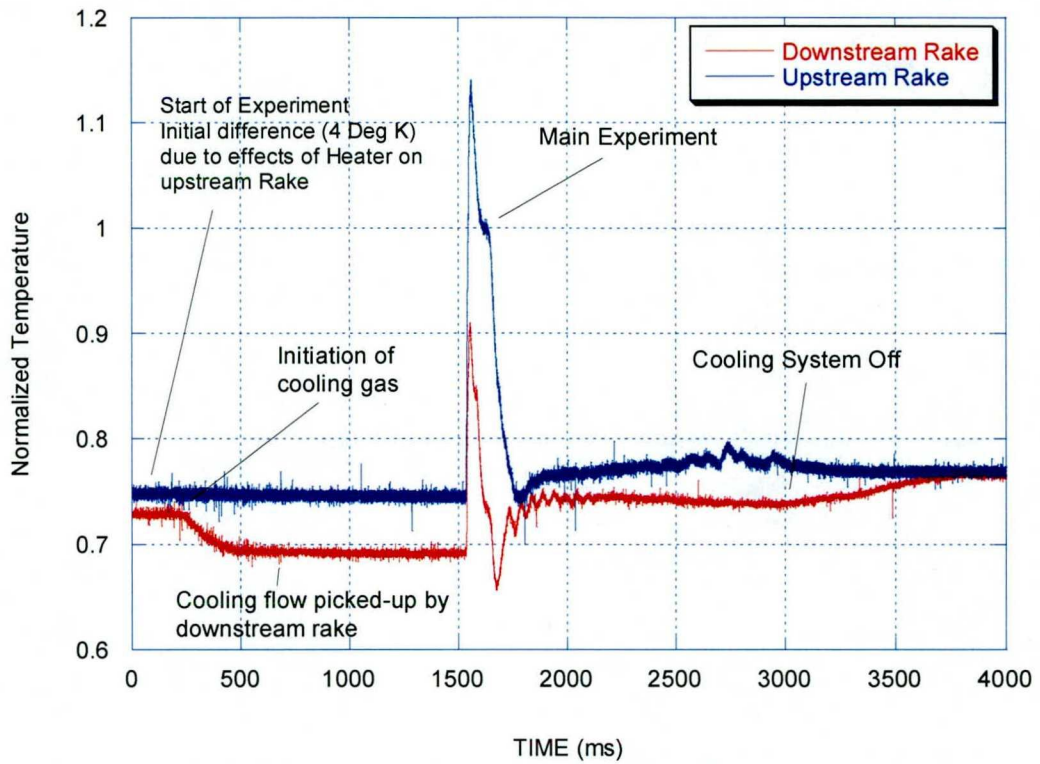
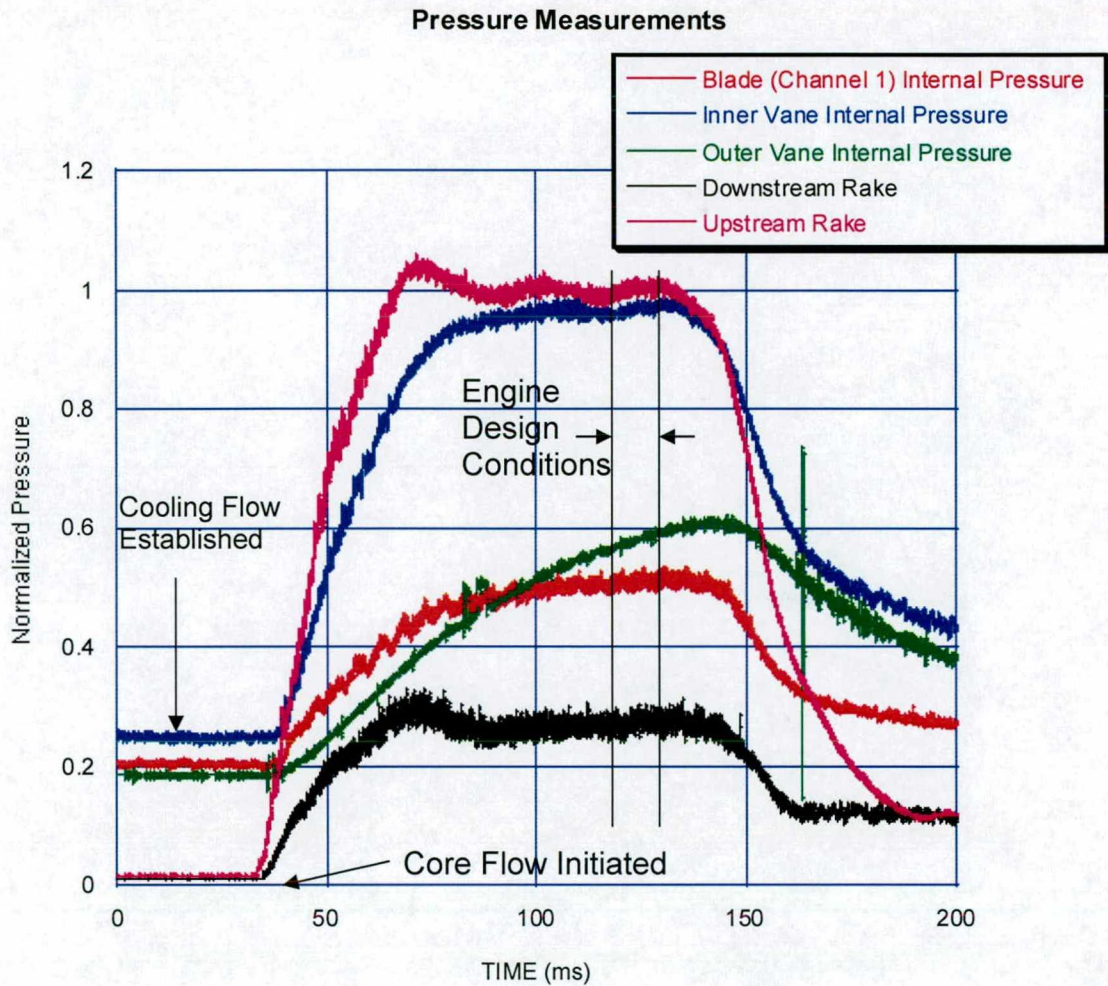


Figure 43. Flow Path Temperature Rake Measurement



**Figure 44. Stage Pressure Measurements**

## 5.2 Estimates of Blowing Ratio and Mass Flow

### 5.2.1 Blowing Ratio on the Blade

Calculation of the blowing ratio for various locations on the blade is based on the local freestream density and velocity, and the coolant gas density and velocity at the exit of the individual cooling hole as defined in Equation 1. The freestream density is calculated based upon the static pressure distribution as measured (normalized distribution in Figure 45) and CFD predictions of the local Mach number (Figure 46) and

local static temperature. Local freestream velocity is calculated based on the Mach number and the local static temperature predictions using Equation 2.

$$Blowing\_Ratio = \frac{\rho_c * V_c}{\rho_\infty * V_\infty}$$

**Equation 1. Blowing Ratio**

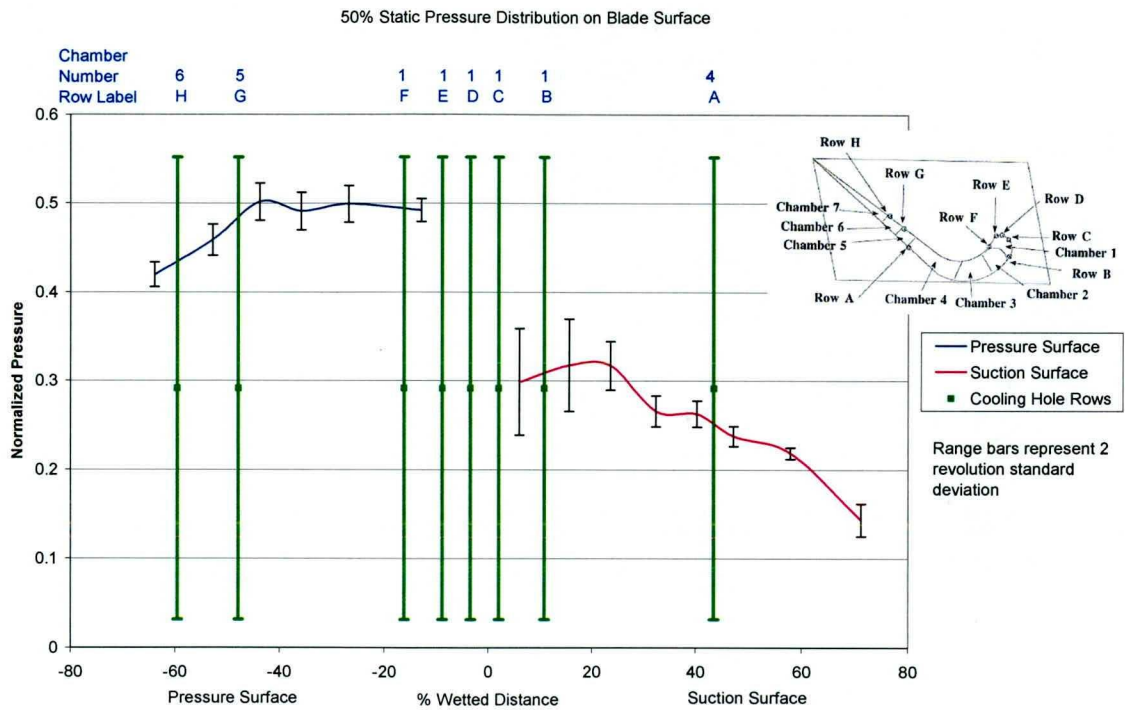


**Figure 45. Normalized Static Pressure Distribution on Blade**

URETI Rotor Mach Number Distribution at 50% Span

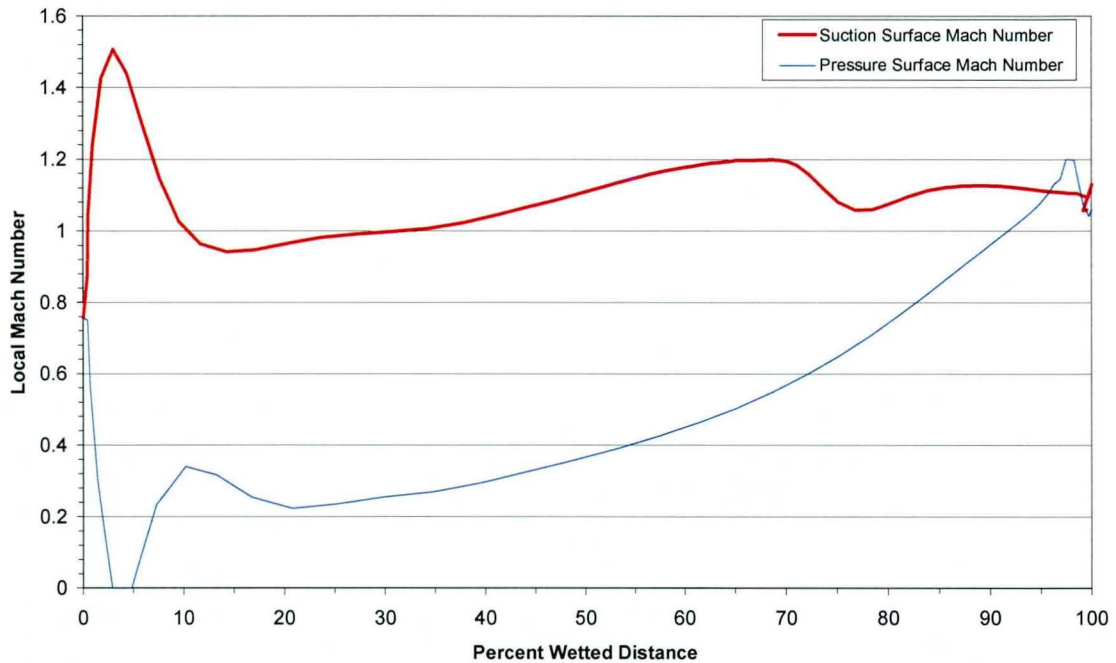


Figure 46. Local Mach Number Distribution CFD Prediction (provided by Honeywell)

$$M = \frac{V}{a} = \frac{V}{\sqrt{\gamma RT}}$$

**Equation 2. Mach number / velocity relation**

Calculating the density and velocity of the cooling gas at the exit of the cooling hole requires a couple of assumptions as described in Section 3.1.1. To refresh, the first assumption is to set the static pressure at the hole exit equal to the local static pressure on the blade surface (from Figure 45). The second assumption is to estimate the total pressure in the internal channels of the airfoil, which can be done in two ways. First (Method A) by assuming the total pressure is constant or second (Method B) by setting



the total pressure equal to the internal pressure measured which fluctuates to a relatively small degree with each vane passing. The cooling gas velocity and density is calculated with both methods by using Equation 3 (a) to calculate the Mach number based on the total pressure and the static pressure on the airfoil surface. Using the calculated Mach number and total temperature with Equation 3 (b) the static temperature can be calculated. From the static temperatures and pressures the density and velocity of the cooling gas are calculated.

$$\text{a.) } \frac{P_o}{P} = \left(1 + \frac{\gamma - 1}{2} M^2\right)^{\frac{\gamma}{\gamma - 1}} \quad \text{b.) } \frac{T_o}{T} = 1 + \frac{\gamma - 1}{2} M^2$$

**Equation 3. Isentropic flow equations (a.) Pressure (b.) Temperature**

Blowing ratio results for the suction surface gill holes (cooling holes located next to leading edge shower head holes) are displayed in Figure 47 with the surface static pressure and the internal pressure (from the channel which supplies the cooling gas to that row) normalized with the upstream total pressure. Cooling holes in this location are designed for a blowing ratio of 1.44 on this particular turbine, which is higher than the 1.05 average as calculated suggesting that the initial pressure in the LCF was set too low for this particular experiment. This issue will be revisited in a later discussion. The peaks in the surface pressure are a clear display of the vane wake passing over the blade which corresponds to a drop in the blowing ratio. As will be illustrated later in this chapter, the blade internal pressure measurements and the FFTs of the blade internal pressure histories also show a dominant signal at vane passing frequency suggesting that

the coolant supply cavity is well aware of disturbances coming from the vane wakes/shocks.

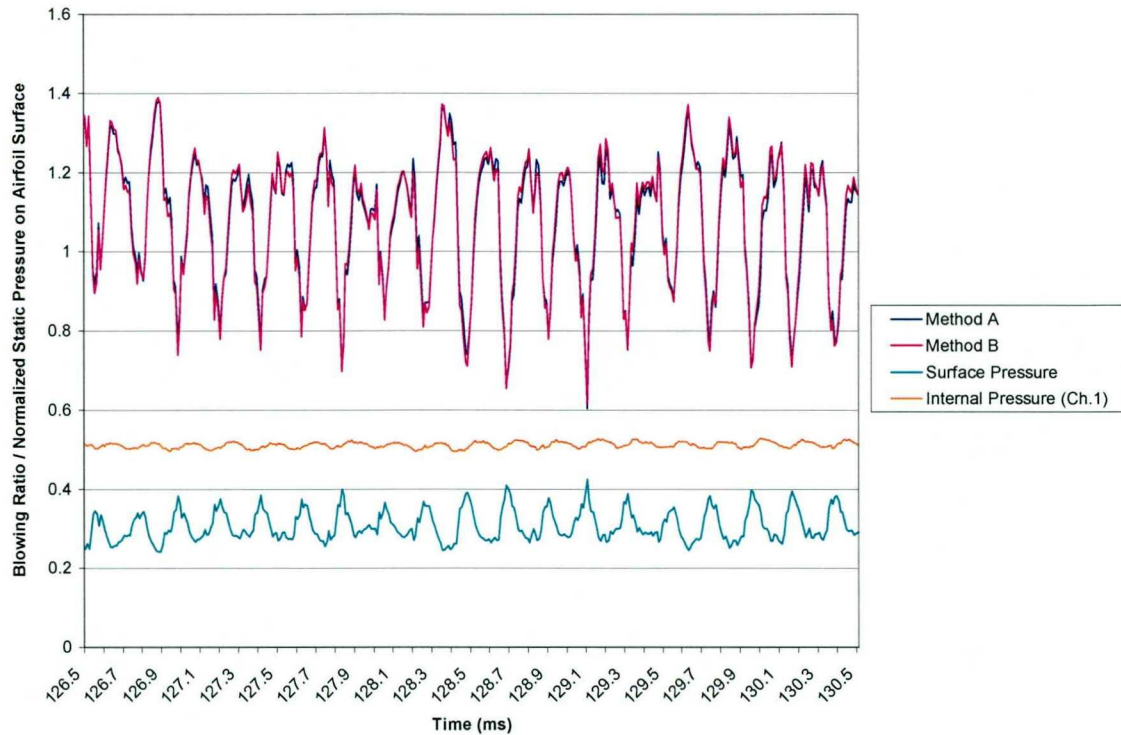


**Figure 47. Estimated Blowing Ratio for Suction Surface Gill Holes**

From the results presented in Figure 47 the two methods appear to be equivalent implying that the assumptions between Method A and B are comparable near the leading edge of the suction surface. The results presented in Figure 48 indicate the two methods average a slight difference of 0.1 at the mid-chord location on the suction surface.

However, the results in Figure 49 for the pressure surface near mid-chord suggest that the two Methods are clearly different. Method A indicates an average blowing ratio of 1.24 which is well below the design blowing ratio of 2.3 indicating a low pressure in the LCF. Method B shows an unreasonably high fluctuation in the blowing ratio (investigated in

uncertainty analysis) and indicates probable ingestion when the pressure ratio drops to zero. From the nature of the calculations the blowing ratio is limited to zero which explains the incapability of the graph to show a negative value when the core flow is ingested through the cooling holes.

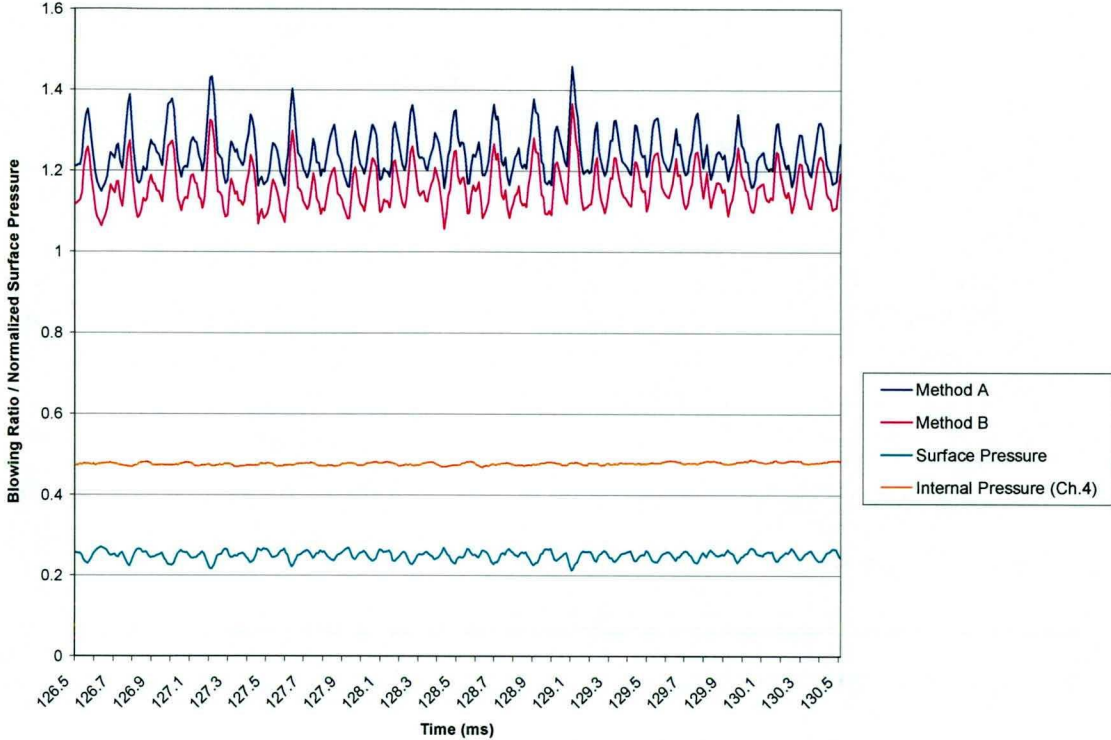


**Figure 48. Estimated Blowing Ratio for Suction Surface Mid-Chord Holes**

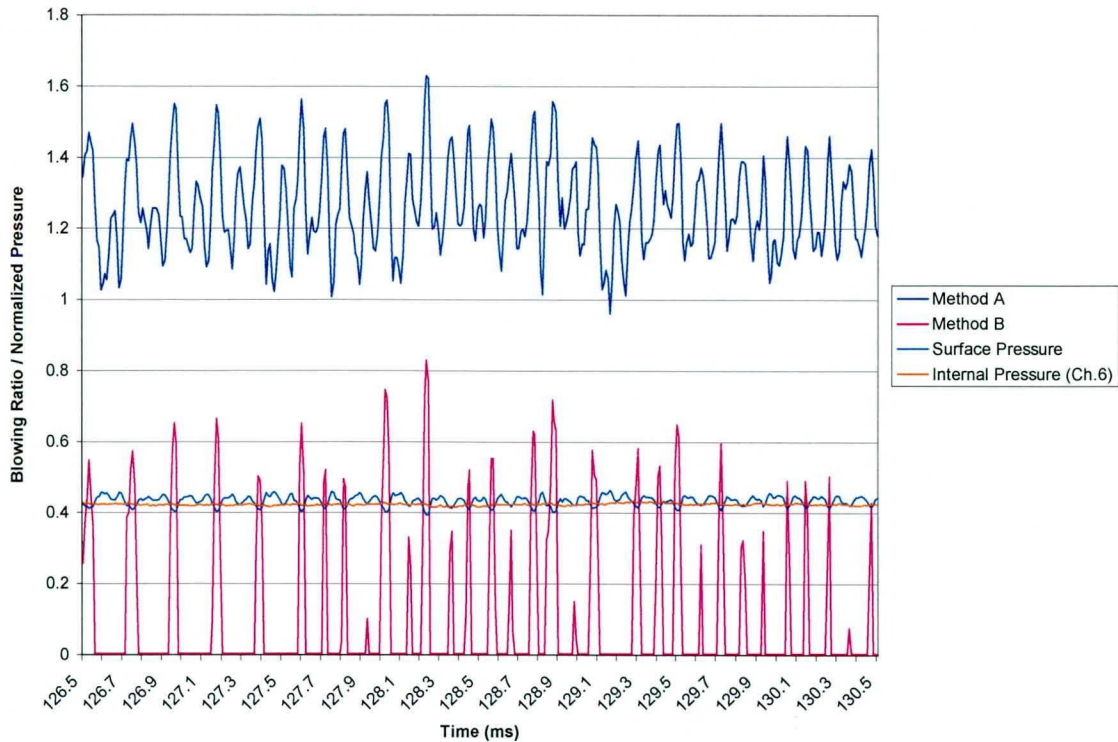


**Figure 49. Estimated Blowing Ratio for Pressure Surface Holes near Mid-Chord**

An interesting feature of this experiment is the ability to observe the unsteadiness in the internal blade passages caused by the vane wakes. To the author’s knowledge, this is the first time that internal coolant passage pressure measurements have been presented as in Figure 50 and the FFTs in Figure 51. Three key results noted in the internal pressure measurements are the phase differences in channels 1 and 2, the wake effect of the vane is barely noticeable in channel 6 compared to the leading edge (1), and the lower pressures closer to the trailing edge. The phase difference in channels 1 and 2 are believed to be a result of the internal geometry of the blade where the fluctuation in channel 2 is a forced response of the fluctuation in channel 1. The pressure drop in the channels indicates that the assumption of a constant coolant total pressure may be

incorrect but the result could also be a result of the flow speeding up due to less mass flow in the channels. Unsteadiness in the channels is a clear result of the vane wakes/shocks as demonstrated by the FFTs in Figure 51, which also demonstrates different levels of unsteadiness in each channel.

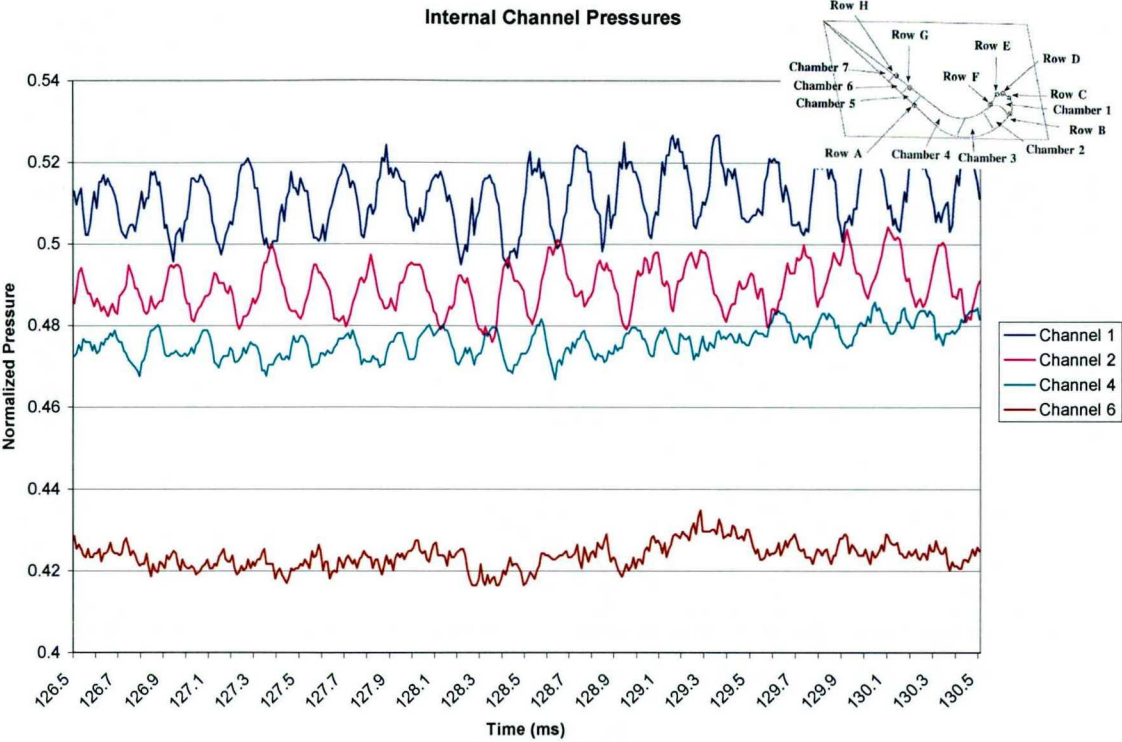


**Figure 50. Internal Channel Pressure Measurements**

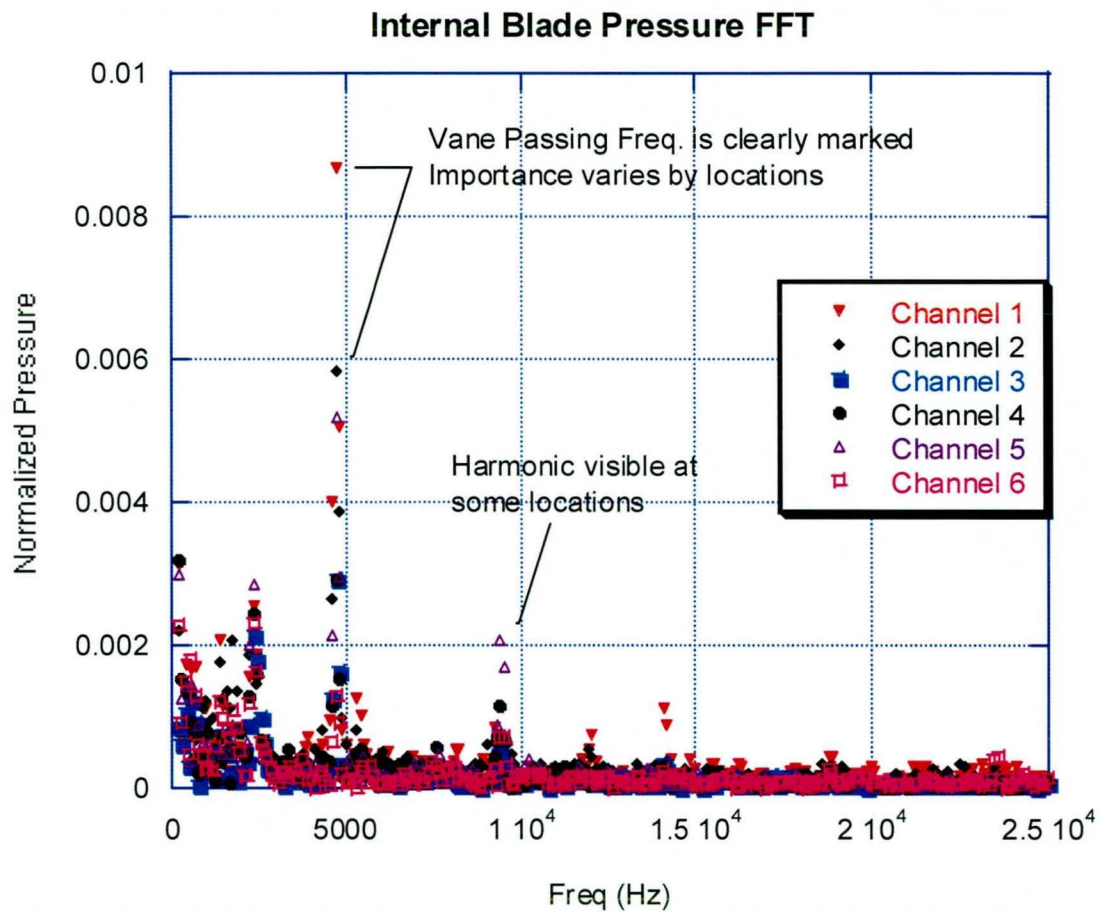


**Figure 51. FFT of Internal Pressure Measurements in Blade**

Twice in the above discussion, implications were made to the initial pressure in the LCF being set too low for this particular experiment. Figure 52 displays the normalized internal pressures for the inner vane, outer vane, rotor, and the LCF pressure during the experiment. From the data the rotor blade pressures increased and stabilized as expected. However, as mentioned in Section 3.1.2 the mass flow is divided into the three sections using six venturi chokes and requires a pressure ratio of approximately 2 across the venturi for the flow to remain choked. The inner vane cavity (which feeds the leading edge cooling holes) pressure measurements indicate that the pressure was stable

during the run but clearly did not maintain the pressure ratio with the LCF and unchoked. The outer vane cavity (which feeds the trailing edge slots) pressure measurements also unchoked late but increased throughout the experiment and stabilized late indicating that the section was starved of coolant gas. Due to the unchoking of the inner and outer vane sections at the venturi chokes the supplied mass flow is unknown after the initiation of the core flow.

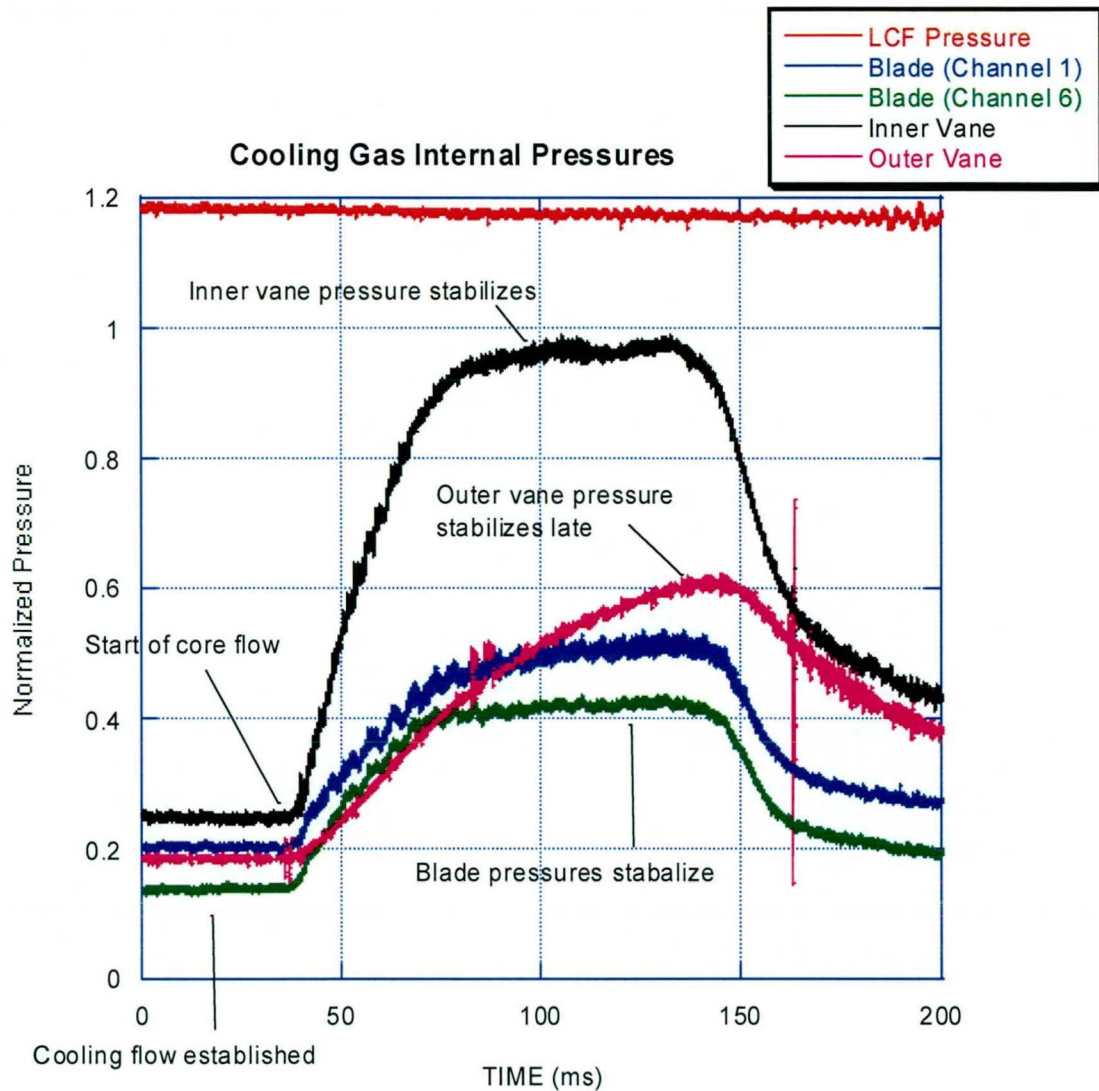


**Figure 52. Cooling Gas Internal Pressures**

### 5.2.2 Coolant Gas Mass Flow Calculations

The coolant gas mass flow to the rig is set by the temperature and pressure of the LCF and with six venturi chokes that divide the flow into the three sections between the exit of the LCF and the entrance to the super-cooler. Calculation of the mass flow is done at these venturi chokes and then again at the cooling exit holes for each of the three



sections. Verification that the mass flows are equivalent at both locations is a useful check done on each section to verify continuity in the experiment and to calculate the inherent leaks in the system feeding the rotor blades and the vane sections.

Calculating the mass flow supplied by the LCF first requires measuring the effective area of the venturi chokes with the super-cooler downstream using a blowdown experimental method (Equation 4 where  $C_g$  is a constant that is a function of temperature and gamma). Using in-house LabVIEW virtual instruments, the time constant ( $\tau$ ) is calculated based upon the differential pressure drop with time. With Equation 5 the mass flow is calculated using the effective area calculated from the blowdown experiments. Density is calculated from the static temperature and pressure measurements from Equation 3 where Mach number equals 1 and the total properties are measured from the LCF conditions. And velocity is calculated in the chokes where the Mach number equals 1. The mass flow delivered to each section of the rig is calculated using an area ratio of the venturi chokes with the total mass flow. Calculations are presented in Appendix C.

$$Choke\_Area = \frac{Volume}{\tau * C_g}, \quad C_g = \sqrt{\gamma R T_o} \left( \frac{\gamma - 1}{2} \right) \left( \frac{2}{\gamma + 1} \right)^{\frac{\gamma + 1}{2\gamma - 2}}$$

**Equation 4. Blowdown experimental relation [41]**

$$\dot{m} = \rho A V$$

**Equation 5. Mass Flow**

A discharge coefficient of 0.95 intrinsic to the super-cooler was measured by conducting area verification experiments using the blowdown experimental methods with the super-cooler connected downstream of the chokes. The verification experiments also

revealed several small leaks in the super-cooler, but when measured, all leaks were determined to be negligible.

Finding the mass flow at the blades and vanes is possible by using the measurements obtained after the cooling flow is established but before the core flow begins. During this time the pressure in the internal coolant plenums is sufficiently high to choke the flow through the cooling holes making the Mach number equal to 1 and the mass flow a simple function of the integrated cooling hole area and the supply temperature and pressure (Equation 5). The cooling hole area was previously measured for all of the blades using the blowdown experimental method previously discussed with Equation 4. However, only a few vanes were able to be flow tested due to time and experimental difficulties so the calculations were performed with the vane cooling hole areas in question.

For the vane, the internal coolant pressure and temperature sensors measure the static flow properties prior to entering the internal chambers of the vanes. Using the area Mach number relation in Equation 6 the Mach numbers at the sensors locations were small enough to deem the measurements as total properties of the coolant flow. The blade sensors are located inside the labyrinthine coolant passages of the blade where the cross-sectional area of the flow is unknown. Using an approximate cross sectional area and the area Mach number relation an approximate Mach number of 0.3 was obtained but as this is an assumption the effects will be investigated in the uncertainty analysis. The internal pressure used for the blade calculations is from channel 3 which is the only channel that measures the flow prior to any cooling holes exiting to the surface. With the isentropic gas flow equations shown in Equation 7 the static temperature and pressure

measurements at the film cooling hole exits can be calculated. Mass flow is then calculated using these values where the velocity is obtained from using  $\sqrt{\gamma RT^*}$ . The mass flow calculations for all three sections are carried out in Appendix C.

$$\left(\frac{A}{A^*}\right)^2 = \frac{1}{M^2} \left[ \frac{2}{\gamma+1} \left( 1 + \frac{\gamma-1}{2} M^2 \right) \right]^{\frac{\gamma+1}{\gamma-1}}$$

**Equation 6. Area Mach number relation**

$$\text{a.) } \frac{T^*}{T_o} = \frac{2}{\gamma+1} \quad \text{b.) } \frac{p^*}{p_o} = \left( \frac{2}{\gamma+1} \right)^{\frac{\gamma}{\gamma-1}}$$

**Equation 7. Isentropic gas flow equations with Mach number equal to 1**  
**a.) Temperature b.) Pressure**

The results of the mass flow calculations are located in Table 2. Calculations for the blade show an 8% difference between the mass flow supplied from the LCF and the mass flow calculated at the blade cooling exit holes. This difference is a combination of leaks and uncertainty of the calculations. As previously mentioned the results of the vane calculations are questionable due to the uncertainty of the cooling holes measured from the blowdown experiments.

Section	Mass Flow (lb/s)		Difference (lb/s)
	From LCF	At Airfoils	
Inner Vane	0.2354	0.2105	0.0249
Outer Vane	0.1296	0.0860	0.0436
Rotor	0.2227	0.2046	0.0181

**Table 2. Mass flows at venturi chokes and at the vanes and blades**

### 5.3 Uncertainty Analysis

Each uncertainty analysis will be comprised of two key parts: an error propagation analysis for parameters of the experiment conducted and a characterization of the behavior of the influence coefficients to aid in the direction of future experiments. The error propagation analysis uses influence coefficients to determine the key variables driving the uncertainty of the function. The influence coefficient is found from multiplying the partial derivative of a variable to the variable divided by the function. Overall uncertainty in the function is then calculated using Equation 8. Appendix D contains the error propagation analysis for the blowing ratio and mass flow calculations.

$$\text{Uncertainty\_in\_function} := \sqrt{\sum_i (\text{influence\_coefficients} \cdot \text{parameter\_uncertainty})^2}$$

#### Equation 8. Error Propagation Analysis

##### 5.3.1 Uncertainty in Blowing Ratio

The results of the error propagation analysis on the blowing ratio at the suction surface gill holes (cooling holes near leading edge) yield the influence coefficients given in Table 3. Uncertainties in the parameters are based on a peak to peak range of the measurements and are 0.25 psia for pressure measurements, 5.4°F for temperature, and approximated as 10% for the Mach number prediction. The total uncertainty in the blowing ratio as calculated is 11% with the key parameters influencing this error according to the influence coefficients is the pressure data and the Mach number.

Blowing Ratio Error Propagation Analysis at SS Gill Holes		
	Influence Coefficient	Parameter Uncertainty (%)
Static Pressure on Blade Surface	1.19	2.7
Coolant Gas Total Pressure	1.19	3
Core Flow Mach Number	1	10
Coolant Gas Total Temperature	0.5	1.1
Core Flow Static Temperature	0.5	0.9

**Table 3. Error Propagation Analysis for SS Gill Holes Blowing Ratio**

To characterize the effect the different variables have on the influence coefficients the coefficients are solved symbolically without any parameter input. If the result is a constant then the coefficient will not change for different operating conditions. This is the case of the temperature parameters and core flow local Mach number where the influence coefficients are 0.5 (temperature parameter) and 1 (Mach number parameter) for all operating conditions.

The influence coefficients associated with the coolant gas total pressure and the static pressure on blade surface are equal and a function of the coolant gas total pressure, static pressure, and gamma of the coolant flow. To characterize the coefficients that vary based on three variables the influence coefficient was plotted using a contour plot while holding different parameters to constant values. The plots (Appendix D.1) indicated an increase in the coefficient when the static pressure on the blade surface approached the coolant gas total pressure. Using this knowledge the coefficient function was rewritten as a function of gamma and a pressure ratio as displayed in Figure 53. From the results, gamma (x-axis) has very little effect on the coefficient but as the static pressure gets near the total pressure the influence coefficient increases dramatically. This serves as a clear

explanation of the unrealistic blowing ratio found in Figure 49 (Method B). Another look at the influence coefficients of the static and total pressure variables with a constant gamma (1.4) is displayed in Figure 54, which reveals the singularity between the variables. The lesson learned from Figure 53 and Figure 54 is to design experiments with a static-to-total pressure ratio below 0.9 for the coolant flow that also results in higher velocities of the coolant gas at the cooling hole exit.

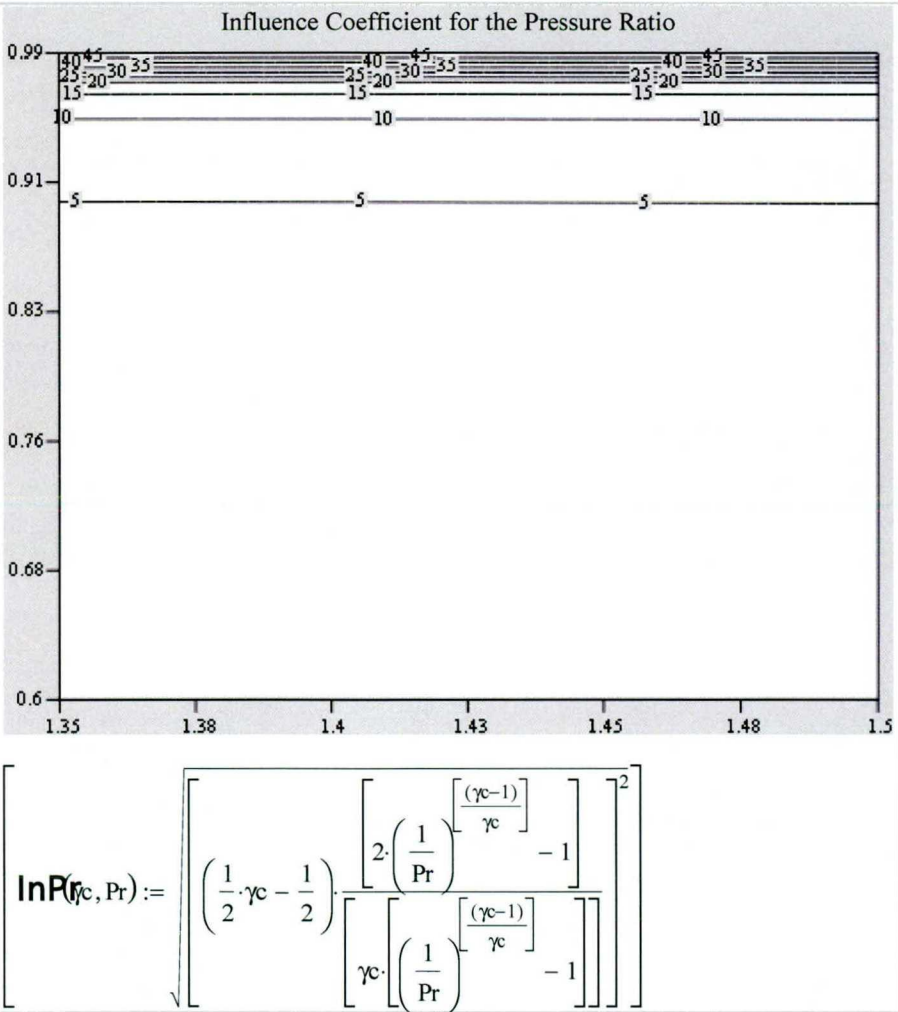


**Figure 53. Influence Coefficient for the Static to Total Pressure Ratio in Blade Cooling Hole (x-axis:  $\gamma_c$ , y-axis: Pr)**

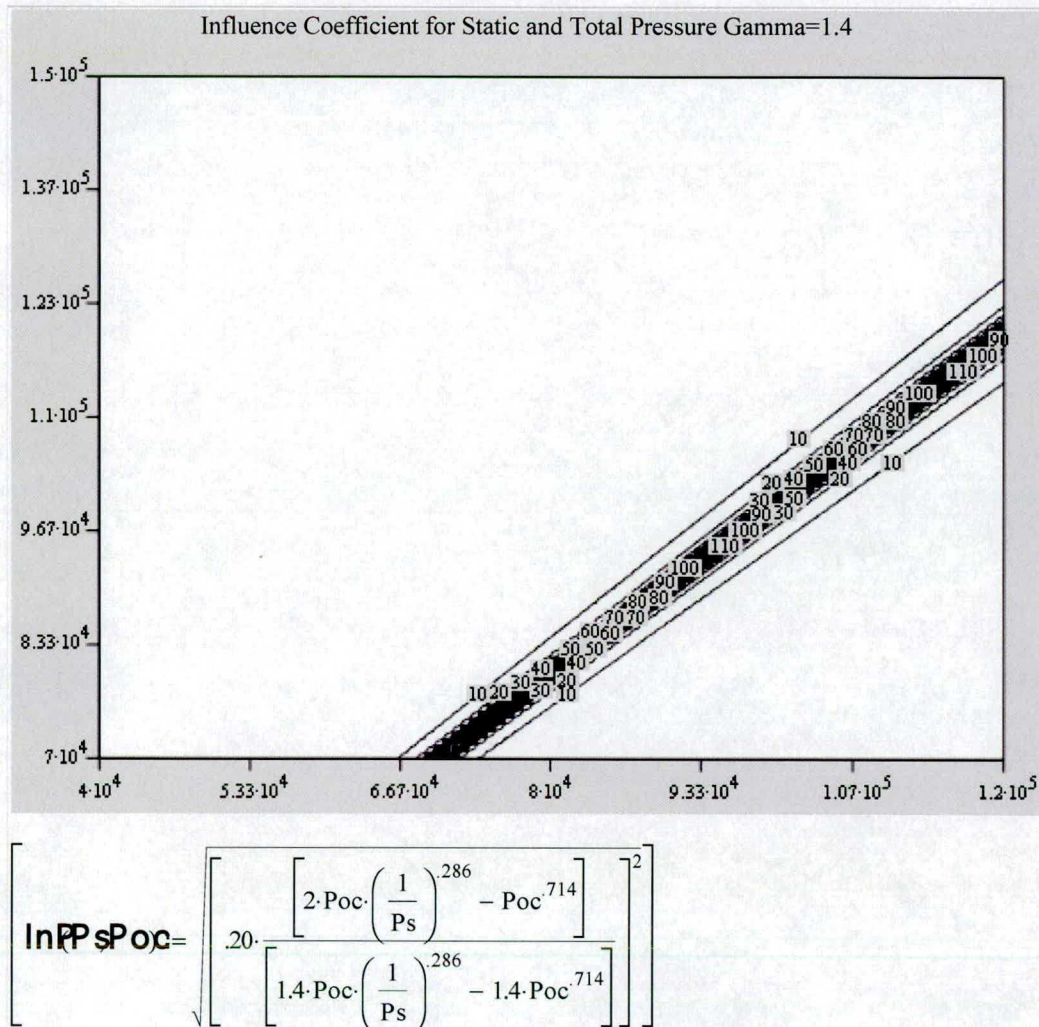


**Figure 54. Influence Coefficient for Static and Total Pressure Variables (Gamma=1.4) (x-axis:  $P_s$ , y-axis:  $P_{oc}$ )**

### 5.3.2 Uncertainty in Mass Flow Supplied by LCF

Conducting the error propagation analysis on the mass flow supplied by the LCF reveals that all of the parameters with the exception of gamma equally contribute to the overall uncertainty in the mass flow calculations which total 1.2%. Parameter uncertainties for these measurements are calculated based on accuracies of 0.075 psia for pressure (calibration accuracy), 0.45°F for Temperature (RTD calibration), and 0.5 s for

the time constant ( $\tau$ ) as in Table 4. Symbolically solving for the influence coefficients shows the coefficient associated with  $\gamma$  varies as a function of  $\gamma$  alone and the other coefficients remain constants. Figure 55 is a plot that shows that the change in influence coefficient verse  $\gamma$  remains small enough that when combined with the uncertainty in  $\gamma$  it is sufficiently small and the parameter can be neglected in the total mass flow uncertainty calculation.

Error Propagation Analysis for Mass Flow Supplied by LCF		
	Influence Coefficient	Parameter Uncertainty (%)
Total Pressure	1	0.2
Total Temperature	1	0.1
Tau	1	0.6
Volume of LCF	1	1
Gamma	3.452	0.04

**Table 4. Error Propagation Analysis for Mass Flow Supplied by LCF**

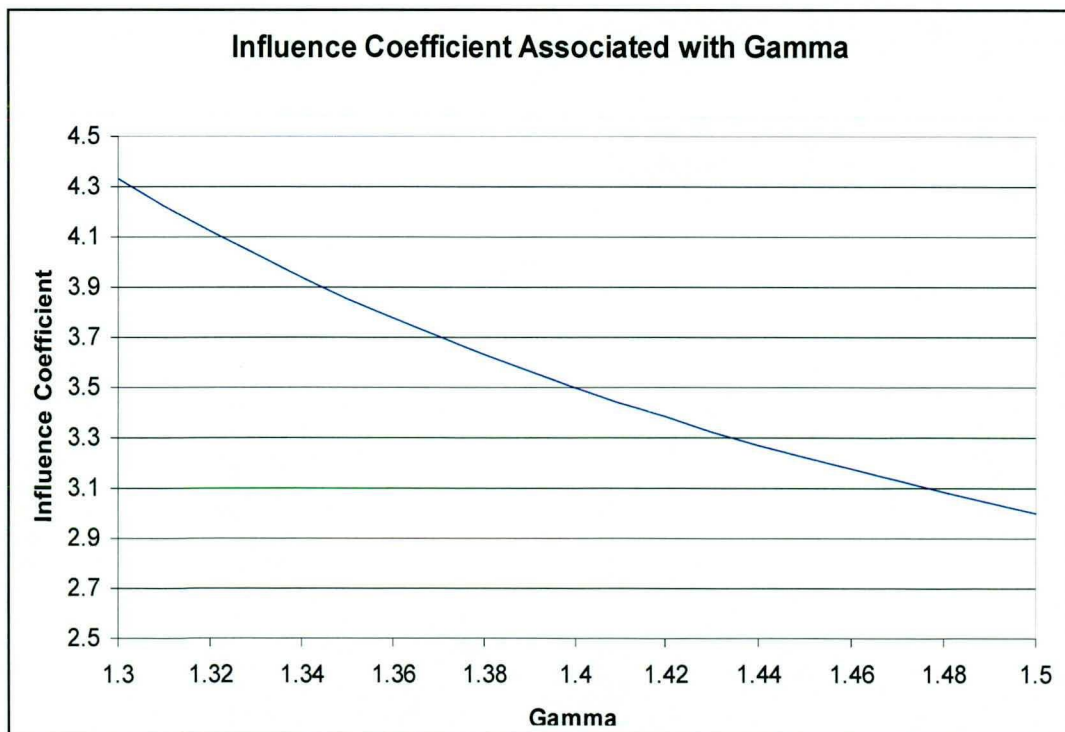


**Figure 55. Influence Coefficient for Gamma**



### 5.3.3 Uncertainty in Mass Flow at Rotor Blade Cooling Holes

The error propagation analysis on the mass flow calculations at the blade cooling holes exposes the integrated effective area of the cooling holes and the pressure measurement as the two key parameters driving the overall uncertainty of 4%.

Uncertainties in the parameters were calculated using the peak to peak variation 0.25 psia for the pressure and 5.4°F for the temperature. The uncertainty in the area measurements was calculated by using the average of peak to peak variations on each blade for multiple blades. A standard deviation of the blade area or a peak to peak variation over all of the blades would not accurately describe the uncertainty in cooling hole area since the blade cooling hole configurations vary slightly. The 10% uncertainty in the Mach numbers over the sensors was selected to be a conservative value.

Error Propagation Analysis for Mass Flow at the Rotor Blade Cooling Holes		
	Influence Coefficient	Parameter Uncertainty (%)
Pressure Measured	1	3.4
Temperature Measured	0.5	1.1
Mach number at Pressure Transducer (Mp)	0.124	10
Mach number at Temperature Sensor (Mt)	0.018	10
Integrated Area of the Cooling Holes	1	1.5
Gamma	0.345	0.04

**Table 5. Error Propagation Analysis for Mass Flow Calculated at Rotor Blade Cooling Holes**

From solving for the influence coefficients symbolically, the coefficients associated with the area, pressure, and the temperature measurements are all constant and remain the key drivers in the overall uncertainty for different operating conditions. The influence coefficient associated with the Mach number (Mp) of the flow over the pressure transducer is a function of gamma and Mp. Likewise the influence coefficient with the

Mach number over the temperature sensor is a function of gamma and Mt. From the contour plots in Figure 56 and Figure 57, gamma (x-axis) has little effect on either influence coefficient. Mach numbers do have an effect on the coefficients (pressure more than temperature) but while dealing with low Mach numbers the influence coefficients remain small compared to the pressure and area coefficients. The influence coefficient associated with gamma is a function of gamma, Mp, and Mt. Since it has been shown that gamma has little effect on the Mp and Mt Mach numbers the coefficient is presented as a function of Mp and Mt where gamma assumed to be constant at 1.4 in Figure 58. The coefficient is influenced more by Mt (y-axis) than Mp (x-axis) but with the small uncertainty in gamma all of the coefficients in Figure 58 are small enough to be neglected when calculating the total uncertainty.

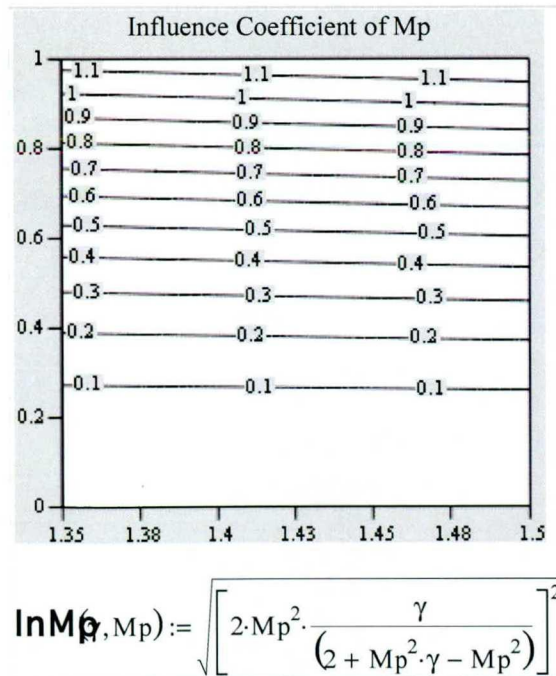


**Figure 56. Influence Coefficient for Mp (x-axis:  $\gamma$ , y-axis: Mp)**

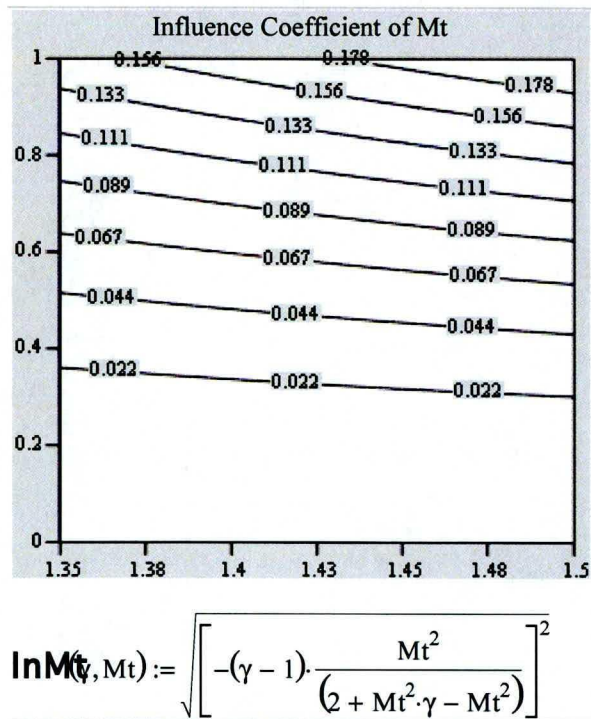
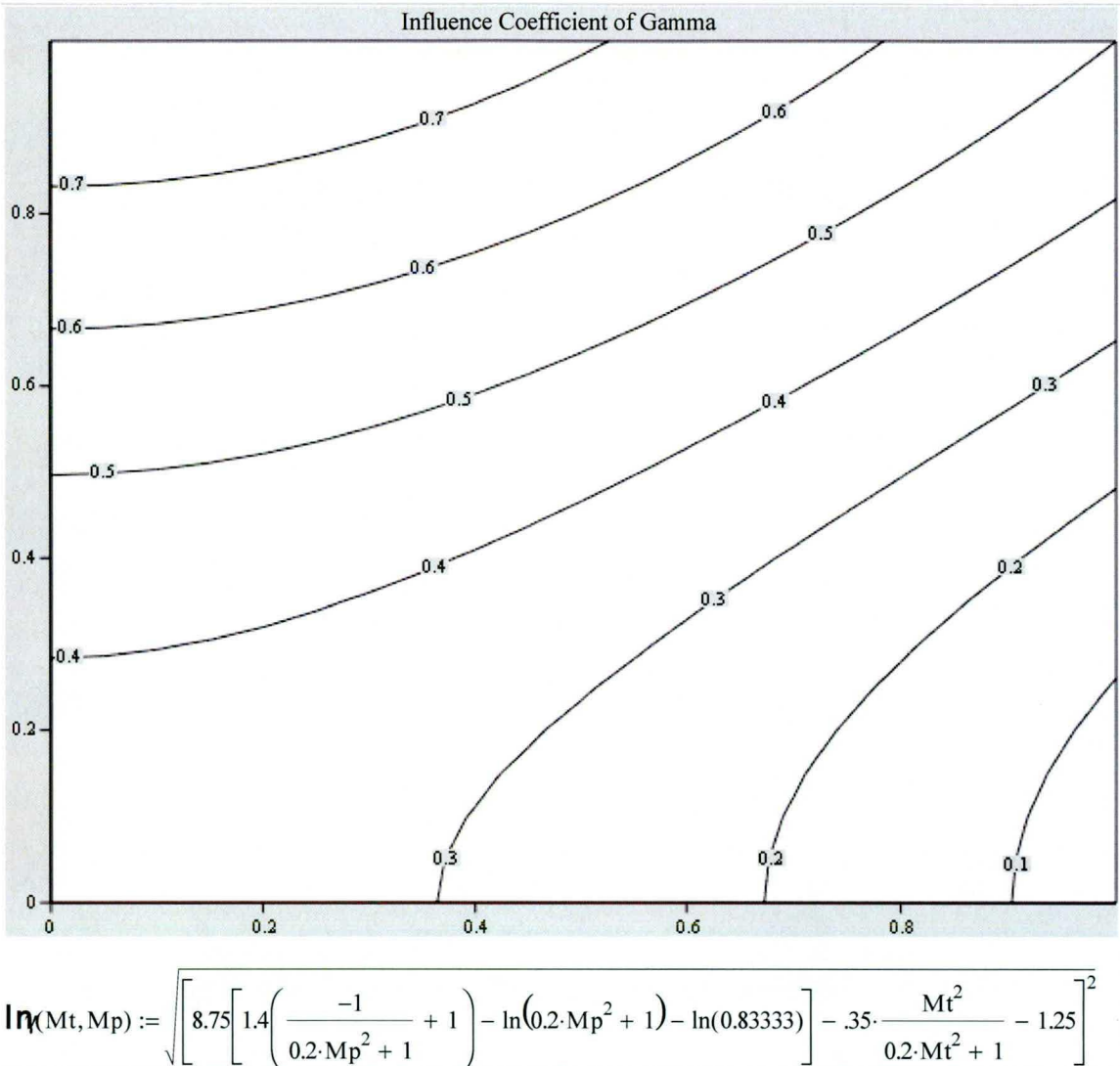


Figure 57. Influence Coefficient for Mt (x-axis:  $\gamma$ , y-axis: Mt)



**Figure 58. Influence Coefficient for Gamma (x-axis: Mt, y-axis: Mp)**

#### 5.4 Future Experimentation

From the data results presented and the uncertainty analysis future experiments can be designed to better understand the cooling flow physics and assumptions. Figure 50 presented the internal channel pressures in the blade, which decreased as the coolant gas traveled through the labyrinthine coolant passages. This pressure drop could be attributed to the decrease in mass flow from the film cooling which would increase the

speed of the flow making the measurement a static property of the flow. Or, it is more likely that the assumption of a constant total pressure (Method A) for the coolant gas is incorrect. Conducting an experiment with higher coolant pressure will either clarify which assumption is most accurate or it will result in a smaller pressure drop in the internal channels showing both assumptions are comparable.

A rule of thumb for future experiments can be directly derived from the blowing ratio uncertainty analysis: Avoid a static to total coolant pressure ratio above 0.9 (which makes a lot of sense physically) in the cooling holes consequently keeping the coolant gas Mach number above 0.4 at the exit of the cooling holes. Pressure ratios near 1 indicate a very low coolant flow Mach number, which is associated with the singularity in Figure 54 and high uncertainty. Using this rule the uncertainty in the blowing ratio should be reasonable (below 20%) and will allow for more accurate blowing ratios above 0.5.

To compare the mass flows calculated as supplied by the LCF and calculated at the cooling holes requires accurate knowledge of the vane cooling hole areas and experiments designed to decrease the uncertainties in the calculations. It is not feasible to flow test (blowdown experimental method) all of the vanes at this time so the two vane sections can be calculated as a unit in the rig. Using an experimental setup designed to reduce the uncertainties in the mass flow calculations the vane areas can be calculated based on the mass flow supplied by the LCF. To do this the experiment should be designed for high-pressure coolant flow to decrease the uncertainty in the pressure measurement. Operating at an elevated temperature would also help to reduce the uncertainty but will have a minimal effect compared to the pressure and is unfavorable

when conducting film cooling experiments due to the design temperature ratios needed. Using a statistical average the experiments should yield an accurate and repeatable area measurement for the inner and outer vane sections. Most importantly from the experiments the leakage in the labyrinth seal around the rotor can be measured. Knowledge of the leakage can allow proper adjustment in sizing the venturi chokes for proper coolant gas mass flow distribution and also aid in the seal design for future experimental rigs.

## **CHAPTER 6**

### **CONCLUSIONS**

Measurements have now been obtained for a fully cooled high-pressure turbine stage operating at design corrected conditions. This thesis describes the current experimental approach, the integration of a coolant gas supply system with the turbine stage, several important details of performing the experiment, and presentation of some of the initial results of the measurement. Integration of the cooling gas supply system with the blowdown facility housing the turbine stage was an integral part of this thesis effort. This included detailed research related to the operation, control, and cooling cycle of the cooling gas supply along with the activation system to allow the coolant gas to become fully established prior to initiation of the core flow.

The experimental results have been used to calculate the blowing ratio for selected locations on the blade and these values are shown to compare favorably with the design values. In addition, coolant gas mass flow was calculated for two specific locations and shown to compare favorably with the anticipated values. The results of the blowing ratio calculation suggest that for the experimental condition used for the calculations presented in this thesis the initial charge pressure in the coolant supply tank was a bit lower than desired. This is an easy problem to fix and the pressure will be increased for subsequent experiments. The low coolant charge pressure was verified in

that the inner and outer vane sections unchoked and the outer vane pressures stabilized quite late during the test time period.

The design of future experiments has been assisted by the uncertainty analysis conducted as part of this thesis. Low blowing ratio calculations can be foreseen to be associated with a large uncertainty similar to any small measurement (e.g. pressure transducers have higher noise to signal ratios at lower pressures). However, the key to the blowing ratio is to keep the coolant gas Mach number at the cooling hole exit above 0.4 or likewise the static-to-total coolant pressure ratio below 0.9. Using a guideline of keeping the blowing ratio above 0.5 is not sufficient due to the possibility of higher blowing ratios resulting from the low local Mach number near the leading edge of the pressure surface as seen in Figure 46. Film-cooling experiments typically require blowing ratios above 1 which also include higher coolant gas Mach numbers and should not be a concern, but it is very important to remember when designing experiments for off-design engine operation.

Verification that the calculated mass flow of coolant gas supplied by the LCF is approximately equal to that determined at the respective cooling holes is a necessary step to obtain an indication of potential leaks in the coolant gas supply system. Little focus was placed on the mass flow verification because of some uncertainty in the vane cooling hole area measurements. However, using properly design experiments it is possible to determine the vane cooling hole areas.

Reducing the uncertainty in the calculations requires increased accuracies of two key parameters as determined from the error propagation calculations; all pressure measurements, and the local Mach number prediction of the flow. Increasing the supply



pressure helps with the uncertainty because in doing so one effectively decreases the noise to signal ratio.

With the successful operation and integration of the LCF with the TTF, the OSU GTL has the ability to design and conduct a multitude of film cooling experiments. Current experiments are ongoing to produce the film cooling film effectiveness data results for the entire turbine stage. Future work is likely to include (but not limited to) film-cooling results on the blade platform and tip regions.

## **APPENDIX A**

### **EXPERIMENTAL RESULTS OF FAV TO UNDERSTAND “HIC-CUP”**

The following experimental test matrix and results show an attempt to characterize the “hic-cup” which occurred in the FAV opening sequence. Variables in the test matrix included LCF pressure, LCF temperature, valve activation pressure, test section pressure, and a test section bleed. The experiments produced inconclusive results as to which variable may be the driving factor. In the following tables the highlighted columns are the expected operating conditions in which the film cooling experiments will be conducted.

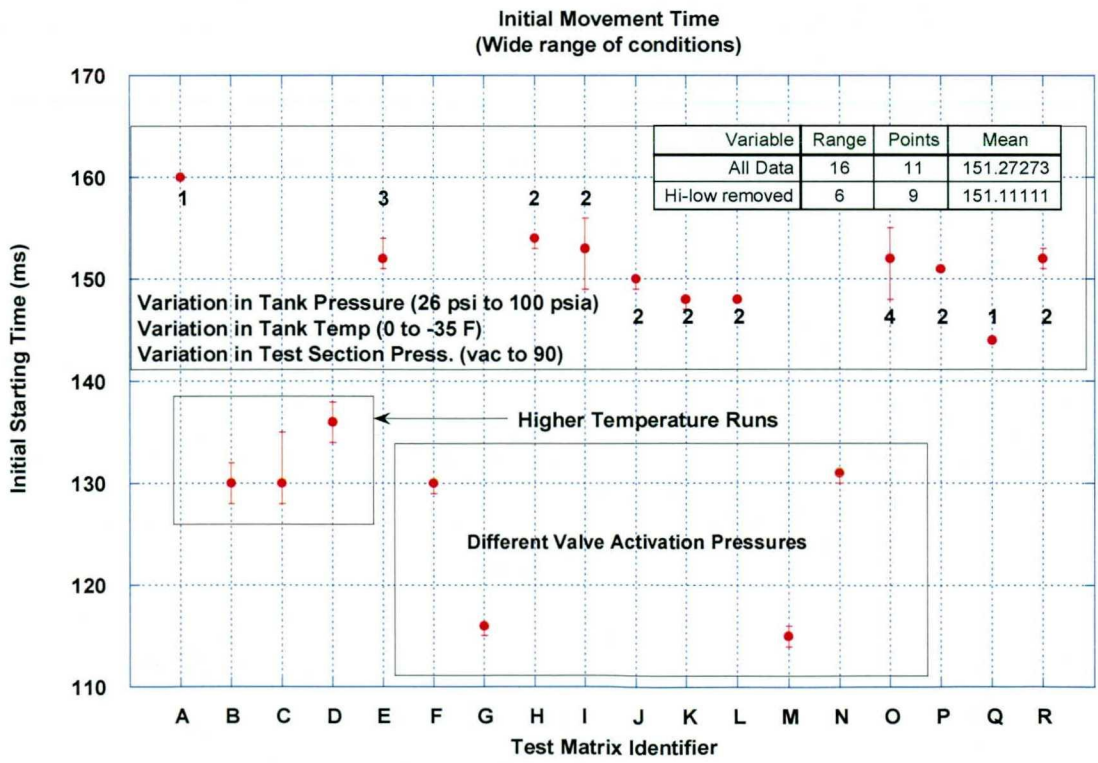
	Tank Pressure			Temperature			Test Section Bleed				Test Section Pressure				VAP (psia)			
	14.3	~26	75 to 90	>0	0 to -30	-30 to -40	Closed	Partial open	Open	Removed	14.3	Vac	equal	E/w Tank/atm	Above Tank P	75	100	120
A		X				X	X					X				X		
B		X		X			X								X	X		
C		X		X			X			X						X		
D		X		X			X					X				X		
E			X			X	X					X				X		
F			X			X	X					X					X	
G			X			X	X					X						X
H			X		X		X						X			X		
I			X		X		X			X						X		
J			X		X			X		X						X		
K			X		X			X		X						X		
L			X		X				X	X						X		
M					X		X					X						X
N					X		X					X					X	
O					X		X					X				X		
P					X		X							X		X		
Q					X		X						X			X		
R					X		X			X						X		

\*Highlighted columns indicate expected Ureti condition.

VAP: Valve Activation Pressure

	Tests	Start of Movement		Time for Valve to Unchoke		Total Pressure Difference Tank - T.S.
		Average	Range	Average	Range	
A	1	160		174		26
B	5	130	±2	144	±2.5	-50
C	4	130	±3.5	144	±3	8
D	2	136	±2	149	±2	26
E	3	152	±1.5	190	±2.5	86
F	2	130	±0.5	158	±0.5	80
G	2	116	±0.5	130	±0.5	80
H	2	154	±0.5	182	±1.5	64
I	2	153	±3.5	183	±2.5	68
J	2	150	±0.5	180	±0.0	64
K	2	148	±0.5	179	±0.5	64
L	2	148	±0.0	178	±0.0	64
M	2	115	±1	145	±0.0	95
N	2	131	±0.5	165	±0.0	95
O	4	152	±3.5	190	±1.5	95
P	2	151	±0.0	169	±1.5	30.5
Q	1	144		160		0
R	2	152	±1	185	±1	81

Notice the small ranges for each set of tests.

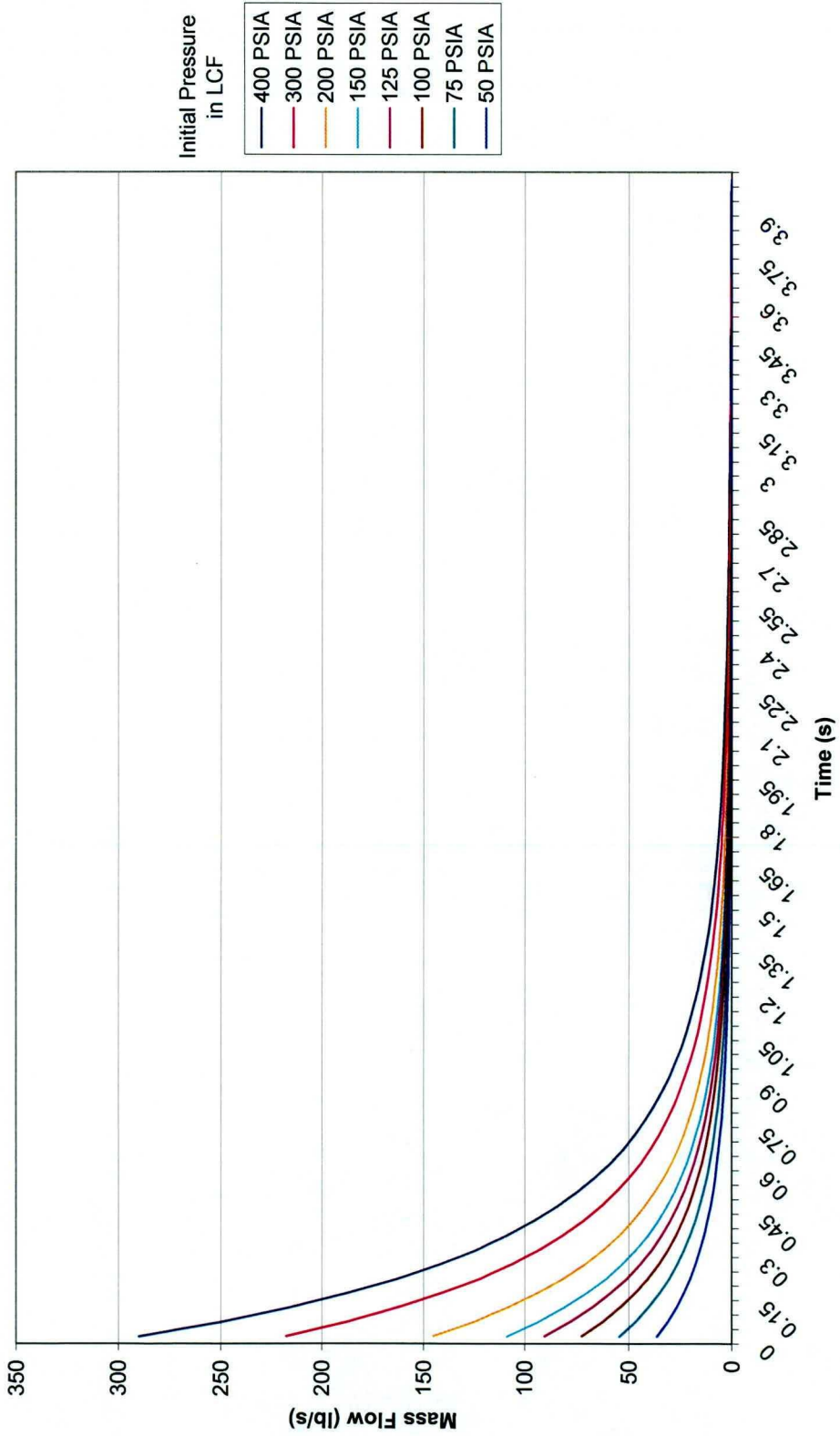


## **APPENDIX B**

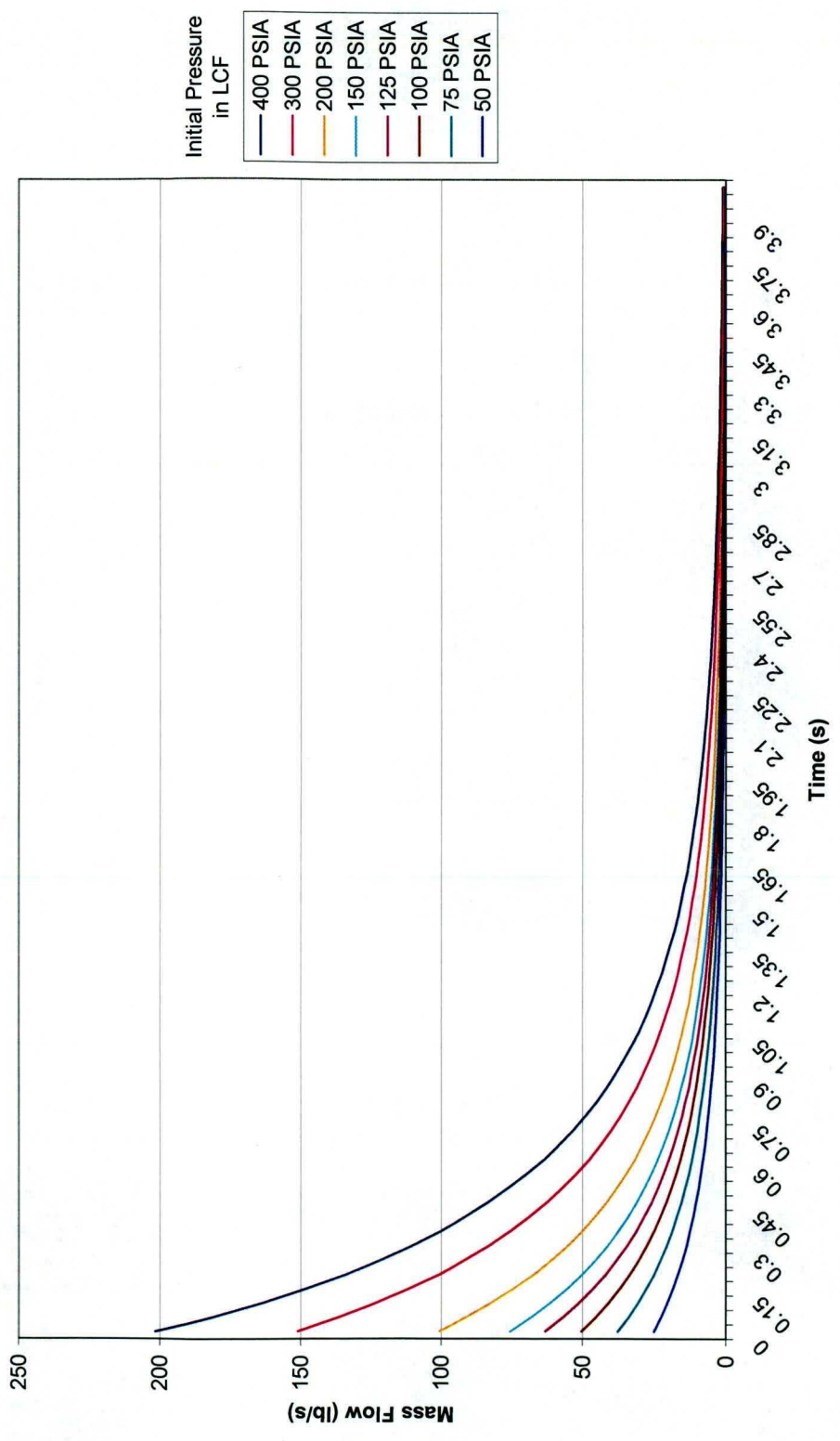
### **LCF CHARACTERIZATION CHARTS**

As a design aid to future experiments the mass flow capabilities of the LCF was characterized using a series of charts. The charts plot the mass flow as a function of time for a given choke area, initial pressure, and initial temperature. Initial temperature values were determined from the current experimental setup by using the low temperature attainable from only using the Julabo chiller (-30°F) and using both the Julabo and the FTS chillers (-45°F). Using the charts researchers can determine approximately what initial pressure is required in the LCF to provide the design mass flow when the initial temperature and estimated delay (time required to establish cooling flow) are known.

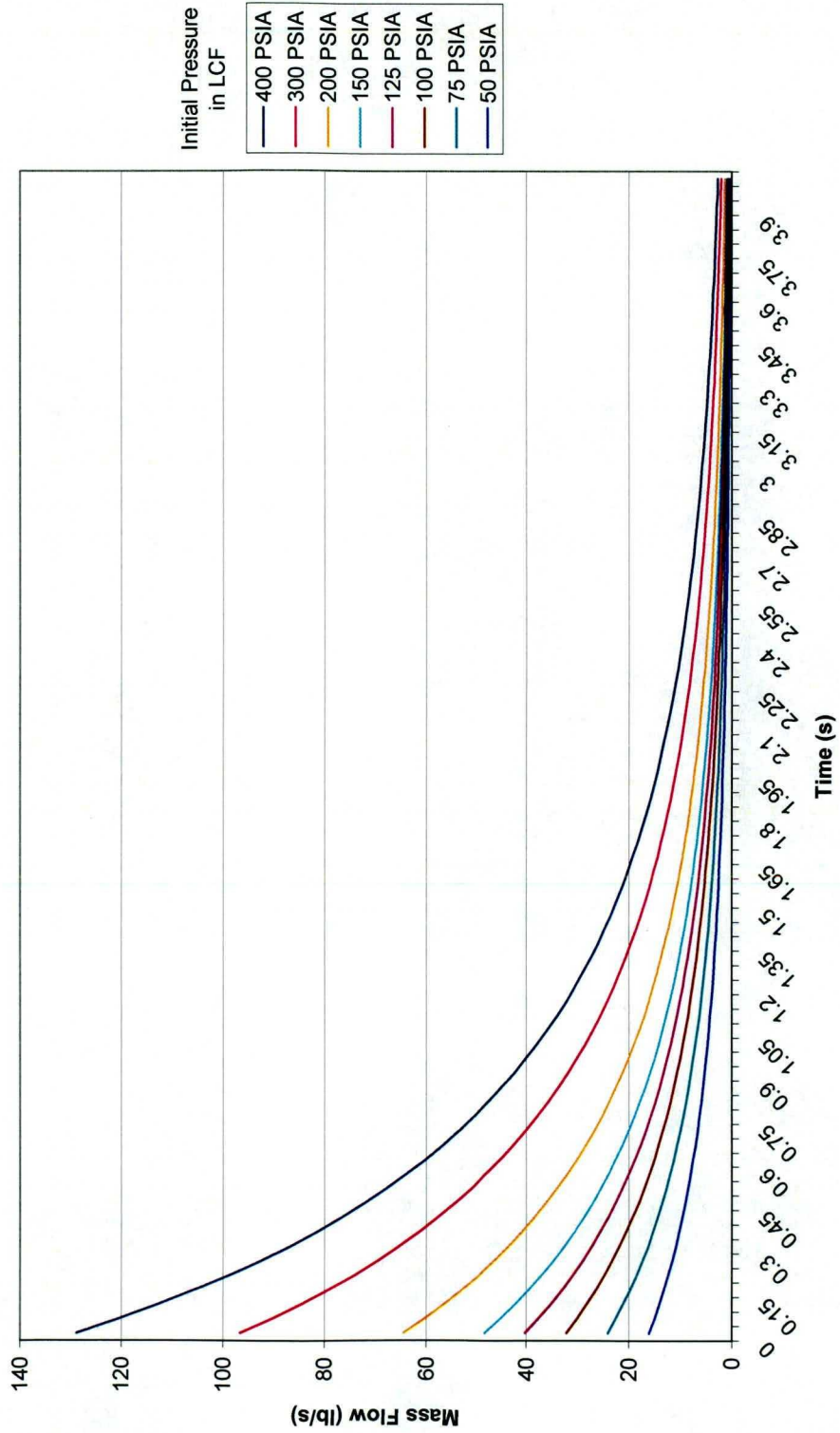
**6" Diameter Choke (Max flow from LCF)**  
**T<sub>o</sub> = -30 F**



5" Diameter Choke  
To=-30 F

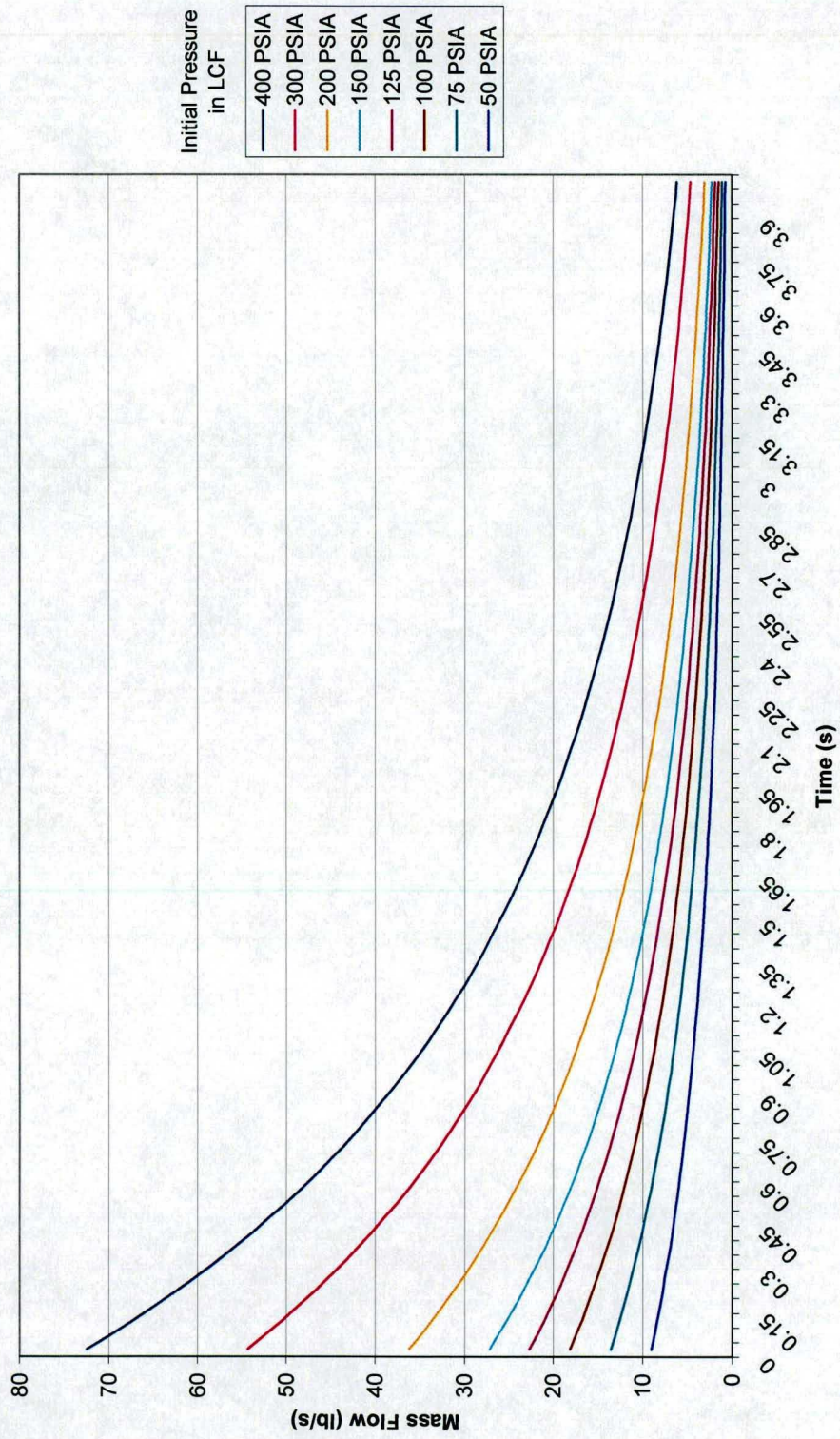


**4" Diameter Choke  
To=-30 F**

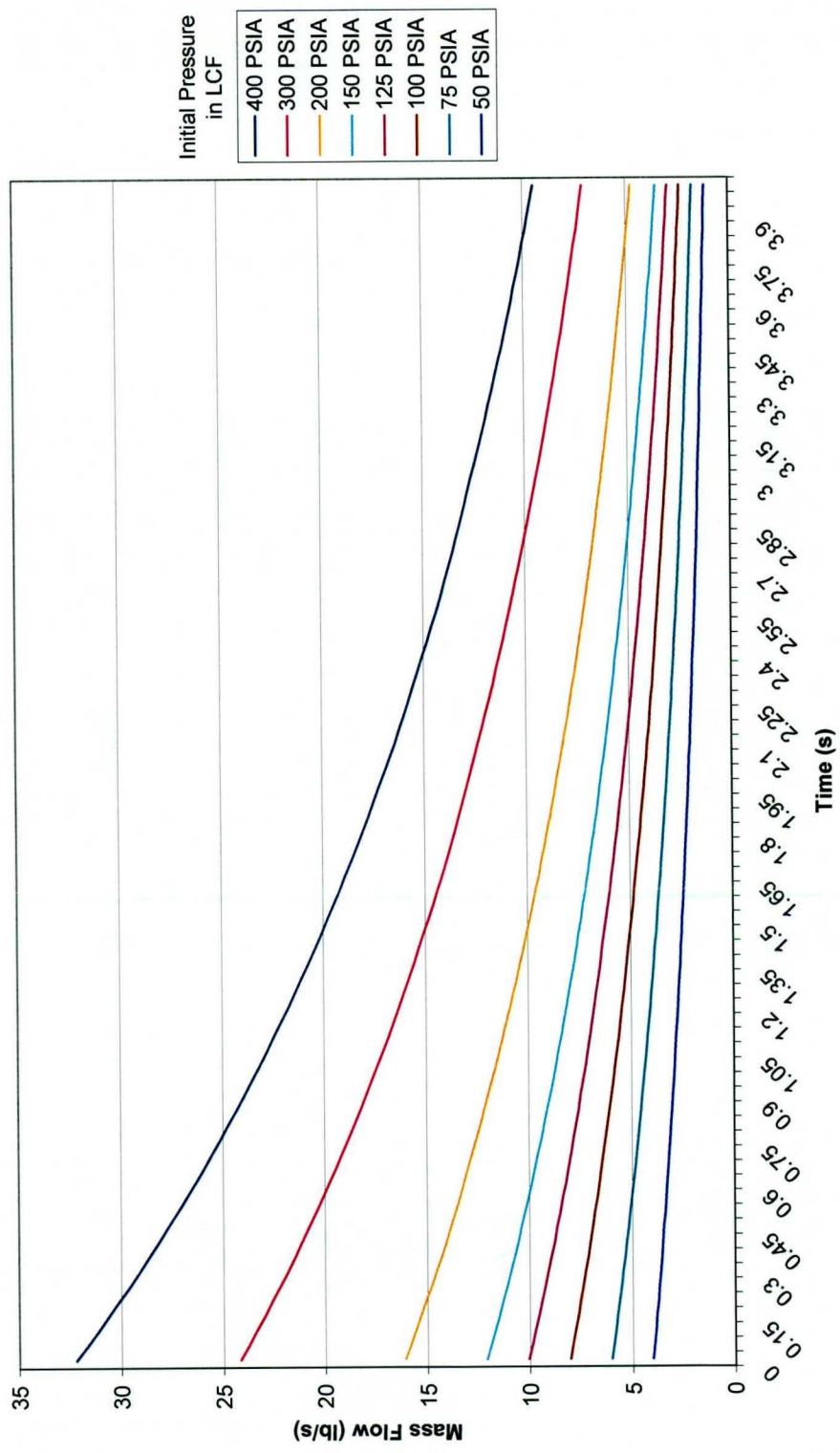




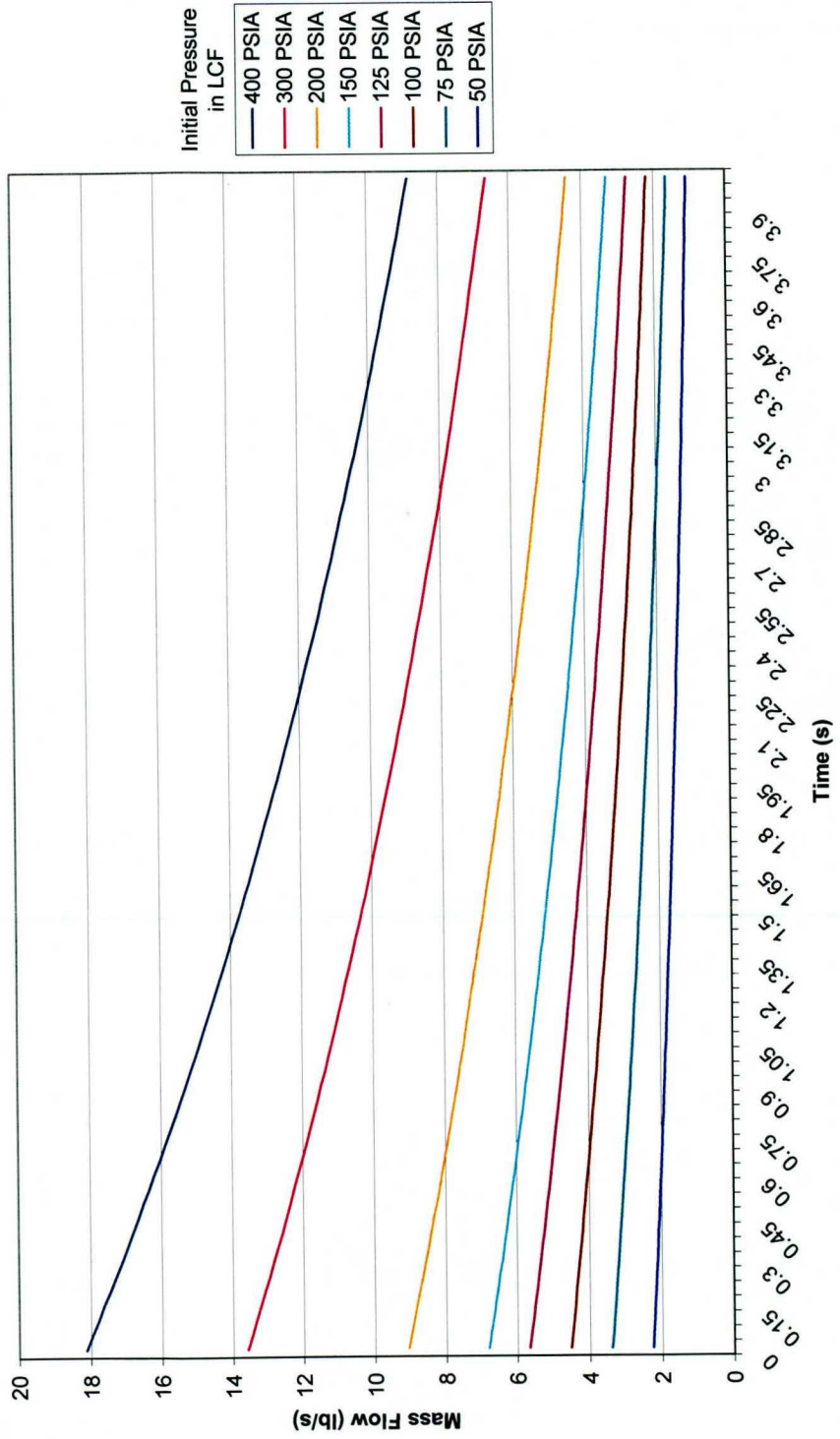
3" Diameter Choke  
To=-30 F



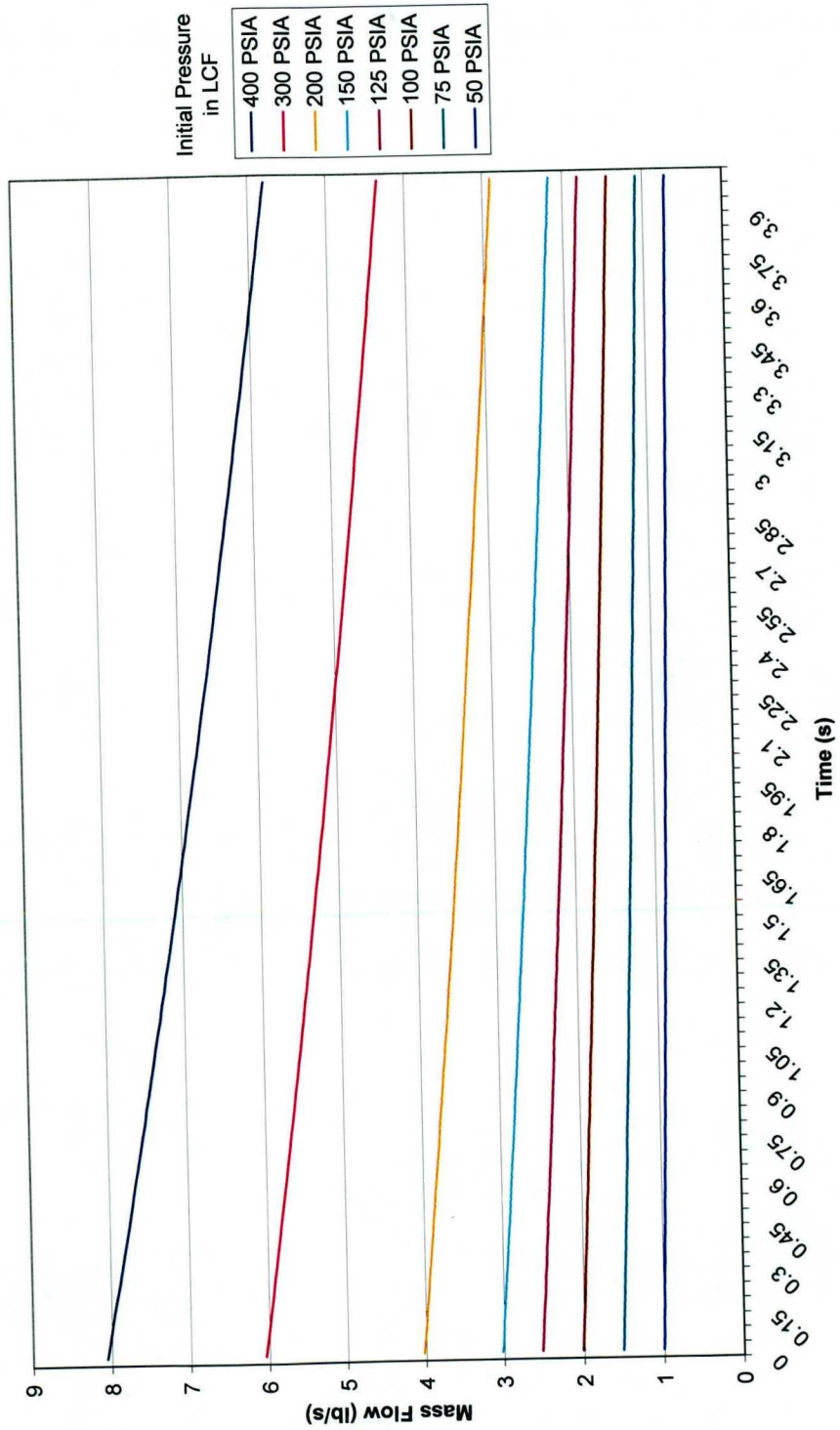
2" Diameter Choke  
To=-30 F



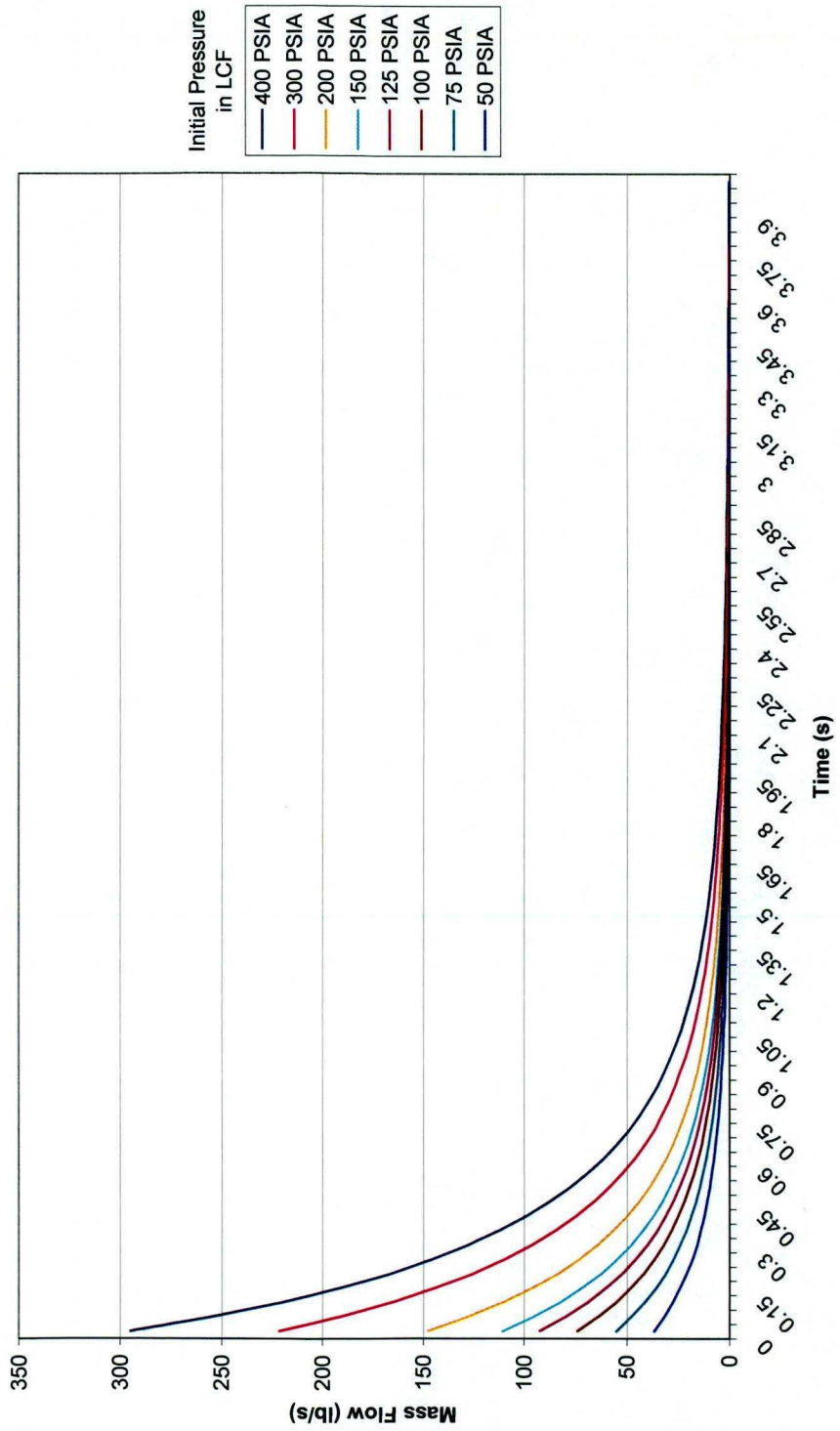
**1.5" Diameter Choke  
To=-30 F**



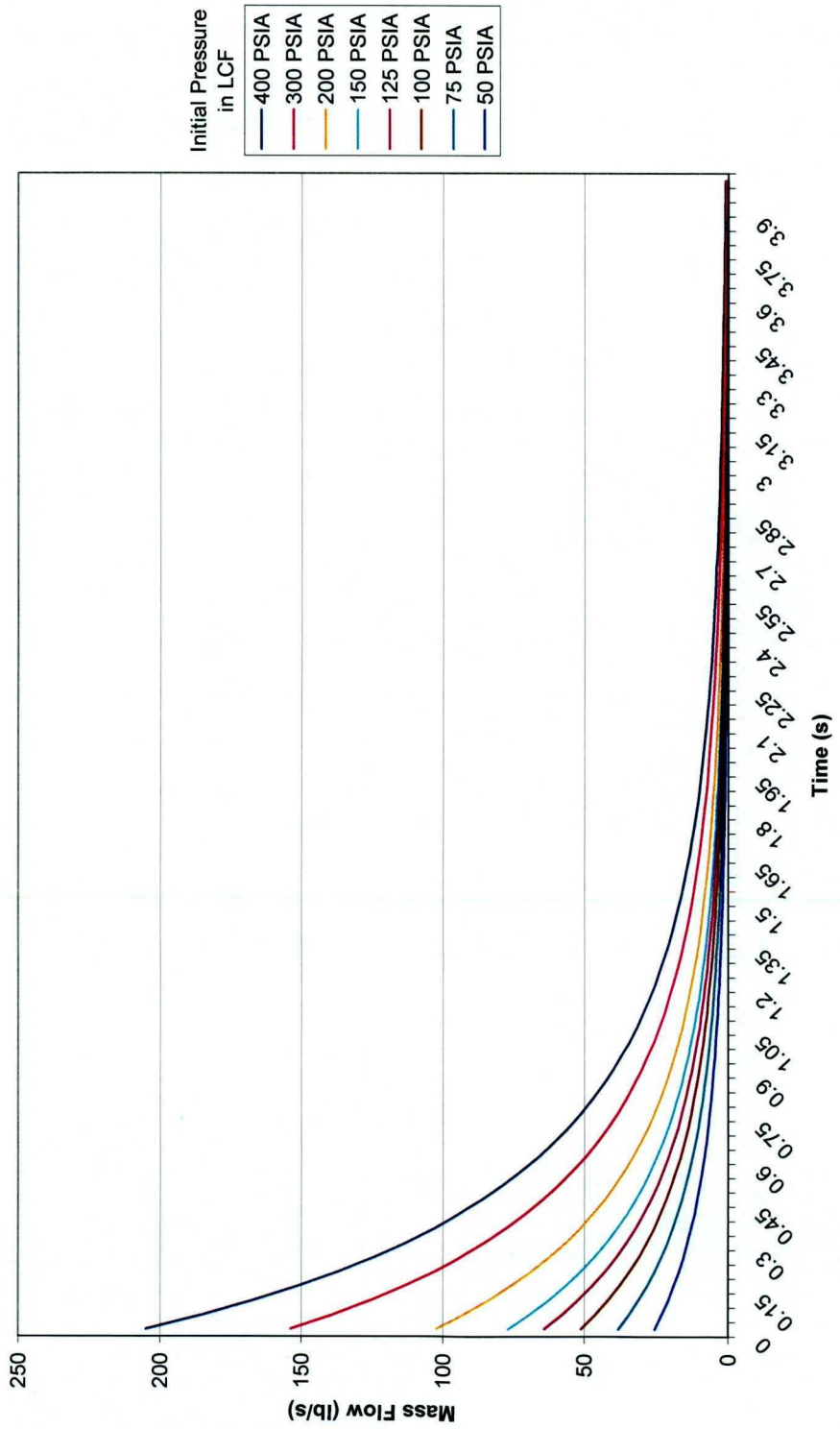
1" Diameter Choke  
To=-30 F



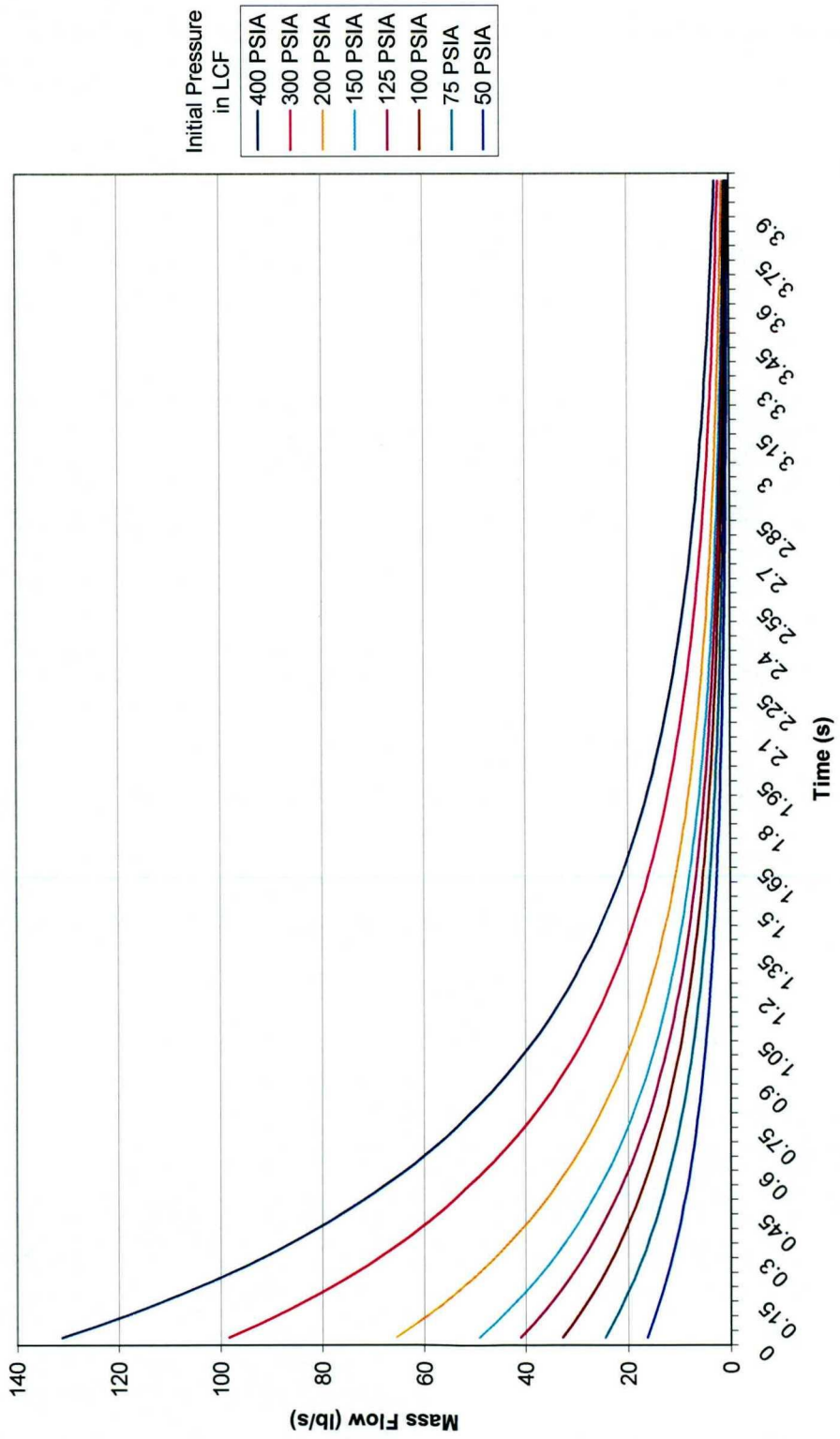
**6" Diameter Choke (Max flow from LCF)  
To=-45 F**



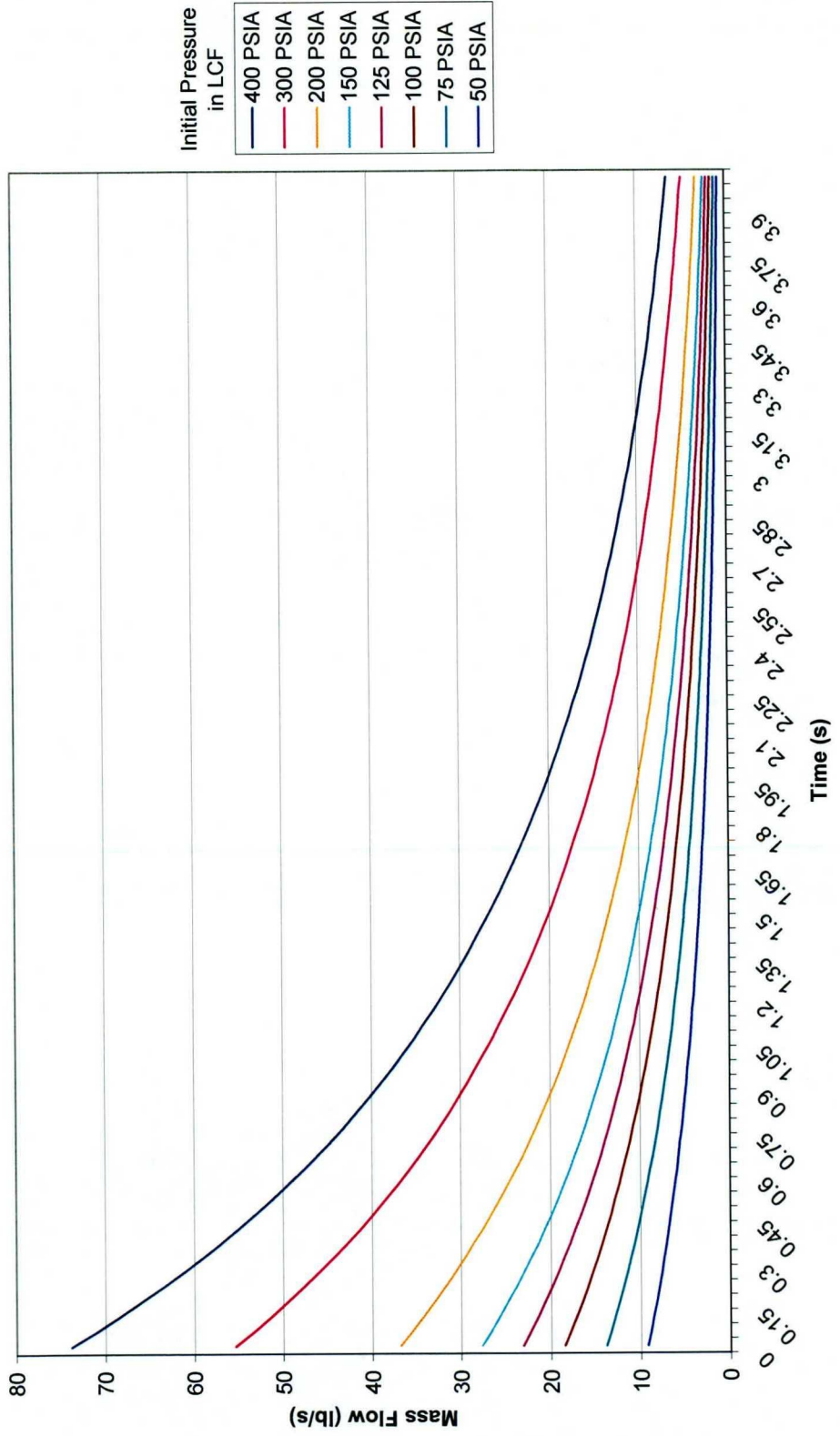
**5" Diameter Choke  
To=-45 F**



4" Diameter Choke  
T<sub>o</sub>=45 F

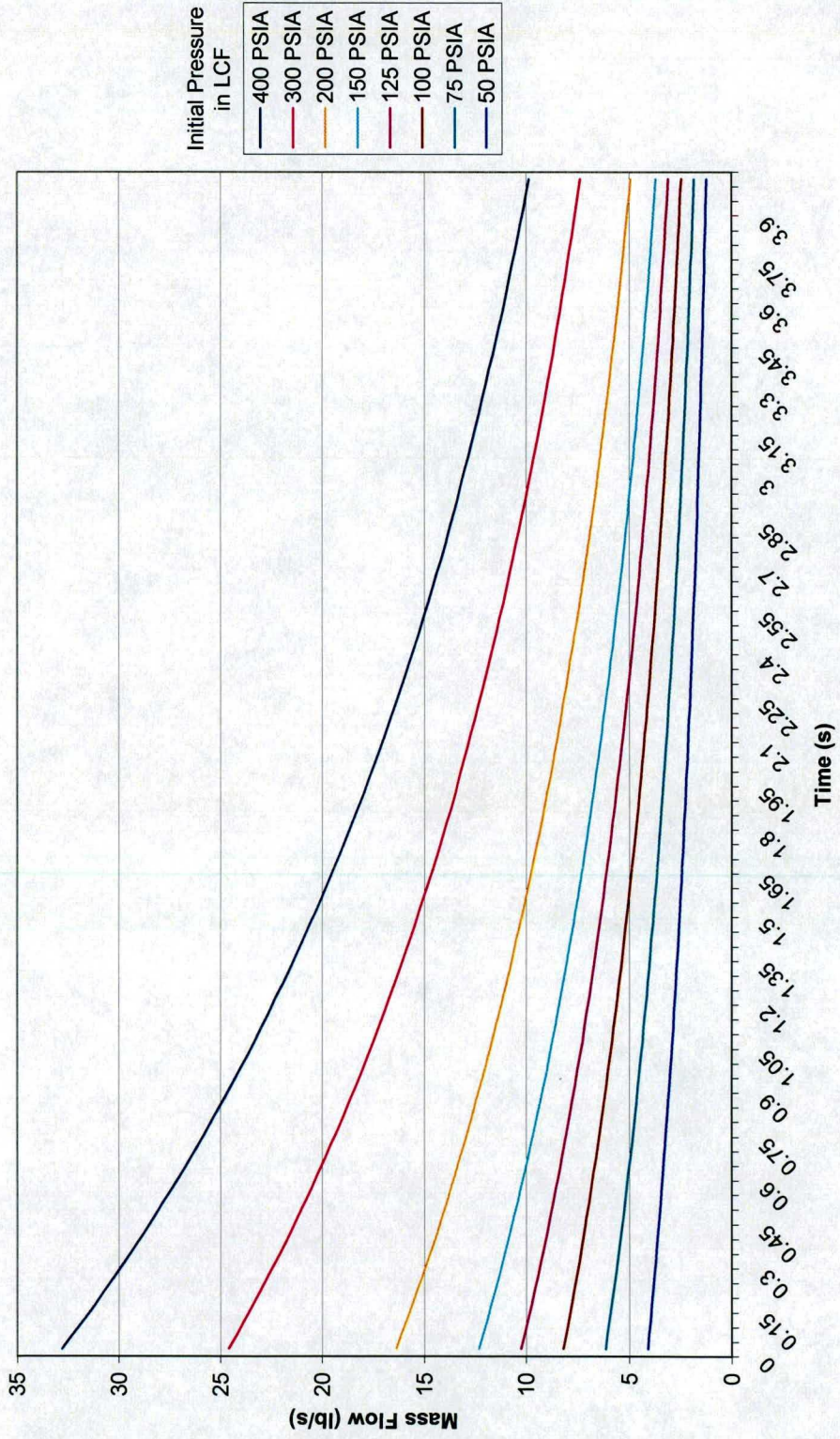


**3" Diameter Choke  
To=-45 F**

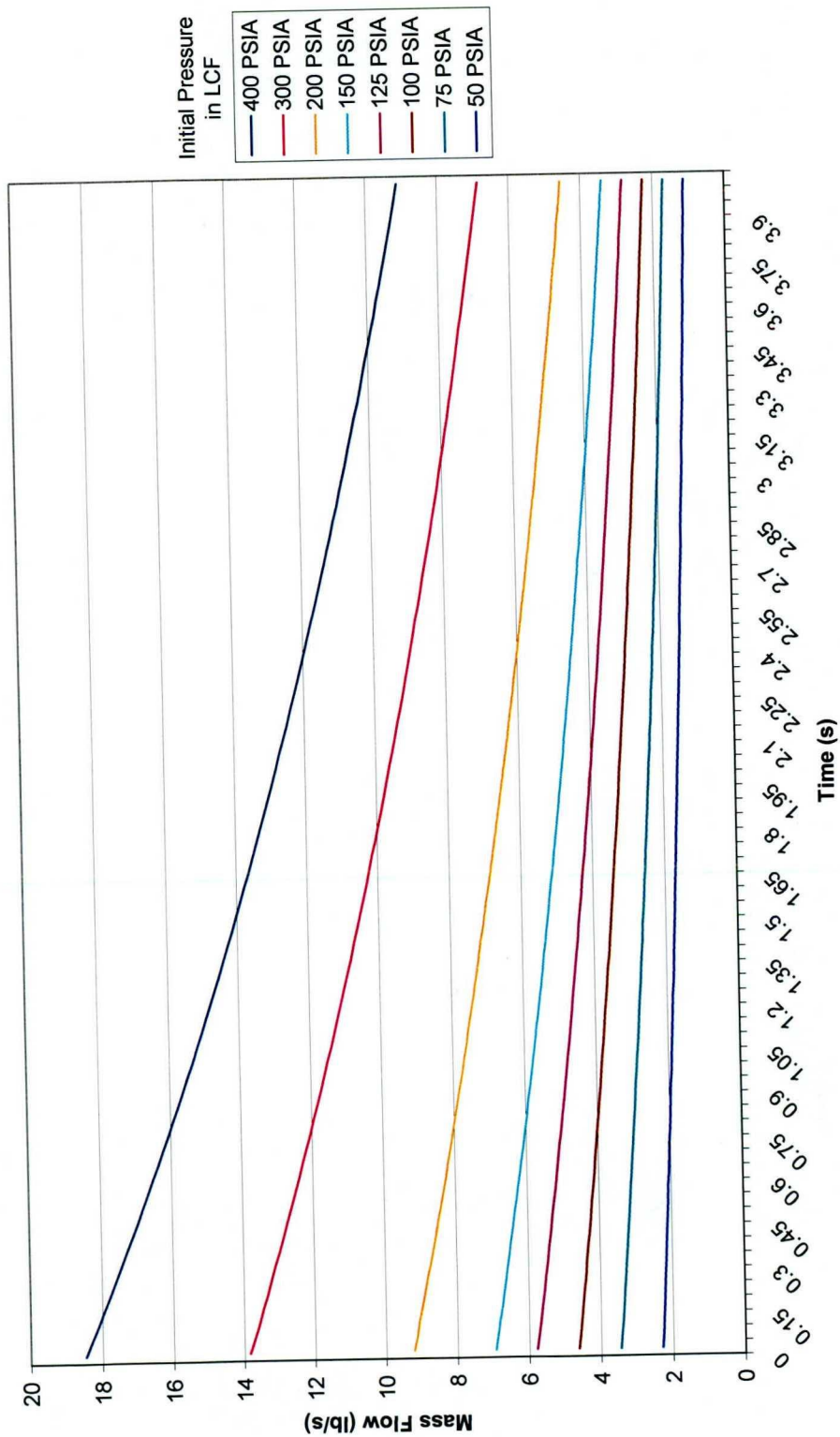




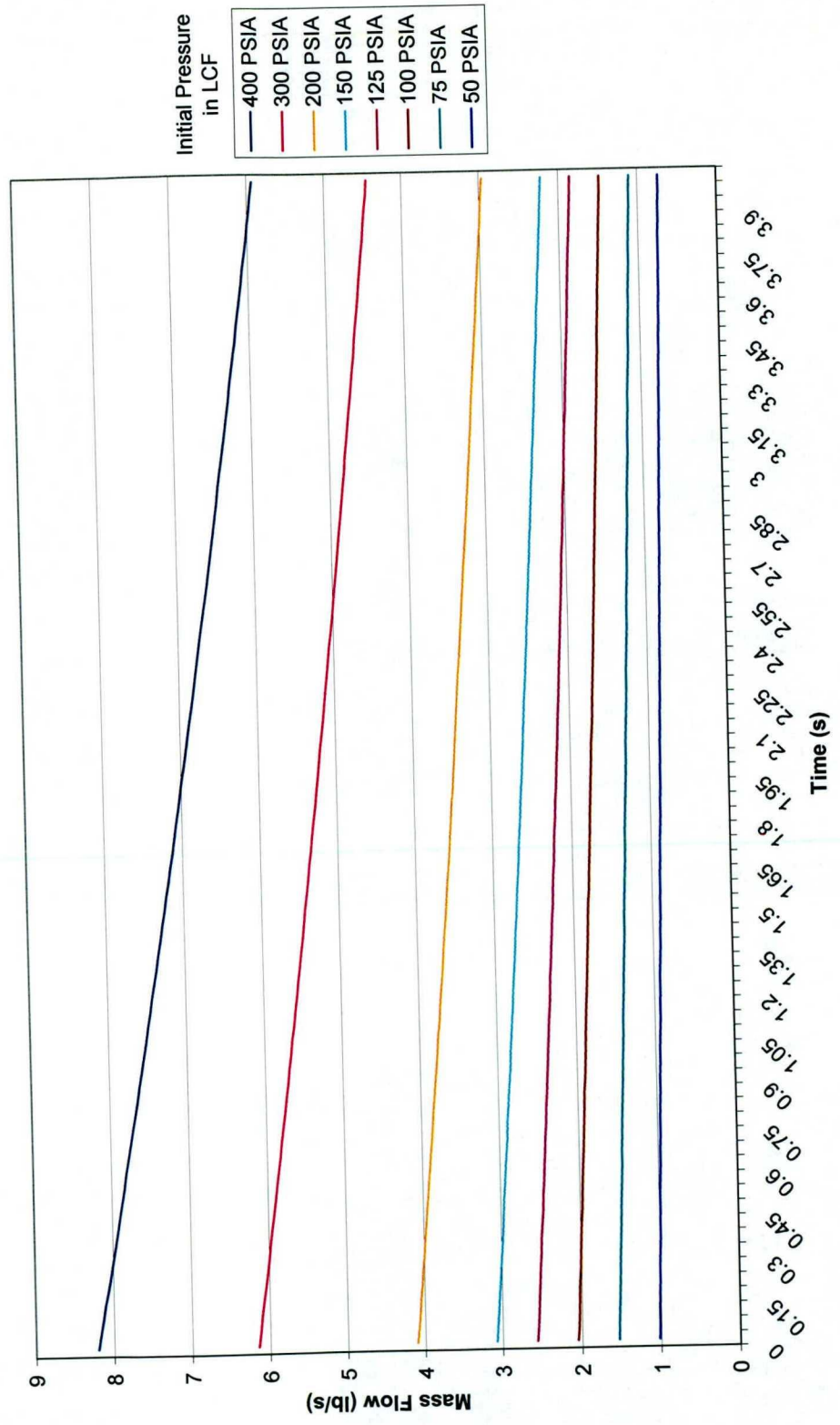
2" Diameter Choke  
T<sub>0</sub> = -45 F



**1.5" Diameter Choke  
T<sub>0</sub>=-45 F**



**1" Diameter Choke  
To=-45 F**



## APPENDIX C

### COOLANT GAS MASS FLOW CALCULATIONS

#### Coolant Gas Mass Flow supplied by LCF

$P_o := 260000 \frac{\text{N}}{\text{m}^2}$ (37.71_psia)	$T_o := 240 \text{ K}$ (-27.67_F)	$\text{Vol} := 1.27444 \text{ m}^3$ (45.0_ft <sup>3</sup> )	$P_o$ Total Pressure in LCF $T_o$ Total Temperature in LCF $\text{Vol}$ Volume of LCF $\tau$ Time Constant of LCF $\text{GC}$ Gas Constant
$\gamma := 1.40788$	$\tau := 85.5 \text{ s}$	$\text{GC} := 296.822 \frac{\text{J}}{\text{kg}\cdot\text{K}}$	

$$\text{Mdot}(P_o, T_o, \tau, \text{Vol}, \text{GC}, \gamma) := \frac{P_o \cdot \left(\frac{2}{\gamma+1}\right)^{\frac{\gamma}{\gamma-1}} \cdot \text{Vol}}{\text{GC} \cdot T_o \cdot \left(\frac{2}{\gamma+1}\right)^{\frac{\gamma+1}{2\gamma-2}} \cdot \tau \cdot \sqrt{\text{GC} \cdot T_o} \cdot \gamma \cdot \left(\frac{\gamma-1}{2}\right) \cdot \left(\frac{2}{\gamma+1}\right)^{\frac{\gamma+1}{2\gamma-2}}} \cdot \sqrt{\gamma \cdot \text{GC} \cdot T_o \cdot \left(\frac{2}{\gamma+1}\right)}$$

Total Mass Flow	$\text{Mdot}(P_o, T_o, \tau, \text{Vol}, \text{GC}, \gamma) = 0.2668 \frac{\text{kg}}{\text{s}} \left(0.588 \frac{\text{lb}}{\text{s}}\right)$	
-----------------	--	--

<p style="text-align: center;">Total effective area of Venturi chokes</p> $A_t := \frac{\text{Vol}}{\tau \cdot \sqrt{\text{GC} \cdot T_o} \cdot \gamma \cdot \left(\frac{\gamma-1}{2}\right) \cdot \left(\frac{2}{\gamma+1}\right)^{\frac{\gamma+1}{2\gamma-2}}}$ $A_t = 3.991 \times 10^{-4} \text{ m}^2$ (0.619_in <sup>2</sup> )	<p style="text-align: center;">Choke areas by section</p> <table style="width: 100%; border-collapse: collapse;"> <tr> <td style="width: 20%;">Inner Vane</td> <td style="width: 30%;"> <math>A_{iv} := 1.598 \cdot 10^{-4} \text{ m}^2</math> </td> <td style="width: 50%;">(0.248_in<sup>2</sup>)</td> </tr> <tr> <td>Outer Vane</td> <td> <math>A_{ov} := 8.799 \cdot 10^{-5} \text{ m}^2</math> </td> <td>(0.136_in<sup>2</sup>)</td> </tr> <tr> <td>Rotor</td> <td> <math>A_r := 1.512 \cdot 10^{-4} \text{ m}^2</math> </td> <td>(0.234_in<sup>2</sup>)</td> </tr> </table>	Inner Vane	$A_{iv} := 1.598 \cdot 10^{-4} \text{ m}^2$	(0.248_in <sup>2</sup> )	Outer Vane	$A_{ov} := 8.799 \cdot 10^{-5} \text{ m}^2$	(0.136_in <sup>2</sup> )	Rotor	$A_r := 1.512 \cdot 10^{-4} \text{ m}^2$	(0.234_in <sup>2</sup> )
Inner Vane	$A_{iv} := 1.598 \cdot 10^{-4} \text{ m}^2$	(0.248_in <sup>2</sup> )								
Outer Vane	$A_{ov} := 8.799 \cdot 10^{-5} \text{ m}^2$	(0.136_in <sup>2</sup> )								
Rotor	$A_r := 1.512 \cdot 10^{-4} \text{ m}^2$	(0.234_in <sup>2</sup> )								

Mass Flow supplied to each section

Inner Vane	$\text{MF}_{iv} := \text{Mdot}(P_o, T_o, \tau, \text{Vol}, \text{GC}, \gamma) \cdot \frac{A_{iv}}{A_t}$	$\text{MF}_{iv} = 0.1068 \frac{\text{kg}}{\text{s}}$	$\left(0.235 \cdot \frac{\text{lb}}{\text{s}}\right)$
Outer Vane	$\text{MF}_{ov} := \text{Mdot}(P_o, T_o, \tau, \text{Vol}, \text{GC}, \gamma) \cdot \frac{A_{ov}}{A_t}$	$\text{MF}_{ov} = 0.0588 \frac{\text{kg}}{\text{s}}$	$\left(0.130 \cdot \frac{\text{lb}}{\text{s}}\right)$
Rotor	$\text{MF}_r := \text{Mdot}(P_o, T_o, \tau, \text{Vol}, \text{GC}, \gamma) \cdot \frac{A_r}{A_t}$	$\text{MF}_r = 0.101 \frac{\text{kg}}{\text{s}}$	$\left(0.223 \cdot \frac{\text{lb}}{\text{s}}\right)$

### Coolant Gas Mass Flow Calculated at Inner Vane Cooling Holes

$$\begin{array}{llll}
 p_o := 51000 \frac{\text{N}}{\text{m}^2} & T_o := 265 \text{ K} & \text{AreaVI} := 7.6684 \times 10^{-4} \text{ m}^2 & \gamma := 1.401 & \text{GC} := 296.822 \frac{\text{J}}{\text{kg}\cdot\text{K}} \\
 (7.40_{\text{psia}}) & (17.33_{\text{F}}) & (1.189_{\text{in}^2}) & & \text{gas constant}
 \end{array}$$

internal pressure measured      internal temperature measured      cooling hole area measured by blowdown experiments

Cooling gas static properties at cooling holes when choked

$$\begin{array}{ll}
 p_s := p_o \left( \frac{2}{\gamma + 1} \right)^{\frac{\gamma}{\gamma - 1}} & p_s = 26934 \frac{\text{N}}{\text{m}^2} \quad (3.91_{\text{psia}}) \\
 T_s := \frac{T_o \cdot 2}{\gamma + 1} & T_s = 220.7 \text{ K} \quad (-62.4_{\text{F}})
 \end{array}$$

Mass flow out of inner vane cooling holes

$$\dot{M} := \left( \frac{p_s}{\text{GC} \cdot T_s} \cdot \text{AreaVI} \cdot \sqrt{\gamma \cdot \text{GC} \cdot T_s} \right)$$

$$\dot{M} = 0.09551 \frac{\text{kg}}{\text{s}} \quad \left( 0.210 \frac{\text{lb}}{\text{s}} \right)$$

### Coolant Gas Mass Flow Calculated at Outer Vane Cooling Holes

$$\begin{array}{lllll}
 p_o := 38000 \frac{\text{N}}{\text{m}^2} & T_o := 265 \text{ K} & \text{AreaVO} := 4.20386 \times 10^{-4} \text{ m}^2 & \gamma := 1.4009 & \text{GC} := 296.822 \frac{\text{J}}{\text{kg} \cdot \text{K}} \\
 (5.51_{\text{psia}}) & (17.33_{\text{F}}) & (0.652_{\text{in}^2}) & & \text{gas constant}
 \end{array}$$

internal pressure measured      internal temperature measured      cooling hole area measured by blowdown experiments

Cooling gas static properties at cooling holes when choked

$$p_s := p_o \left( \frac{2}{\gamma + 1} \right)^{\frac{\gamma}{\gamma - 1}} \qquad p_s = 20069 \frac{\text{N}}{\text{m}^2} \quad (2.91_{\text{psia}})$$

$$T_s := \frac{T_o \cdot 2}{\gamma + 1} \qquad T_s = 220.8 \text{ K} \quad (-62.2_{\text{F}})$$

Mass flow out of outer vane cooling holes

$$\dot{M} := \left( \frac{p_s}{\text{GC} \cdot T_s} \cdot \text{AreaVO} \cdot \sqrt{\gamma \cdot \text{GC} \cdot T_s} \right)$$

$$\dot{M} = 0.03901 \frac{\text{kg}}{\text{s}} \quad \left( 0.086 \frac{\text{lb}}{\text{s}} \right)$$

## Coolant Gas Mass Flow Calculated at Rotor Blade Cooling Holes

$$\begin{array}{llll}
 p_m := 51000 \frac{\text{N}}{\text{m}^2} & T_m := 265 \text{ K} & \text{AreaR} := 7.0606 \times 10^{-4} \text{ m}^2 & \gamma := 1.401 & \text{GC} := 296.822 \frac{\text{J}}{\text{kg}\cdot\text{K}} \\
 (7.40_{\text{psia}}) & (17.33_{\text{F}}) & (1.094_{\text{in}^2}) & & \text{gas constant}
 \end{array}$$

internal pressure measured      internal temperature measured      cooling hole area measured by blowdown experiments

$$M_p := 0.3 \quad M_t := 0.3$$

Mach numbers at pressure and temperature sensors estimated using the area Mach number relation

Cooling gas total properties in rotor

$$\begin{array}{ll}
 p_o := p_m \cdot \left( 1 + \frac{\gamma - 1}{2} \cdot M_p^2 \right)^{\frac{\gamma}{\gamma - 1}} & p_o = 54288 \frac{\text{N}}{\text{m}^2} \quad (7.87_{\text{psia}}) \\
 T_o := T_m \cdot \left( 1 + \frac{\gamma - 1}{2} \cdot M_t^2 \right) & T_o = 269.8 \text{ K} \quad (26.0_{\text{F}})
 \end{array}$$

Cooling gas static properties at cooling holes when choked

$$\begin{array}{ll}
 p_s := p_o \left( \frac{2}{\gamma + 1} \right)^{\frac{\gamma}{\gamma - 1}} & p_s = 28670 \frac{\text{N}}{\text{m}^2} \quad (4.16_{\text{psia}}) \\
 T_s := \frac{T_o \cdot 2}{\gamma + 1} & T_s = 224.7 \text{ K} \quad (-55.2_{\text{F}})
 \end{array}$$

Mass flow out of rotor cooling holes

$$\begin{aligned}
 \dot{M} &:= \frac{p_s}{\text{GC} \cdot T_s} \cdot \text{AreaR} \cdot \sqrt{\gamma \cdot \text{GC} \cdot T_s} \\
 \dot{M} &= 0.09277 \frac{\text{kg}}{\text{s}} \\
 &\quad \left( 0.204 \frac{\text{lb}}{\text{s}} \right)
 \end{aligned}$$

## APPENDIX D

### UNCERTAINTY ANALYSIS CALCULATIONS

**Blowing Ratio Error Propagation Analysis SS Gill Holes**

$P_s := 63000 \frac{N}{m^2} \quad (9.14\_psia)$ $P_{oc} := 105200 \frac{N}{m^2} \quad (15.26\_psia)$ $M\alpha := .98$ $T_{oc} := 265 \quad K \quad (17.33\_F)$ $T_s := 344.32 \quad K \quad (160.11\_F)$	$R_c := 296.822 \frac{J}{kg \cdot K}$ $\gamma_c := 1.4$ $R\alpha := 286.986 \frac{J}{kg \cdot K}$ $\gamma\alpha := 1.4$	$P_s$ Static Pressure on Blade Surface $P_{oc}$ Coolant Gas Total Pressure $M\alpha$ Core Flow Mach Number $T_{oc}$ Coolant Gas Total Temperature $T\alpha$ Core Flow Total Temperature
--	--	---

$$BR(\gamma\alpha, M\alpha) := \frac{R_c \cdot \frac{P_s}{\left[1 + \frac{\gamma_c - 1}{2} \left[ \left( \frac{P_{oc}}{P_s} \right)^{\frac{\gamma_c - 1}{\gamma_c}} - 1 \right] \cdot \frac{2}{\gamma_c - 1} \right]} \cdot \sqrt{\left[ \left( \frac{P_{oc}}{P_s} \right)^{\frac{\gamma_c - 1}{\gamma_c}} - 1 \right] \cdot \frac{2}{\gamma_c - 1}} \cdot \sqrt{\frac{T_{oc}}{1 + \frac{\gamma_c - 1}{2} \left[ \left( \frac{P_{oc}}{P_s} \right)^{\frac{\gamma_c - 1}{\gamma_c}} - 1 \right] \cdot \frac{2}{\gamma_c - 1}}}}{\frac{P_s}{R\alpha \cdot T_s} \cdot M\alpha \cdot \sqrt{\gamma\alpha \cdot R\alpha \cdot T_s}}$$
  

$$BR(P_s, R_c, T_{oc}, \gamma_c, P_{oc}, R\alpha, T_s, \gamma\alpha, M\alpha) = 1.1$$

$a := \left( \frac{\partial}{\partial P_s} BR(P_s, R_c, T_{oc}, \gamma_c, P_{oc}, R\alpha, T_s, \gamma\alpha, M\alpha) \right) \cdot \frac{P_s}{BR(P_s, R_c, T_{oc}, \gamma_c, P_{oc}, R\alpha, T_s, \gamma\alpha, M\alpha)}$	$b := \left( \frac{\partial}{\partial P_{oc}} BR(P_s, R_c, T_{oc}, \gamma_c, P_{oc}, R\alpha, T_s, \gamma\alpha, M\alpha) \right) \cdot \frac{P_{oc}}{BR(P_s, R_c, T_{oc}, \gamma_c, P_{oc}, R\alpha, T_s, \gamma\alpha, M\alpha)}$	$c := \left( \frac{\partial}{\partial M\alpha} BR(P_s, R_c, T_{oc}, \gamma_c, P_{oc}, R\alpha, T_s, \gamma\alpha, M\alpha) \right) \cdot \frac{M\alpha}{BR(P_s, R_c, T_{oc}, \gamma_c, P_{oc}, R\alpha, T_s, \gamma\alpha, M\alpha)}$	$d := \left( \frac{\partial}{\partial T_{oc}} BR(P_s, R_c, T_{oc}, \gamma_c, P_{oc}, R\alpha, T_s, \gamma\alpha, M\alpha) \right) \cdot \frac{T_{oc}}{BR(P_s, R_c, T_{oc}, \gamma_c, P_{oc}, R\alpha, T_s, \gamma\alpha, M\alpha)}$	$e := \left( \frac{\partial}{\partial T_s} BR(P_s, R_c, T_{oc}, \gamma_c, P_{oc}, R\alpha, T_s, \gamma\alpha, M\alpha) \right) \cdot \frac{T_s}{BR(P_s, R_c, T_{oc}, \gamma_c, P_{oc}, R\alpha, T_s, \gamma\alpha, M\alpha)}$
---	---	---	---	---

Influence Coefficients for Blowing Ratio	Uncertainties in Variables				
$a = -1.191$	$c = -1$	$e = 0.5$	$\Delta P_s := 2.7 \%$	$\Delta M\alpha := 10 \%$	$\Delta T_s := 0.9 \%$
$b = 1.191$	$d = -0.5$		$\Delta P_{oc} := 1.6 \%$	$\Delta T_{oc} := 1.1 \%$	

$$\Delta BR := \sqrt{\sum_i (\text{influence\_coefficients} \cdot \text{uncertainty})^2}$$
  

$$\Delta BR := \sqrt{(\Delta P_s \cdot a)^2 + (\Delta P_{oc} \cdot b)^2 + (\Delta M\alpha \cdot c)^2 + (\Delta T_{oc} \cdot d)^2 + (\Delta T_s \cdot e)^2}$$
  

Total Uncertainty in Blowing Ratio       $\Delta BR = 10.7 \%$



### Error Propagation Analysis on Coolant Gas Mass Flow supplied by LCF

$$P_o := 260000 \frac{\text{N}}{\text{m}^2}$$

(37.7\_psia)

$$\text{Vol} := 1.27444 \text{ m}^3$$

(45.0\_ft<sup>3</sup>)

$$\gamma := 1.40788$$

$P_o$  Total Pressure in LCF  
 $T_o$  Total Temperature in LCF  
 $\text{Vol}$  Volume of LCF  
 $\tau$  Time Constant of LCF  
 $\text{GC}$  Gas Constant

$$T_o := 240 \text{ K}$$

(-27.67\_F)

$$\tau := 85.5 \text{ s}$$

$$\text{GC} := 296.822 \frac{\text{J}}{\text{kg}\cdot\text{K}}$$

$$\text{Mdot}(P_o, T_o, \tau, \text{Vol}, \text{GC}, \gamma) := \frac{P_o \cdot \left(\frac{2}{\gamma+1}\right)^{\frac{\gamma}{\gamma-1}} \cdot \text{Vol}}{\text{GC} \cdot T_o \cdot \left(\frac{2}{\gamma+1}\right)^{\frac{\gamma+1}{2\gamma-2}}} \cdot \sqrt{\gamma \cdot \text{GC} \cdot T_o \cdot \left(\frac{2}{\gamma+1}\right)}$$

$$a := \left( \frac{d}{dP_o} \text{Mdot}(P_o, T_o, \tau, \text{Vol}, \text{GC}, \gamma) \right) \cdot \frac{P_o}{\text{Mdot}(P_o, T_o, \tau, \text{Vol}, \text{GC}, \gamma)}$$

$$b := \left( \frac{d}{dT_o} \text{Mdot}(P_o, T_o, \tau, \text{Vol}, \text{GC}, \gamma) \right) \cdot \frac{T_o}{\text{Mdot}(P_o, T_o, \tau, \text{Vol}, \text{GC}, \gamma)}$$

$$c := \left( \frac{d}{d\tau} \text{Mdot}(P_o, T_o, \tau, \text{Vol}, \text{GC}, \gamma) \right) \cdot \frac{\tau}{\text{Mdot}(P_o, T_o, \tau, \text{Vol}, \text{GC}, \gamma)}$$

$$d := \left( \frac{d}{d\text{Vol}} \text{Mdot}(P_o, T_o, \tau, \text{Vol}, \text{GC}, \gamma) \right) \cdot \frac{\text{Vol}}{\text{Mdot}(P_o, T_o, \tau, \text{Vol}, \text{GC}, \gamma)}$$

$$e := \left( \frac{d}{d\gamma} \text{Mdot}(P_o, T_o, \tau, \text{Vol}, \text{GC}, \gamma) \right) \cdot \frac{\gamma}{\text{Mdot}(P_o, T_o, \tau, \text{Vol}, \text{GC}, \gamma)}$$

#### Influence Coefficients

$$a = 1 \quad b = -1 \quad c = -1 \quad d = 1 \quad e = -3.452$$

#### Uncertainties in Variables

$$\Delta P_o := 0.2 \% \quad \Delta \tau := 0.6 \% \quad \Delta \gamma := 0.04 \%$$

$$\Delta T_o := 0.1 \% \quad \Delta \text{Vol} := 1 \%$$

$$\Delta \text{Mdot} := \sqrt{\sum (\text{influence\_coefficients} \cdot \text{uncertainty})^2}$$

$$\Delta \text{Mdot} := \sqrt{(\Delta P_o \cdot a)^2 + (\Delta T_o \cdot b)^2 + (\Delta \tau \cdot c)^2 + (\Delta \text{Vol} \cdot d)^2 + (\Delta \gamma \cdot e)^2}$$

$$\% \text{ Uncertainty for Mdot} \quad \Delta \text{Mdot} = 1.2 \%$$

## Error Propagation Analysis on Mass Flow Calculations at the Rotor Blade Cooling Holes

$$\begin{aligned}
 GC &:= 296.822 \frac{\text{J}}{\text{kg}\cdot\text{K}} & \gamma &:= 1.401 & \text{Area} &:= 7.0606 \cdot 10^{-4} \text{ m}^2 & & \text{Pm} & \text{Pressure measured} \\
 & & & & & (1.094_{\text{in}}^2) & & \text{Tm} & \text{Temperature measured} \\
 \text{Pm} &:= 51000 \frac{\text{N}}{\text{m}^2} & \text{Tm} &:= 265 \text{ K} & \text{Mp} &:= 0.3 & \text{Mt} &:= 0.3 & \text{Mp} & \text{Mach at Pressure transducer} \\
 & (7.40_{\text{psia}}) & & (17.3_{\text{F}}) & & & & & \text{Mt} & \text{Mach at Temperature sensor} \\
 & & & & & & & & \text{GC} & \text{Gas Constant}
 \end{aligned}$$

$$\text{Mdot}(\text{Pm}, \text{Tm}, \text{Mp}, \text{Mt}, \text{GC}, \text{Area}, \gamma) := \left[ \frac{\left[ \text{Pm} \cdot \left( 1 + \frac{\gamma-1}{2} \cdot \text{Mp}^2 \right)^{\frac{\gamma}{\gamma-1}} \cdot \left( \frac{2}{\gamma+1} \right)^{\frac{\gamma}{\gamma-1}} \right]}{\text{GC} \cdot \left[ \frac{2}{\gamma+1} \cdot \text{Tm} \cdot \left( 1 + \frac{\gamma-1}{2} \cdot \text{Mt}^2 \right) \right]} \right] \cdot \text{Area} \cdot \sqrt{\gamma \cdot \text{GC} \cdot \left[ \frac{2}{\gamma+1} \cdot \text{Tm} \cdot \left( 1 + \frac{\gamma-1}{2} \cdot \text{Mt}^2 \right) \right]}$$

$$a := \left( \frac{d}{d\text{Pm}} \text{Mdot}(\text{Pm}, \text{Tm}, \text{Mp}, \text{Mt}, \text{GC}, \text{Area}, \gamma) \right) \cdot \frac{\text{Pm}}{\text{Mdot}(\text{Pm}, \text{Tm}, \text{Mp}, \text{Mt}, \text{GC}, \text{Area}, \gamma)}$$

$$b := \left( \frac{d}{dTm} \text{Mdot}(\text{Pm}, \text{Tm}, \text{Mp}, \text{Mt}, \text{GC}, \text{Area}, \gamma) \right) \cdot \frac{\text{Tm}}{\text{Mdot}(\text{Pm}, \text{Tm}, \text{Mp}, \text{Mt}, \text{GC}, \text{Area}, \gamma)}$$

$$c := \left( \frac{d}{d\text{Mp}} \text{Mdot}(\text{Pm}, \text{Tm}, \text{Mp}, \text{Mt}, \text{GC}, \text{Area}, \gamma) \right) \cdot \frac{\text{Mp}}{\text{Mdot}(\text{Pm}, \text{Tm}, \text{Mp}, \text{Mt}, \text{GC}, \text{Area}, \gamma)}$$

$$d := \left( \frac{d}{d\text{Mt}} \text{Mdot}(\text{Pm}, \text{Tm}, \text{Mp}, \text{Mt}, \text{GC}, \text{Area}, \gamma) \right) \cdot \frac{\text{Mt}}{\text{Mdot}(\text{Pm}, \text{Tm}, \text{Mp}, \text{Mt}, \text{GC}, \text{Area}, \gamma)}$$

$$e := \left( \frac{d}{d\text{Area}} \text{Mdot}(\text{Pm}, \text{Tm}, \text{Mp}, \text{Mt}, \text{GC}, \text{Area}, \gamma) \right) \cdot \frac{\text{Area}}{\text{Mdot}(\text{Pm}, \text{Tm}, \text{Mp}, \text{Mt}, \text{GC}, \text{Area}, \gamma)}$$

$$f := \left( \frac{d}{d\gamma} \text{Mdot}(\text{Pm}, \text{Tm}, \text{Mp}, \text{Mt}, \text{GC}, \text{Area}, \gamma) \right) \cdot \frac{\gamma}{\text{Mdot}(\text{Pm}, \text{Tm}, \text{Mp}, \text{Mt}, \text{GC}, \text{Area}, \gamma)}$$

### Influence Coefficients for Mass Flow at Cooling holes

$$a = 1 \qquad c = 0.1239 \qquad e = 1$$

$$b = -0.5 \qquad d = -0.0177 \qquad f = 0.3748$$

### Uncertainties in Variables

$$\Delta\text{Pm} := 3.4 \text{ \%} \qquad \Delta\text{Mp} := 10 \text{ \%} \qquad \Delta\text{Area} := 1.5 \text{ \%}$$

$$\Delta\text{Tm} := 1.1 \text{ \%} \qquad \Delta\text{Mt} := 10 \text{ \%} \qquad \Delta\gamma := 0.04 \text{ \%}$$

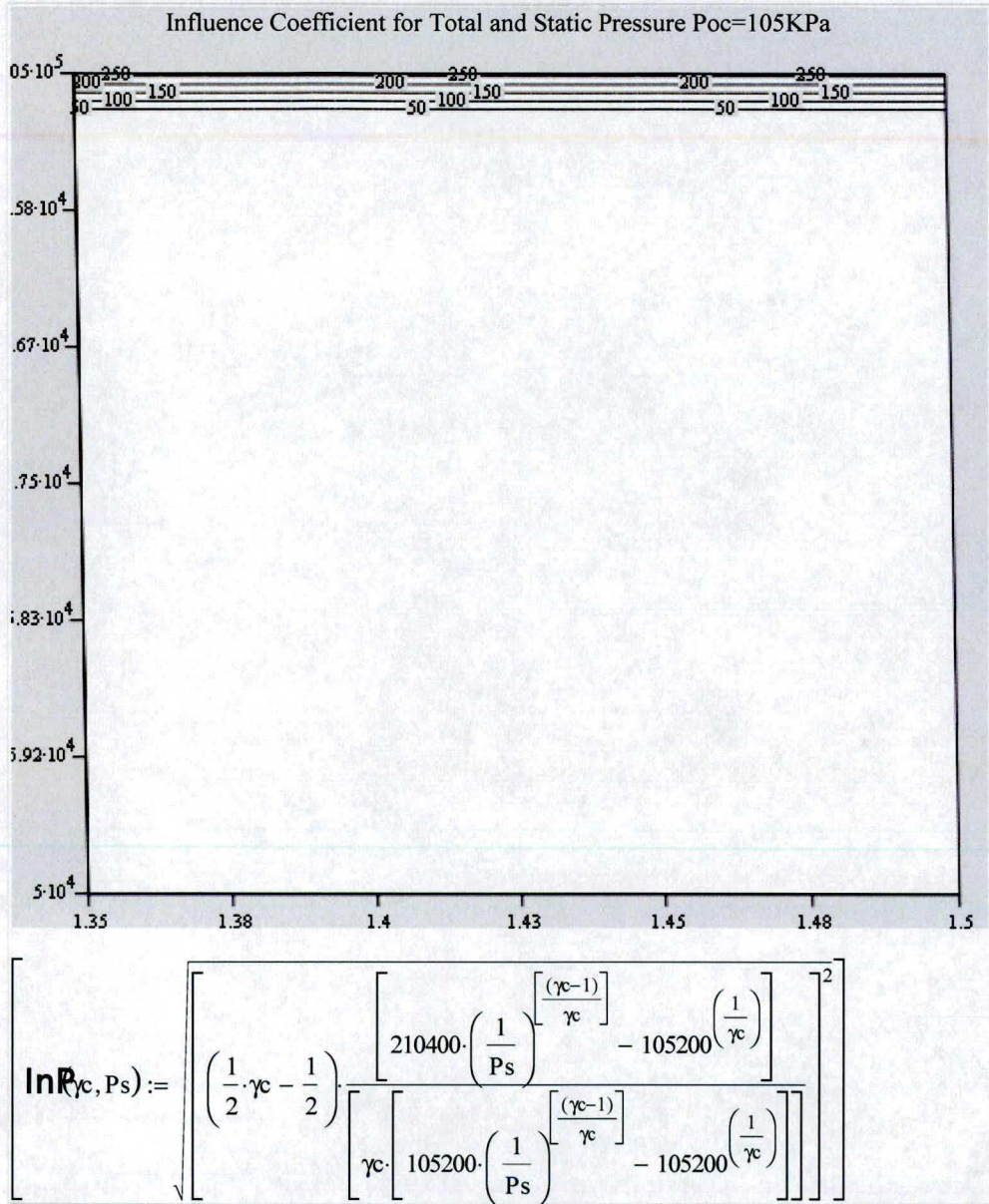
$$\Delta\text{Mdot} := \sqrt{\sum_i (\text{influence\_coefficients} \cdot \text{uncertainty})^2}$$

$$\Delta\text{Mdot} := \sqrt{(\Delta\text{Pm} \cdot a)^2 + (\Delta\text{Tm} \cdot b)^2 + (\Delta\text{Mp} \cdot c)^2 + (\Delta\text{Mt} \cdot d)^2 + (\Delta\text{Area} \cdot e)^2 + (\Delta\gamma \cdot f)^2}$$

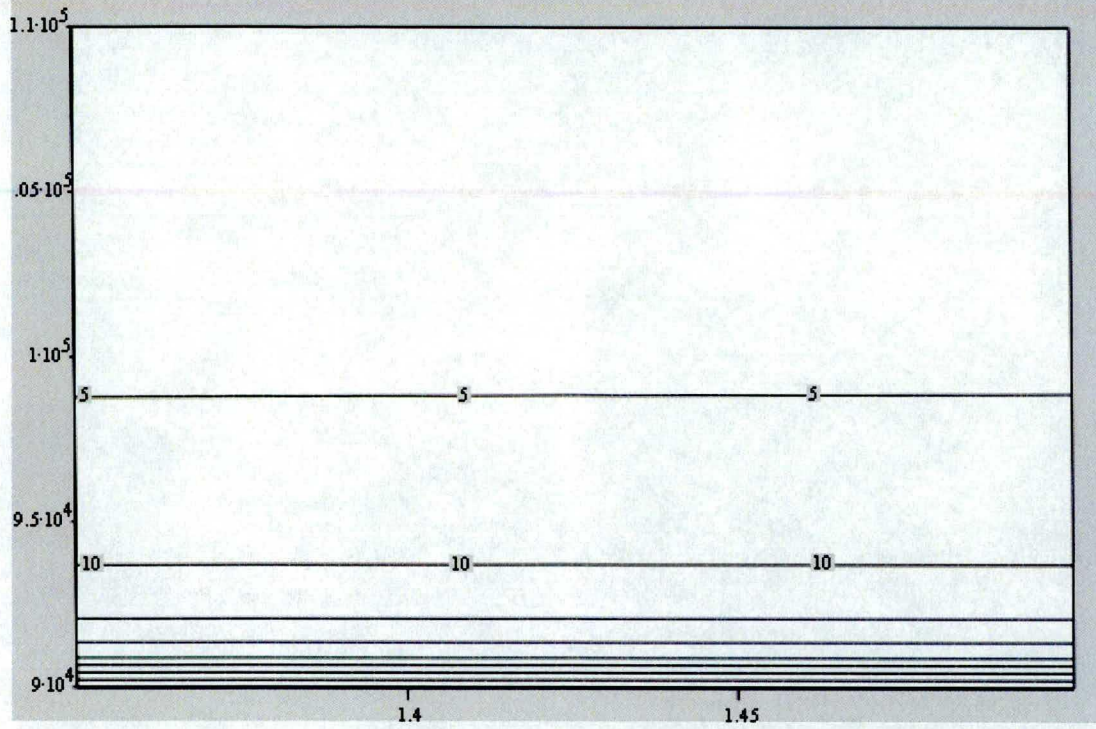
% Uncertainty for Mdot

$$\Delta\text{Mdot} = 3.96 \text{ \%}$$

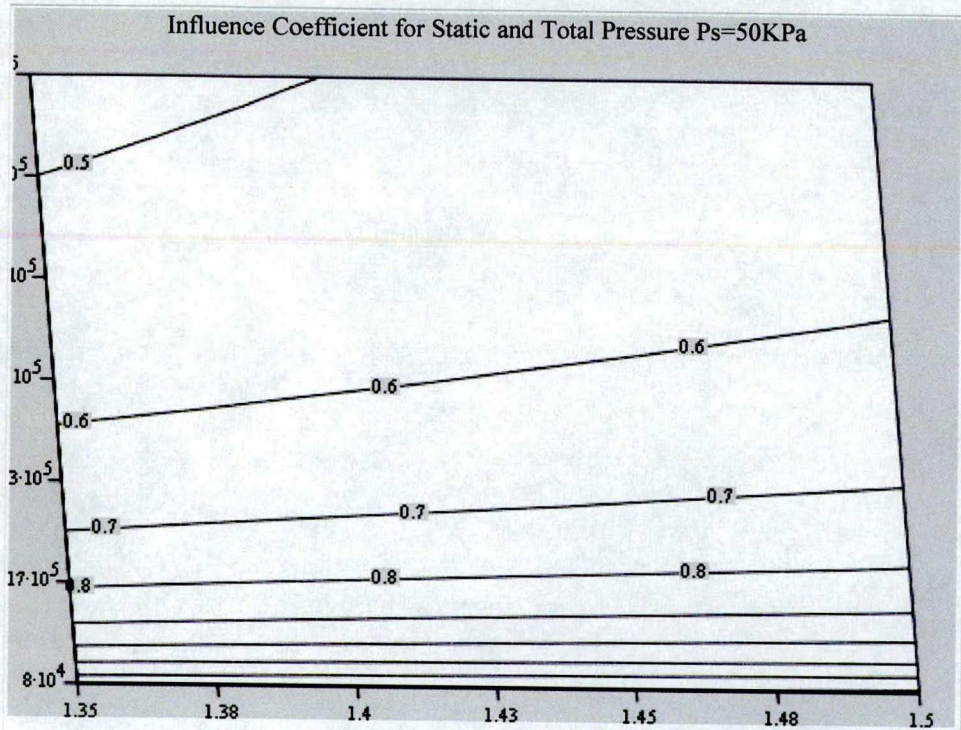
## D.1 Blowing Ratio Influence Coefficients Characterization Plots



Influence Coefficient for Static and Total Pressure Ps=89KPa



$$\ln R_{(\gamma, P_{oc})} := \sqrt{\left[ \left( \frac{1}{2} \cdot \gamma - \frac{1}{2} \right) \cdot \frac{\left[ 2 \cdot P_{oc} \cdot \left( \frac{1}{89000} \right)^{\frac{(\gamma-1)}{\gamma}} - P_{oc} \left( \frac{1}{\gamma} \right) \right]^2}{\left[ \gamma \cdot \left[ P_{oc} \cdot \left( \frac{1}{89000} \right)^{\frac{(\gamma-1)}{\gamma}} - P_{oc} \left( \frac{1}{\gamma} \right) \right] \right]^2} \right]}$$



$$\ln R_{(\gamma_c, P_{oc})} := \sqrt{\left[ \left( \frac{1}{2} \cdot \gamma_c - \frac{1}{2} \right) \cdot \frac{\left[ 2 \cdot P_{oc} \cdot \left( \frac{1}{50000} \right)^{\frac{(\gamma_c-1)}{\gamma_c}} - P_{oc} \left( \frac{1}{\gamma_c} \right) \right]^2}{\left[ \gamma_c \cdot \left[ P_{oc} \cdot \left( \frac{1}{50000} \right)^{\frac{(\gamma_c-1)}{\gamma_c}} - P_{oc} \left( \frac{1}{\gamma_c} \right) \right] \right]} \right]}$$

## BIBLIOGRAPHY

1. Cumpsty, N., *Jet Propulsion: A Simple Guide to the Aerodynamic and Thermodynamic Design and Performance of Jet Engines*. 2nd ed. 2003, Cambridge, UK: Cambridge University Press. 303.
2. Gladden, H.J. and R.J. Simoneau, *Review and Assessment of the Database and Numerical Modeling for Turbine Heat Transfer*, in *Toward Improved Durability in Advanced Aircraft Engine Hot Sections*, K.E. Sokolowski, Editor. 1988. p. 39-55.
3. Abhari, R.S. and A.H. Epstein. *An Experimental Study of Film Cooling in a Rotating Transonic Turbine*. in *IGTI*. 1992. Cologne, Germany, 92-GT-201.
4. Dring, R.P., M.F. Blair, and H.D. Joslyn, *An Experimental Investigation of Film Cooling on a Turbine Rotor Blade*. *Journal of Engineering for Power*, 1980. **102**: p. 81-87,
5. Takeishi, K., S. Aoki, T. Sato, and K. Tsukagoshi. *Film Cooling on a Gas Turbine Rotor Blade*. in *International Gas Turbine and Aeroengine Congress and Exposition*. 1991. Orlando, Florida, 91-GT-279.
6. Abhari, R.S., *Impact of Rotor-Stator Interaction on Turbine Blade Film Cooling*. *Journal of Turbomachinery*, 1996. **118**: p. 123-133,
7. Dénos, R. and G. Paniagua. *Influence of the Hub Endwall Cavity Flow on the Time-Averaged and Time-Resolved Aero-Thermodynamics of an Axial HP Turbine Stage*. in *ASME Turbo Expo 2002*. 2002. Amsterdam, The Netherlands, GT-2002-30185.

8. Didier, F., R. Dénos, and T. Arts. *Unsteady Rotor Heat Transfer in a Transonic Turbine Stage*. in *ASME Turbo Expo 2002*. 2002. Amsterdam, The Netherlands, GT-2002-30195.
9. Zilles, D., *Design and Operation of The Ohio State University Gas Turbine Lab's Large Calibration Facility*. 1998, OSU: Columbus. p. 37.
10. Green, B.R., J.W. Barter, C.W. Haldeman, and M.G. Dunn. *Time-Averaged and Time-Accurate Aero-Dynamics for the Recessed Tip Cavity of a High-Pressure Turbine Blade and the Outer Stationary Shroud: Comparison of Computational and Experimental Results*. in *IGTI*. 2004. Vienna, Austria, GT2004-53443.
11. Molter, S., M.G. Dunn, C.W. Haldeman, R.F. Bergholz, and P. Vitt. *Heat-Flux Measurements and Predictions for the Blade Tip Region of a High-Pressure Turbine*. in *IGTI*. 2006. Barcelona, Spain GT2006-9004.
12. Sen, B., D.L. Schmidt, and D.G. Bogard, *Film Cooling with Compound Angle Holes: Heat Transfer*. *Journal of Turbomachinery*, 1996. **118**: p. 800-806,
13. Leylek, J.H. and R.D. Zerkel, *Discrete-Jet Film Cooling: A Comparison of Computational Results with Experiments*. *ASME Journal of Turbomachinery*, 1994. **Vol. 116**: p. pp. 358-368,
14. Bernsdorf, S., M.G. Rose, and R.S. Abhari. *Modeling of Film Cooling - Part I: Experimental Study of Flow Structure*. in *ASME Turbo Expo 2005*. 2005. Reno-Tahoe, Nevada, USA, GT2005-68783.
15. Burdet, A., R.S. Abhari, and M.G. Rose. *Modeling of Film Cooling - Part II: Model for use in 3D CFD*. in *ASME Turbo Expo 2005*. 2005. Reno-Tahoe, Nevada, USA, GT2005-68780.
16. Montomoli, F., S.D. Gatta, P. Adami, and F. Martelli. *Conjugate Heat Transfer Modeling in Film Cooled Blades*. in *ASME Turbo Expo 2004 Power for Land, Sea, and Air*. 2004. Vienna, Austria: ASME, GT2004-53177.

17. Albert, J.E., D.G. Bogard, and F. Cunha. *Adiabatic and Overall Effectiveness for a Film Cooled Blade*. in *ASME Turbo Expo 2004*. 2004. Vienna, Austria, GT2004-53998.
18. Berhe, M.K. and S.V. Patankar, *Investigation of Discrete-Hole Film Cooling Parameters Using Curved-Plate Models*. *Journal of Turbomachinery*, 1999. **121**: p. 792-803,
19. Ahn, J., S. Mhetras, and J.-C. Han. *Film-Cooling Effectiveness on a Gas Turbine Blade Tip Using Pressure Sensitive Paint*. in *ASME Turbo Expo 2004*. 2004. Vienna, Austria, GT2004-53249.
20. Doorly, D.J. and M.L.G. Oldfield. *Simulation of the Effects of Shack Wave Passing on a Turbine Rotor Blade*. in *ASME*. 1985, 85-GT-112.
21. Doorly, D.J., M.L.G. Oldfield, and C.T.J. Scrivener. *Wake Passing in a Turbine Rotor Cascade*. in *AGARD*. 1985. Bergen, Norway,
22. Zhang, D. and J.-C. Han, *Combined Effect of Free-Stream Turbulence and Unsteady Wake on Heat Transfer Coefficients from a Gas Turbine Blade*. *ASME Journal of Heat Transfer*, 1995. **Vol. 117**: p. pp. 296-302,
23. Zhang, D. and J.-C. Han, *Influence of Mainstream Turbulence on Heat Transfer Coefficients from a Gas Turbine Blade*. *ASME Journal of Heat Transfer*, 1994. **Vol. 116**: p. pp. 896-903,
24. Mehendale, A.B., J.-C. Han, S. Ou, and C.P. Lee, *Unsteady Wake Over a Linear Turbine Blade Cascade with Air and CO<sub>2</sub> Film Injection. Part II: Effect on Film Effectiveness and Heat Transfer Distributions*. *ASME Journal of Turbomachinery*, 1995. **Vol. 116**: p. pp. 730-737,
25. Yaras, M.I. and S.A. Sjolander. *Effects of Simulated Rotation on Tip Leakage in a Planar Cascade of Turbine Blades*. in *ASME*. 1991, 91-GT-127.



26. Bathie, W.W., *Fundamentals of Gas Turbines*. 1984, New York: John Wiley & Sons, Inc. 358.
27. Ashworth, K.A., J.E. LaGraff, K.L. Schultz, and K.J. Grindrod, *Unsteady Aerodynamic and Heat Transfer Processes in a Transonic Turbine Stage*. ASME Journal of Engineering for Gas Turbines and Power, 1985. **107**: p. pp. 1022-1030,
28. Nasir, H., S.V. Ekkad, R.S. Bunker, and S. Prakash. *Effects of Tip Gap Film Ingestion from Plain and Squealer Blade Tips*. in *ASME Turbo Expo 2004*. 2004. Vienna, Austria, GT2004-53455
29. Kwak, J.S., J. Ahn, J.-C. Han, C.P. Lee, R.S. Bunker, R. Boyle, and R. Gaugler. *Heat Transfer Coefficients on the Squealer Tip and Near Tip Regions of a Gas Turbine Blade with Single or Double Squealer*. in *ASME Turbo Expo 2003*. 2003. Atlanta, Georgia, GT2003-38907.
30. Kwak, J.S. and J.-C. Han. *Heat Transfer Coefficient and Film-Cooling Effectiveness on the Squealer Tip of a Gas Turbine Blade*. in *ASME Turbo Expo 2002*. 2002. Amsterdam, The Netherlands, GT-2002-30555.
31. Dunn, M.G., *Convective Heat Transfer and Aerodynamics in Axial Flow Turbine*. Journal of Turbomachinery, 2001. **123**: p. 637-686,
32. Popp, O., D.E. Smith, J.V. Bubb, H.C. Grabowski, T.E. Diller, J.A. Schetz, and W.-F. Ng. *Steady and Unsteady Heat Transfer in a Transonic Film Cooled Turbine Cascade*. in *International Gas Turbine & Aeroengine Congress & Exhibition*. 1999. Indianapolis, Indiana 99-GT-259.
33. Epstein, A.H., G.R. Guenette, R.J.G. Norton, and C. Yuzhang, *High Frequency Response Heat Flux Gauge*. Review of Scientific Instruments, 1985. **75**(4): p. 639-649,
34. Rigby, M.N., A.B. Johnson, and M.L.G. Oldfield. *Gas Turbine Rotor Blade Film Cooling With and Without Simulated MGW Shock Waves and Wakes*. in *ASME*. 1990, 90-GT-78.

35. Schultz, D.L., T.V. Jones, M.L.G. Oldfield, and L.C. Daniels. *A New Transient Cascade Facility for the Measurement of Heat Transfer Rates*. in *AGARD CP*. 1977, No. 229.
36. Miller, R.J., R.W. Moss, S.J. Payne, R.W. Ainsworth, C.K. Horwood, and N.W. Harvey, *HP/LP (Military), HP/LP (Civil) Aerodynamic Interaction Investigation in the Oxford Rotor Facility*. 1998.
37. Haldeman, C.W., M.G. Dunn, C.D. MacArthur, and C.G. Murawski. *The USAF Advanced Turbine Aerothermal Research Rig (ATARR)*. in *AGARD Conference Proceedings 527*. 1992,
38. Dunn, M.G., J.C. Moller, and R.C. Steele, *Operating Point Verification Data for a Large Shock Tunnel Test Facility*. 1989: Dayton.
39. Haldeman, C.W., R.M. Mathison, and M.G. Dunn. *Design, Construction, and Operation of a Combustor Emulator for Short-Duration High-Pressure Turbine Experiments*. in *AIAA Joint Propulsion Conference*. 2004. Fort Lauderdale, Florida, AIAA-2004-3829.
40. Han, J.-C., S. Dutta, and S. Ekkad, *Gas Turbine Heat Transfer and Cooling Technology*. 2000, Great Britain: Taylor & Francis. 646.
41. Epstein, A.H., G.R. Guenette, and R.J.G. Norton, *The Design of the MIT Blowdown Turbine Facility*. 1985.